VISVESVARAYA TECHNOLOGICAL UNIVERSITY

Jnana Sangama, Belagavi - 590 018, Karnataka

A Thesis on

Design, Development and Optimization of Electromagnetic Vibration Energy Harvesting Device

Submitted for the award of the degree of

DOCTOR OF PHILOSOPHY

IN

MECHANICAL ENGINEERING

By

Mr. Vijay Balkrishna Patil

Seat No: 2BL13PMN01

Under the Guidance of

Research Co-Supervisor

Dr. P. V. Malaji

Associate Professor

Department of Mechanical Engineering

Research Supervisor

Dr. M. I. Sakri

Professor

Department of Mechanical Engineering

Research Center

BLDEA's V. P. Dr. P.G. Halakatti

COLLEGE OF ENGINEERING AND TECHNOLOGY

Vijayapur – 586103

November 2022

BLDEA's V. P. Dr. P.G. Halakatti
COLLEGE OF ENGINEERING AND TECHNOLOGY
Vijayapur – 586103

VISVESVARAYA TECHNOLOGICAL UNIVERSITY
Jnana Sangama, Belagavi - 590 018, Karnataka

Research Center

BLDEA's V. P. Dr. P.G. Halakatti
College of Engineering and Technology,
Vijayapur – 586103

CERTIFICATE

This is to certify that the work incorporated in the thesis entitled, **"Design, Development and Optimization of Electromagnetic Vibration Energy Harvesting Device"** is submitted by **Mr. Vijay Balkrishna Patil (USN: 2BL13PMN01),** the research scholar of VTU, Research Center: BLDEA's V. P. Dr. P.G. Halakatti College of Engineering and Technology, Vijayapur, for the award of the degree of **"Doctor of Philosophy"** in Mechanical Engineering. It is certified that his work has been carried out under our supervision and guidance, the material in the thesis is his original work and material that has been obtained from the other sources has been duly acknowledged in the thesis.

Co-Supervisor
Dr. P. V. Malaji
Associate Professor,
Department of Mechanical Engineering

Supervisor
Dr. M. I. Sakri
Professor,
Department of Mechanical Engineering

BLDEA's V. P. Dr. P.G. Halakatti College of Engineering and Technology,
Vijayapur – 586103

HOD
Mechanical Engg. Dept.
BLDEA's V.P.Dr. P.G.Halakatti
College of Engg. & Tech. Vijayapur

Signature of the Head of the Research Centre
BLDEA's V. P. Dr. P.G. Halakatti College of Engineering and Technology,
Vijayapur – 586103

for

Head of the Institution
Principal,
B.L.D.E.A's V.P. Dr. P.G.H
College of Engg. & Tech
VIJAYAPUR-586103.

External Viva-voce

Name of the Examiners — Signature with date

1. _____

2. _____

VISVESVARAYA TECHNOLOGICAL UNIVERSITY
Jnana Sangama, Belagavi - 590 018, Karnataka
Research Center
BLDEA's V. P. Dr. P.G. Halakatti
College of Engineering and Technology,
Vijayapur – 586103

DECLARATION

I hereby declare that, the research work embedded in this doctoral thesis entitled, **"Design, Development and Optimization of Electromagnetic Vibration Energy Harvesting Device"**, submitted for the award of the degree of Doctor of Philosophy in Mechanical Engineering has been carried out by me under the guidance of Supervisor **Dr. M. I. Sakri,** Professor and Co-supervisor **Dr. P.V. Malaji,** Associate Professor, Department of Mechanical Engineering, BLDEA's V. P. Dr. P.G. Halakatti College of Engineering and Technology, Vijayapur.

I declare that the contents of this thesis and the results of this research work has not been submitted in part or full for the award of any diploma or degree of this or any other University.

Date: 25·11·22

Place: Vijayapur

Mr. Vijay Balkrishna Patil

(USN: 2BL13PMN01)

ABSTRACT

In this thesis report, an account of research work carried out on the design, development, and optimization of the power output of a vibration-based electromagnetic energy device (VBEH) is presented. The topic selected is based on the research gaps identified in an exhaustive literature review conducted in the area of energy harvester in general and vibration-based energy harvester, in particular. VBEH transforms ambient vibration energy (KE) into electrical energy. A laboratory model of Single Degree Freedom Vibration-Based Electromagnetic Energy Harvester (SDOF VBEH) has been designed and developed, which consists of a mechanical system of spring-mass-damper connected to an electrical load circuit through a vibration transducer. The vibration transducer comprises of high residual flux density cylindrical permanent magnet which oscillates in a copper coil and produces electro-motive-force (EMF) across the coil terminals to which the electrical load circuit is connected. The design and development of the copper coil has been carried out as per coil design guidelines, and proper copper fill factor and high residual flux density rare earth magnetic material Neodymium Iron Boron (NdFeB) has been selected as an oscillating magnet.

The harvester mass of the VBEH is suspended on a helical compression spring, and the other end of the spring is connected to the base of the VBEH device. The vibration transducer is placed parallel to the suspension spring such that the transducer magnet is connected to the harvester mass and the coil is connected to the base facilitating the in-line relative displacement between magnet and coil to convert vibration KE energy into electrical voltage.

An experimental test is a setup with the necessary instrumentation for the performance analysis of the developed model of SDOF VBEH. The sensors for i) measurement of harvester mass displacement response and the VBEH base displacement ii) voltage (EMF) across the vibration transducer copper coil and iii) the speed measurement of variable speed electric drive motor have been provided. The base of VBEH is subjected to variable frequency harmonic excitation by a cam-follower mechanism driven by a variable speed DC motor. The cam eccentricity provides the necessary value of the amplitude of excitation.

In this experimental test setup, first of all, i) the relative displacement between harvester mass and base, without and with vibration transducer has been measured at various

frequencies of excitation. Using these results, the values of mechanical damping ratio ζ_m and electrical damping ratio ζ_e have been calculated ii) the effect of variation of the values of ζ_m and ζ_e on the maximum average power of VBEH is analyzed and iii) the pure resistive load across the transducer coil is varied, and its effect on the maximum average power output is analyzed at various excitation frequencies.

From this analysis, it is observed that i) for maximum average power generated from VBEH, the values of ζ_m and ζ_e should be equal and ii) the values of ζ_m should be as less as possible, and for maximum average power harvested from a VBEH, the electrical load resistance should be nearly equal to the internal resistance of the copper coil of the vibration transducer. As such, it is important and necessary to determine ζ_m and ζ_e experimentally for the VBEH performance analysis. Hence in the next phase of research, the effect of variation of resistive, inductive, and capacitive load impedances on the maximum average power harvested from VBEH is investigated. In this case, the electrical load circuit parameters viz. resistance (R), inductance (L), and capacitance (C) are so chosen that the natural frequency ω_e ($\omega_e = \frac{1}{\sqrt{LC}}$) of the electrical R-L-C load circuit is made equal to the natural frequency ω_n ($\omega_n = \sqrt{\frac{K}{m}}$) of the mechanical sub-system of VBEH, which in turn, is tuned to the resonant frequencyof the harmonic excitation. The electrical circuit load resistance controls the electrical damping ratio ζ_e. As such, the effect of combined R-L-C load impedance on the maximum average harvested power is studied using the experimental setup developed for the same. From the experimental results, it is seen that the average harvested power is maximum at the resonant frequency, which is also equal to the natural frequency of the R-L-C load circuit. The maximum values occur when the resistive load is equal to the internal resistance of the transducer coil. This result is significant from the point of view of SDOF VBEH design for the given application. Also, it is observed that the value of electrical damping ratio ζ_e obtained experimentally is less than that obtained from its analytical expression. As such, it is important to determine electrical damping ratio ζ_e experimentally for estimation of power harvested from a VBEH when combined resistive, inductive, and capacitive loads are connected to VBEH, especially when the value of electrical damping ratio ζ_e is very small compared to mechanical damping ratio ζ_m. These findings are useful for deciding allowable electrical R-L-C load to obtain maximum harvested power from VBEH.

The power output of an SDOF VBEH is at maximum at or near resonance and over a small frequency band. In order to enhance the power output of traditional SDOF VBEH and to widen its operational frequency band, in the next phase of research, the SDOF VBEH design has been transformed into a Two Degree Freedom Vibration Based Electromagnetic Energy Harvester (2DOF VBEH) to amplify the vibration received by harvester mass by inserting a dynamic magnifier mass in between the base and the harvester mass-spring-system. It is shown that this change in design also helps to widen the effective operational frequency range of SDOF VBEH. For this purpose, an expression for the power generated by 2DOF VBEH has been derived using the approach of Tang and Zuo [28]. The effect of mass ratio μ harvester mass to amplifier mass and frequency tuning ratio f on the effective operational frequency bandwidth b_e of the developed 2DOF VBEH has been investigated using the expression derived for the effective operational frequency band. Using the experimental test setup developed for 2DOF VBEH, the effect of change in mass ratio μ on the harvested power of the 2DOF VBEH is analyzed.

The findings of this investigation will be useful to provide the guidelines for selecting an appropriate value of mass ratio μ and tuning ratio f for the design of a 2DOF VBEH to enhance the power output and widen the effective operational frequency band of a traditional SDOF VBEH.

In the final stage of the research, the analysis of the optimization of a power output of a 2DOF VBEH is carried out using the method of surface plots and associated contour diagrams. It is shown that these diagrams will be useful for obtaining the value of the optimal power output from 2DOF VBEH and its effective operational frequency band under a given set of values of mass ratio μ, tuning ratio f, and electrical damping ratio ζ_e at various excitation frequencies.

In the last place, a discussion on the results of research work carried out is taken up, and conclusions are presented.

Dedication

I dedicate this thesis to my Beloved Parents **Late Balkrishna Pandurang Patil** and **Late Sunanda Balkrishna Patil** without their blessings I would not have completed my research work. I see their presence in every page of this thesis.

ACKNOWLEDGEMENTS

First and foremost, I offer my sincere gratitude to research supervisor, **Prof. Dr. M. I. Sakri** and co- supervisor **Dr. P.V. Malaji** who have supported me throughout this research work and thesis writing with their knowledge whilst allowing me the room to work in my own way. I would like to gratefully acknowledge their enthusiastic supervision and I am honestly thankful towards them for constantly encouraging me throughout this research work.

My sincere thanks to Principal, **Prof. Dr. V. G. Sangam,** Vice Principal Administration **Dr.(Smt.) G.V. Patil,** Vice Principal Academic **Dr. P. V. Malaji,** and Research Coordinator **Prof. Dr. R. S. Malladi,** and head of Mechanical Engineering Department **Dr. R.N. Jeeragal,** BLDEA's Dr. P. G. Halakatti College of Engineering and Technology, Vijayapur for providing all the necessary facilities.

I am very much thankful to the Research Doctoral Committee members **Prof. Dr. S. G. Joshi,** Formerly Head, Department of Mechanical Engineering, Walchand college of engineering, Sangli, and **Dr. G. S. Shivshankar,** Professor, Department of Mechanical Engineering, Siddhaganga Institute of Technology, Tumkar for regular review of my progress and critical comments and valuable suggestions which helped me to find my role as a researcher during these years. I would like to express my thanks to the faculty of Mechanical Engineering Department, BLDEA Vijayapur for their critical assessment and useful suggestions during the progress presentations.

My keen appreciation goes to Hon. **Rajendra R. Dange,** Secretary, **Sant Dnyaneshwar Shikshan Sanstha, Islampur** for his help and encouragement. I am express my sincere gratitude to **Prof. R. A. Kanai,** Executive Director, Sant Dnyaneshwar Shikshan Sanstha, Islampur, **Dr. Vikram. S. Patil,** Director, **Prof. S. B. Hivrekar** Registrar, **Dr. S. V. Taralkar,** Dean Academics, **Dr. S. P. Chavan,** Dean consultancy, **Prof. M.M. Jadhav,** Head, Department of Mechanical Engineering and faculty members of Mechanical Engineering Department, Annasaheb Dange College of Engineering and Technology, Ashta for their support. I am also thankful to **Dr. R.G. Todkar, Mr. Anup Joshi and Mr. Elahi Sande** for helping me a lot in my research work.

I am grateful to all the collogue friends for their continued moral support, especially, **Prof. S.P. Patil, and Prof A.A. Jadhav,** ADCET Ashta and **Dr. S. S. Ahankari,** Vellore Institute of Technology, **Prof. M.S. Deshmukh** BVCOE, Palus for accompanying and helping me on many occasions during this work.

Finally, I am forever indebted to my mother ***Sunanda,*** father ***Balkrishan,*** sister **Lata,** Brother **Sanjeev,** Manager, Emerson Technologies Ltd., sister in law **Swati,** niece **Dr. Mrunalini** and nephew **Rajwardhan** and parents for their support, without their valuable support, motivation, and encouragement I would have never seen these days.

My special appreciation goes to **Vaishnavi,** my wife, daughter ***Girija,*** and son ***Aryan*** for their understanding, endless patience and helping me to concentrate on completing this thesis when it was most required.

Vijay Balkrishna Patil

TABLE OF CONTENTS

LIST OF FIGURES

LIST OF TABLES

NOMENCLATURE

N	:	Speed rpm
$y(t)$	:	Base Excitation
m_1	:	Mass of the magnifier system, Kg
K_1	:	Stiffness of spring of magnifier system, N/m
$x_1(t)$	:	Amplitude of response of magnifier mass, m
z	:	Relative displacement of mass w.r.t. base
Z	:	Relative amplitude (X-Y), m
$\dot{z}$	:	Relative velocity of mass w.r.t. base
$\ddot{z}$	:	Relative acceleration of mass w.r.t. base
Ω	:	Circular excitation frequency, rad/sec
ω_n	:	Circular natural frequency, rad/sec
ω_1	:	Natural frequency of magnifier system, rad/sec
ω_2	:	Natural frequency of harvester system, rad/sec
c_m	:	Mechanical damping coefficient
c_e	:	Electrical damping coefficient
C	:	Damping coefficient $c= c_m + c_e$
ζ_m	:	Mechanical Damping ratio.
ζ_e	:	Electrical damping ratio.
ζ	:	Damping ratio $= \varsigma_m + \varsigma_e$
ζ_{ev}	:	Electrical damping ratio from voltage.
ζ_{ez}	:	Electrical damping ratio from displacement.
$\frac{\omega}{\omega_n}$	:	Frequency ratio
m	:	Mass, Kg
k	:	Spring rate, N/m
z	:	Relative amplitude (X-Y), m
Z_1	:	load Impedance, Ω
Z_2	:	Impedance load, Ω
E	:	Open circuit Voltage, V
V_R	:	Voltage across the load resistance, V
P_{ave}	:	Average generated Power, mW

P_{aveh}	:	Average harvested Power, mW
$\overline{P_{aven}}$	:	Non-dimensional Average harvested Power, mW
$\overline{\omega_e}$	:	Circular natural frequency of the electrical circuit, rad/sec
B	:	Magnetic flux density, T
Br	:	Residual magnetic flux density, T
h_{mag}	:	Height of magnet, m
R_{mag}	:	Radius of the magnet m
X	:	Distance from magnet pole face, m
R_L	:	Resistive load Ω
R_c	:	Resistance of coil Ω
L	:	Inductive load H
C	:	Capacitive load F
m_2	:	Mass of the harvester system, Kg
K_2	:	Stiffness of spring of harvester system, N/m
X_2 (t)	:	Amplitude of response of harvester mass, m
μ	:	Mass ratio = $\frac{m_2}{m_1}$
f	:	Tuning ratio = $\frac{\omega_2}{\omega_1}$
α	:	Frequency ratio = $\frac{\omega}{\omega_n}$
$\overline{\omega_{n_1}}$	:	Non-dimensionless undamped first mode circular natural frequency
$\overline{\omega_{n_2}}$	:	Non-dimensionless undamped second mode circular natural frequency
$\overline{b_e}$	:	Effective operational non-dimensional bandwidth=($\overline{\omega_{n_2}} - \overline{\omega_{n_1}}$)

Chapter – 1

INTRODUCTION

1.0 Energy Harvesting

Energy harvesting is a process in which the energy from an external source or surrounding ambient environment is extracted and transformed into electrical energy. It is sometimes also referred to as power scavenging or energy scavenging. There has been increasing use of (i) smart sensors in the plant industry, industrial automation, machine monitoring, etc., and (ii) the use of wireless sensor networks (WSNs). These miniaturized low-power electronic devices are powered, at present, by batteries and other energy devices such as micro fuel cells, solar cells, etc., which require replacement or recharging, involving serious and costly maintenance problems. As such, in the last few decades, science and engineering research workers have focused their research on the development of devices which can convert the non-electric ambient energy available around the operational environment into electricity. These devices are known as energy harvesters. The research effort, at present, is to develop a variety of energy harvesters which can use external sources of energy such as solar, heat, tide, wind, RF, and vibrations to obtain electrical energy from them. Solar, heat, wind and tidal energies are available on a large scale. The solar energy harvesters use the principle of the photoelectric effect to convert light into electric energy, whereas the thermoelectric effect is used to transform heat into electric voltage in thermoelectric energy harvesters. In the radio frequency (RF) energy harvesters, the floating gate transistor effect is employed to transform RF energy into electrical energy. In capacitive RF energy harvesters, the electrostatic effect is used.

1.1 Vibration-Based Energy Harvesters (VBEHs)

The small-scale ambient energy source is the kinetic energy of vibration. The low-frequency vibrations of industrial machinery, civil structures, car engine, the instrument panel of the car, HVAC vents in office buildings, blenders casing, Clothes dryers etc., exist in small amounts as unwanted or wasted energy. This energy can be captured and transformed into electrical energy by vibration-based or vibration-driven energy harvesters (VBEHs). This electrical power can be used directly to run small electronic devices or suitably stored in batteries where necessary. In a vibration-based energy

harvester, the mechanism of conversion of vibration energy into electricity can be either of electrostatic, piezoelectric, electromagnetic or magnetostrictive. These harvesters are also referred to as vibration-driven energy harvesters for vibration-powered energy harvesters.

1.2 Types of Vibration-Based Energy Harvesters

1.2.1 Electrostatic Energy Harvesters

The electrostatic energy harvester (ESEH) use a variable capacitor (varacters) in which the plates of initially charged capacitors fluctuate due to vibrations received by them, and the kinetic energy of vibrations is converted into electrical energy due to work done against electrostatic force between plates of capacitor used is shown in figure 1.1

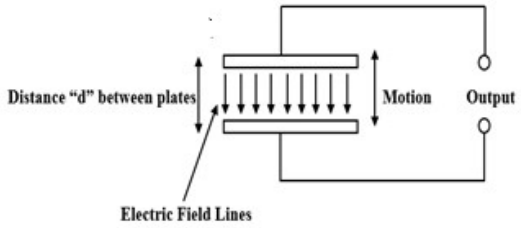

Figure 1.1 Electrostatic Vibration Energy Harvester

In an ESEH, the power output can be increased by (i) connecting an additional capacitor and (ii) by using two-layered structures of materials with high and low permittivity. The advantages of an ESEH are (i) the ability to integrate with microelectronics (ii) smart material is not required. However, ESEHs need an additional voltage source for the initial charging of the capacitor. ESEH is especially useful for powering micro-fabricated devices.

1.2.2 Piezoelectric Energy Harvesters

It is well known that when a pressure, vibration, or force is applied to the smart piezoelectric material, the mechanical energy is transformed into an electrical charge.

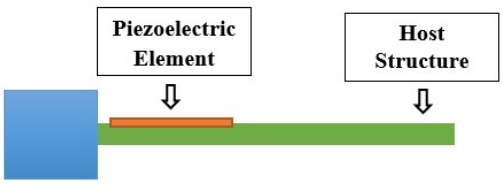

Figure 1.2 Piezoelectric Vibration Energy Harvester

The simplest piezoelectric energy harvester (PEH) shown in figure 1.2 consists of an unimorph piezoelectric cantilever steel beam with a tip or proof mass. In the recent design of PEH, a batch of PZT-5H material is attached over a composite cantilever beam. The position of the patch has an influence on the natural frequency of the beam structure, and maximum voltage is generated for unidirectional composite beam-type PEH. Some innovative designs of PEH to increase its voltage/ power output and broaden the operating frequency range. This design includes a 2DOF VEH, VEH with dynamic magnifier, fix-free multimorph cantilever with or without proof mass, etc. Some materials considered for pH design are polycrystalline ceramic and lead zirconate titanate (PZT). PZT converts mechanical energy into electrical energy at high efficiency. VEHs are compatible with MEMS and can also be used in applications where force and impact are coupled. However, their properties vary with age, stress, and heat.

1.2.3 Vibration-Based Electromagnetic Energy Harvester

A few decades back, the vibration-driven electromagnetic energy harvester was proposed. The vibration-driven electromagnetic energy harvester (VBEH) transforms ambient mechanical vibration into electrical power. The VBEHs are used to power autonomous devices in sensor networks. These self-powered devices can function autonomously and continuously (i.e., maintenance-free). The VBEHs are also referred to in the literature as electromagnetic vibration transducers or power scavenging devices.

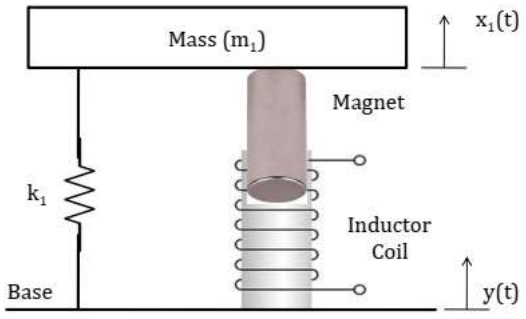

Figure 1.3 (a) Schematic Representation of a SDOF VBEH

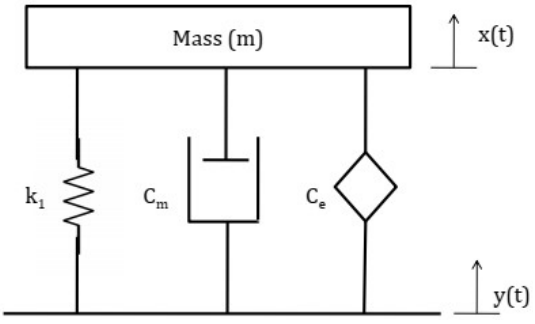

Figure 1. 3 (b) Mathematical Model of a SDOF VBEH

A schematic representation of a typical SDOF VBEH is shown in figure 1.3 (a). The mechanical subsystem of VBEH consists of a harvester mass 'm_1' and suspension spring 'k_1' connected across the mass and the base of VBEH. The base is subjected to harmonic

excitation from the vibration source. The electrical subsystem consists of a cylindrical magnet connected to the mass and the induction coil is connected to the base or vice versa. The coil magnet configuration is the in-line type which allows a relative displacement [$x_1(t)$ - $y(t)$] between magnet and coil. This relative motion [$x_1(t)$ - $y(t)$]generates an electromotive magnetic force (EMF) across the terminals of the induction coil, which drives the electrical load connected to VBEH. The magnitude of this EMF depends on the design of the induction coil and the selection of the magnet. The efficiency of transforming vibration energy into electricity is influenced by the following factors.

i. The type of Electromechanical (coil and magnet) coupling architecture used.
ii. Degree of tuning undamped natural frequency of the mechanical system (SDOF spring-mass system) to the base harmonic excitation frequency.
iii. Values of system or mechanical damping ratio and electrical damping ratio
iv. The nature of electrical load connected to induction coil of VBEH (pure resistive load and or inductive and capacitive load)
v. Coil design: material, number of turns, effective diameter, copper fill factor, etc.
vi. The type of permanent magnet in the coil coupling.

Magnet selection is based on residual flux density (Br), High value of Br is useful to produce high flux linkage to produce high EMF. The VBEHs are low-cost devices having ease in manufacturing, have design flexibility (for example, SDOF system to 2DOF system), and can be designed for cubic centimeter range transducers.

1.3 Research Problem and Objectives

In Chapter 2, an exhaustive literature review of research papers on earlier and present research in the area of vibration-based electromagnetic harvesters (VBEHs) has been presented and based on research gaps in this area, the scope of further research has been outlined. Based on this scope for further research and factor influencing the energy conversion efficiency of VBEH, as discussed in section 1.2.3, the research problem and its main objectives have been decided. These are as follows:

i. To design and develop a prototype of SDOF VBEH and carry out theoretical analysis and experimental analysis to decide the maximum average power that can

be generated from this VBEH and to study the influence of mechanical and electrical damping ratios on the maximum average power generated.

ii. To analyze the effect of electrical load impedances on the maximum average power output that can be obtained from VBEH.

iii. To design and develop a 2DOF VBEH prototype with a view (i) to enhance the maximum average power generated, (ii) to widen the range of operation excitation frequency, and (iii) to analyze the effect of changing the mass ratio on the power harvested.

iv. To obtain global optimal value of power output of 2 DOF vibration-based electromagnetic energy harvester, when the electrical damping ratio ζ_e and normalized excitation frequency α are varied simultaneously for a set of values of tuning ratio f for given mass ratio μ. To achieve this goal, the method of drawing surface plots and contour diagrams will be used.

1.4 Research Work Carried out

i. A comprehensive literature review on the previous and current research work has been carried out with a view to identifying research gaps to decide the scope of the present research work and its objectives.

ii. A prototype of an SDOF VBEH has been manufactured. An experimental laboratory setup has been constructed with the necessary instrumentation to (i) determine the maximum average power that can be generated at the resonant frequency and off the resonant frequency. (ii) to obtain experimental values of mechanical and electrical damping ratios, and (iii) to analyze the effect of these ratios on the power generated from the developed VBEH.

iii. Development of an electrical load circuit with resistive, inductive, and capacitive elements to be shunted to the developed VBEH and to analyze the influence of variations in electrical load impedance on the maximum power output at the resonance and off the resonance conditions.

iv. The design and development of the 2DOF prototype of VBEH with a view to analyze experimentally the enhancement in average power that can be obtained from this developed VBEH and to widen the useful operating range of the excitation frequency over which more harvested power can be obtained. To analyze the effect of changing the ratio of harvester mass to amplifying mass on

the enhancement of harvester power and widening of the useful operating range of excitation frequency.

v. Optimization of the power output of a VBEH using the method of surface plots and contour diagrams.

The details of the research work carried out and significant research findings have been reported in Chapters 2 to 6.

1.5 Organization of the thesis

i. In Chapter 2, the details of the literature review carried out on some selected research papers on the previous and present research on the vibration-based electromagnetic energy harvesters (VBEH) are presented. The research gaps in the earlier research work in this area have been identified, and the scope of further research is outlined.

ii. In chapter 3, the details of some studies on maximum average power output from VBEH using a coupling architecture in which a cylindrical magnet moves in a copper coil are given. An experimental test setup has been developed to study the effect of base excitation frequency and electrical and mechanical damping ratios on maximum average power output from the developed VBEH. The values of electrical and mechanical damping ratios are estimated by experimental analysis.

iii. In chapter 4, the details of experimental studies on the influence of various types of shunted electrical load impedances such as resistive, inductive, and capacitive on the average power output from VBEH are presented. For this purpose, an experimental setup with necessary instrumentation has been developed. The procedure of experimental determination of mechanical damping ratio using the transient open circuit response method and of electrical damping ratio by the loaded impulse response method is explained.

iv. In chapter 5, the method of enhancing the harvested power from an SDOF VBEH by transforming SDOF VBEH into a 2DOF VBEH by adding a magnifier system is explained. The equation for maximum harvesting power of 2 DOF VBEH is derived. Analytical solutions are obtained for the optimum value of the electrical damping ratio at which maximum power can be harvested.

v. In chapter 6, using the surface plots and contour diagrams, it is shown that the global optimal dimensionless power of 2 DOF VBEH depends on the values of

electrical damping ratio, mass ratio, tuning ratio, and normalized excitation frequency. It is also shown that to widen the useful operating frequency range of 2DOF VBEH, it is necessary to choose a proper combination of the mass ratio and the normalized excitation frequency.

vi. In the last chapter, a discussion on the results of the analysis is taken up, and conclusions are presented.

Chapter – 2

LITERATURE REVIEW

2.0 Introduction

When an engineer intends to carry out the research work in the area of his interest, he faces the problem of identifying the subject/ topic for his research work. He has also to formulate the research problem and decide its objectives. For this purpose, he has to search material related to his proposed research topic from the papers based on previous and present research in the area published in international conferences and journals. In this context, it is important to carry out a literature review. From the literature review, the researcher will have the knowledge of theories and practices in the subject of his research, the methods of mathematical modeling and solution procedures, techniques of experimental analysis and instrumentation used, software for simulation, etc., and the significant results from previous research in the topic of interest. From the knowledge of the above-mentioned aspects from the literature review, the researcher can decide the scope of his research work based on the research gaps and recommendations for further research by earlier researchers. Based on this information, the formulation of a research problem and its objectives can be worked out. Thus, the literature review is a prelude to further research.

Therefore, in this chapter, a review of some selected papers published in international journals related to energy harvesters, in general, and the vibration-driven electromagnetic energy harvesters, in particular, has been carried out under the following heads:

i. Electromagnetic energy harvesters: types, design and mathematical modeling techniques.
ii. Methods of theoretical and experimental analysis and simulation.
iii. Methods of the enhancement of the power of electromagnetic energy harvester and Optimization.
iv. Miscellaneous types of energy harvesters.

2.1 Electromagnetic energy harvesters: types, design and mathematical modeling

In the last few decades, engineers have been engaged in the development of a wide variety of vibration-driven electromagnetic energy harvesters by using the principle of electromagnetic induction to power small electronic devices. In this subsection, some recent developments in this area of research are reviewed.

Banerji et al.[1] [2016] have reviewed and discussed the energy harvesters suitable for the wireless sensors for supervising the health of structures. Solar, RF energy Piezoelectric and Electromagnetic harvesters have been studied by the authors. The energy captured from solar panels depends on the solar panel surface area. To improve the efficiency of these systems, new high-efficiency materials, such as black silicon, are being studied. Direct voltage generation is a benefit of piezoelectric harvesters, but they have limitations such as property volatility with age, charge leakage, temperature and stress. Electromagnetic is reliable with small output voltage. To integrate with MEMS, it is difficult. It is a promising area and it has been seen that a substantial amount of work has been carried out by using electromagnetic generators on bridges. The RF harvester can deliver electricity to far places while limiting signal loss. According to the author, the technology that can provide a reliable power supply is a challenge associated with powering wireless sensors.

Mahmud et al. [2] [2016] have discussed the current improvements in piezoelectric, electrostatic and, electromagnetic energy harvesting systems. Various harvesting techniques provide different energy densities, with piezoelectric generating the most, the electromagnetic and electrostatic follows it. These energy harvesters were driven mainly by ambient vibrations.

Electromagnetic energy harvesters: The electrical design of the coils may be adjusted to enhance power production. Nonlinear asymmetric designs also produced more power than linear symmetric designs and were easier to execute in microelectronic devices. In low-frequency vibration applications, such a transducer may produce up to 140 mW and can produce more than 2 W for applications where a high frequency is demanded.

The power output of an electrostatic energy harvester can be increased by adding another capacitor. It can also be achieved by using two-layered structures with materials of high and low permittivity. The power output of an electrostatic energy harvester can be up to

50 watts. In the energy harvesters based on piezoelectric effect, triangular piezoelectric shapes produce larger energy outputs. Furthermore, the change in dimensions of PZT unimorph and PVDF material and the piezoelectric multilayer may boost power. The output power of these can be as high as 12.5 mW.

These energy harvesters are suitable for low-power devices in medical applications like portable medical devices and cardiac implantations. These devices are usually small and low-powered, and they are used to monitor numerous critical factors or to administer a specific therapy. These developments point to a positive future for the expanded application of these technologies.

Sapolan et al. [3] [2016] have discussed the working of an electromechanical energy harvester. A spring-mass-damper represents the energy harvester. The energy dissipated in the damper is stored and to increase the harvester's dynamic range. The response of the energy harvester is obtained by simulation on nonlinear damping and by using the harmonic balancing method. The effect of the base excitation on frequency and amplitude on the response of the harvester system with a time-varying damper is analyzed. It is observed that the system will have instability at certain values of damping. This technique can enhance the power output and operational bandwidth of the energy harvester.

Gatti et al. [4] [2016]have proposed to use a linear single-degree-of-freedom vibration system to study the possibility of getting maximum energy from rail movement in the vertical direction when a train passes over it. To optimize the energy captured, the harvester is tuned to a natural frequency of 17 Hz and should have a mechanical damping ratio near to 0.0045. This results in a vertical relative displacement of rails maximum up to 5 mm. As the train passes through the system, such a device will create around 0.25 J/kg of oscillator mass. The harvester should also be set to the frequency at which the vertical acceleration is highest, which corresponds to one of the train-load frequencies. The transient element of the forced vibration was also found to be highly essential, and the damping should be selected so that the vibration of the mass of the energy harvester does not approach a steady-state throughout the system's operation. It is shown by numerical, analytical analysis that the optimum amount of energy harvested per unit mass is proportional to the product of the square of the input acceleration amplitude and the square of the input time.

Liu et al. [5] [2013] have developed a combined active and passive dynamic vibration absorption system. This absorber has a variable stiffness spring which is used to change

the natural frequency of the dynamic vibration absorber. The structural characteristics of this developed vibration absorber were determined using simulation techniques. The results of the experimental investigation show that this semi-active vibration absorber works well in the frequency adjustment range of 21 Hz to 25 Hz. A significant vibration reduction of 5 dB to 10 dB is possible.

Zuo and Cui [6] [2013] have reported a new method of simultaneous functions of energy harvesting and vibration control using a tuned mass damper (TMD). An electromagnetic harvester connected to a resonant RLC circuit replaces the element that dissipates energy between the tuned mass damper and the primary system. To minimize the vibrations and maximize the harvester output power, the tuning of the natural frequency of TMD with that of the electrical circuit is necessary.

Also, an electromagnetic resonant shunt in series with TMD has been. A case study of concerning the Taipei 101 skyscraper for energy harvesting, vibration control and parameter sensitivity analysis is presented. It is shown that the mechanical and electrical resonance approach for series TMDs for energy harvesting and vibration control is reliable.

Zoller and Dobra [7] [2009] have presented the analysis of electromechanical setup as vibration absorber for SDOF (single degree of freedom) subjected to force excitation at primary mass. The importance of electrical and mechanical system coupling is explained, along with coil design details. The discussions on a simulation program using HP VEE software for modeling and simulation of an electromechanical vibration absorber is done. An electromechanical transducer and a resonant electrical circuit is replaced by a mechanical vibration absorber system. By proper tuning of the electrical circuit, the vibration of the primary can be minimized.

N.G. Stephen [8] [2006] has explained how the maximum power transfer in mechanical, electromechanical and electrical systems can be obtained. For both the purely electrical and purely mechanical systems, the resistance matching leads to maximum power transmission with an efficiency of fifty percent.

It is recommended that in electromechanical systems having losses in both the electrical and mechanical domain, the concept of load matching be used inside the system to which power is harvested to achieve efficiency up to fifty percent.

N.G. Stephen [9] [2006] has presented a theoretical analysis of energy harvester in which either harvester mass force excitation or the base of excitation to extract energy from

ambient vibration. In both the mass and base excitation cases the energy flow is maximum when the frequency of excitation (ω) is equal to the undamped natural frequency (ω_n) of the mechanical subsystem and the net energy flow from the base to the damper is zero when $\omega = \omega_n$ and for the case when $\omega > \omega_n$ it is positive and for $\omega<\omega_n$ it is negative. The maximum power is transferred when electrical load R_L equals coil internal resistance R_C. When the excitation amplitude is variable, the design of the electromagnetic energy harvester should be based on low-frequency vibration excitation.

Fan et al. [10] [2018] have presented 2DOF cylindrical electromagnetic energy harvesters with linear or nonlinear configurations. Theoretical and experimental models for the four 2DOF cylindrical electromagnetic energy harvesters have been developed and their frequency responses are predicted. In comparison with SDOF, the 2DOF electromagnetic energy harvesters operate better under low-frequency excitations. The nonlinear 2DOF electromagnetic energy harvester power output can be improved by altering the spring stiffness and geometric arrangement.

Bakhtiar and Khan [11] [2019] have discussed the method of simulation of an electromagnetic energy harvester drawing energy from a pulsing fluid flow in a pipeline. By putting a bluff body into the flow route in the pipe, the authors have deliberately created a pulsing fluid flow in the pipe, causing the diaphragm to vibrate. An analytical model for voltage and power generation is developed using a single degree of freedom spring-mass-damper system the electromagnetic induction governed by Faraday's law.

Munaz and Chung [12] [2015] have presented a design of a rectangular-shaped multiple magnet vibration-based electromagnetic energy harvester have been designed. Finite element analysis (ANSYS FEA) was used to determine the magnetic field regions and related flux lines of the magnets encircling the coil, as well as magnitude-based vector plots. The developed harvester generated up to 224.72 W of power against a load resistance of 20 ohms with a 6 Hz operating frequency range. It may be used for portable power devices as well as distant sensor node applications. The harvester has a low resonance frequency of 6 Hz, making it suitable for human remote sensor node applications.

Chen and Wu [13] [2016] have presented two degrees of freedom electromagnetic energy harvester to increase the operating frequency bandwidth the harvester has been developed. By incorporating a spiral diaphragm into a U-shaped cantilever. Using finite element analysis, two diaphragms with a slight shift at frequencies lower than 300Hz

have been designed. To enhance the output bandwidth, thick copper coils have been electroplated on both structures using photo resists as electroplating molds. The harvester is tuned into a dual-mode operation by arranging the connection sequences between the U-shaped cantilever and coils on the spiral diaphragm. The harvester generates the power of 22.1 nW and 21.5 nW, at load resistance of 27 Ω, respectively, for the resonance frequencies of 211 and 274 Hz. This forms a duo-mode energy harvester. The comparison of this harvester has been carried out with cantilever-type generators.

Fu et al. [14] [2014] have presented the modeling, simulation, and development of a novel resonator made up of two detachable mass-spring systems. According to simulation data analysis, the velocity-amplifying resonator has a broader bandwidth than that of a normal SDOF resonator. Data fitting analysis with and without Coulomb damping is done for the developed 2-DOF detachable resonator. The model with Coulomb damping agrees well with the experimental results. The comparison of simulation and experimental results reveals that a good correlation under 0.5g acceleration level is achieved when compared to a SDOF conventional configuration. It is observed that the 2-DOF detachable resonator is more efficient than the conventional SDOF configuration.

Ooi and Gilbert [15] [2014] have investigated the dual-resonator technique for increasing the band of frequency of a vibration-based electromagnetic energy harvester. An analytical model of this electromagnetic harvester is analyzed using MATLAB Simulation. The cantilever resonance, stress, and magnetic field distribution are all estimated using the ANSYS finite element modeling (FEM) tool. The prototype is developed on the basis of ANSYS FEM and MATLAB simulation results. When compared to a conventional single resonator generator, a maximum improvement of 58.22 % in output is obtained from a low-frequency vibration source of 0.8 m/s^2. The output is compared to simulation results and experimental results. The authors also suggested that future work should be done to reduce the damping factor of the resonators and the beam of coils.

Naifar et al. [16] [2015] The most difficult aspect of designing vibration energy harvesters is maximizing the energy output in relation to the applied excitation. The electromagnetic and magneto-electric principles are described and categorized according to design considerations. A comparison of electromagnetic and magneto-electric converters is presented in terms of energy produced by these harvesters. It depends on the

nature of vibration excitation. It is found that magneto-electric generators are useful for extremely small devices than electromagnetic one.

Jee Siang [17] [2017] has reviewed different types of vibration energy harvester viz. electromagnetic, piezoelectric, electrostatic, magnetostrictive, flexoelectric or electrostrictive polymers and hybrid harvesters. A comparative study of these principles has been carried out. In order to become a mainstream energy solution, the researchers must focus on specialized applications while still being adaptable enough to support a variety of devices. Vibration energy harvesting will be able to overcome the problem of battery storage once it becomes a commercial product and cost-effective.

Mohanty et al. [18] [2019] present common principles and their operation mechanisms of electromagnetic, electrostatic, piezoelectric and magnetostrictive harvesters. Some key characteristics and composition of magnetic materials is tabulated. Raindrops, sound waves, flow-induced vibration, vortex-induced vibration, and other sources of energy should be harvested in the future with the objective to build more efficient storage circuits and to discover novel materials for improved voltage and power output.

Bang and Park [19] [2013] this paper describe an electromagnetic energy harvester with a bulb micro machined Silicon spiral spring. The basic theory of vibration energy harvester, design of energy harvester and device fabrication are explained. The design is supported with experimental results show successful harvesting of ultra-low level ambient vibrations through an electromagnetic energy harvester. The spiral springs of micro-fabricated silicone are suitable for harvesters using a low-frequency vibration environment. The fabricated device shows excellent power densities at low amplitude vibration.

Zang and Kim [20] [2014] provide a comparative summary of electromagnetic vibration energy harvester for excitation frequency versus power generation. The fabrication of a magnet coil array for vibration energy harvesting is discussed. A miniature model is developed and tested for energy conversion efficiency. This gadget demonstrates the potential of the novel electromagnetic energy conversion concept in both harvesting vibration energy and producing electricity. To harvest electrical power from various vibrating surroundings, the resonance frequency may be altered by design modifications of the mass-spring system of the harvester. A straightforward approach to boost the power is to scale up the number of coils and magnets.

Salar Chamanian et al. [21] [2014] have presented an application of an electromagnetic energy harvester for powering wireless sensor nodes. Experimental analysis shows that a custom-designed electromagnetic energy harvester for low-frequency vibrations may supply enough current to charge the heterogeneous network node's batteries and extend its lifetime by more than ten times.

Zang and Corr [22] [2018] have investigated the effect of resistive and non-resistive load on the performance of electromagnetic vibration energy harvester. The case study with rectifier having resistive, capacitive and parallel combination of resistor and capacitor is presented with mathematical analysis and MATLAB modeling. The performance of devices obtained with pure resistive load cannot be generalized for the electronic component, which may be capacitive, inductive, or switching devices. A rectifier at the output stage of the harvester is responsible for voltage drop. The introduction of the capacitor on the load side shows that the efficiency of the harvester is ensured for the higher bandwidth as compared to a resistive load.

William and Yates [23] [1996] have proposed and an electromagnetic energy harvester comprising of a spring-mass system and magnet coil system where the magnet and coil have a relative motion. Micro energy harvester developed working on this principle has a volume of $25mm^3$. It is shown that the power generated depends on the cube of vibration frequency and the mass displacement should be as large as feasible to maximize the power output. The anticipated power output for a typical device is of the order of $1\mu W$ at a vibration excitation frequency of 70 Hz and of the order of 0.1mW at a harmonic vibration excitation frequency of 330 Hz. Hence the device is not well suited low-frequency vibration source. The design rules for optimizing the power output of an electromagnetic harvester have been presented.

2.2 Methods of Theoretical and experimental analysis and simulation

Malaji and Ali [24] [2016] have described a pendulum array as a broadband energy harvester, in which the parameters of the harvester influence the frequency bandwidth and the magnitude of power. The pendulums of the harvester are with tip magnets. The number of pendulums investigated experimentally is confined to a maximum of five, whereas simulations are carried out for a maximum of twenty pendulums. The maximum power harvested is dominated by the first pendulum with strong grounding, while the remaining pendulums contribute to increasing the bandwidth of the harvesting frequency.

It has been shown that increasing the number of pendulums did not result in a significant improvement in either power or in the bandwidth.

Halim and Park et al. [25] [2015] have developed, analyzed, and implemented an appropriate and reliable electromagnetic energy harvester that can scavenge considerable power from human-limb motion such as hand-shaking and power portable and wearable smart gadgets. A freely moving (non-magnetic) ball within a cylindrical structure is periodically excited, causing two magnets mounted on two helical compression springs at either end of the cylinder to vibrate at higher frequencies. Electromotive force is produced by the relative motion of the magnets and coils (voltage).To reduce power loss, high-frequency oscillators have been developed using the design characteristics such as frequency, spring stiffness, mechanical, and electrical damping. Both vibration exciter and manual hand-shaking were used to test a fabricated prototype. During the vibration exciter test, the prototype displayed non-resonant behavior. A hand-shaking vibration frequency of 5.17 Hz and acceleration of 20.2 m/s^2 generated an average output of 2.15 mW. The device has a power density of $0.33mWcm^3$, which is significantly greater than current technologies in the field of frequency up-conversion energy harvesting (Frequency < 20 Hz).

Daqaq et al. [26] [2014] have studied the effect of nonlinearities in energy harvesting based on ambient vibrations. The absence of appropriate scalable energy sources required to operate and sustain low-power devices such as medical implants, wireless sensing, data transmission, etc., is an obstacle to their implementation. It has been noted that batteries which are still reliable power sources, could not match with the requirements of these gadgets, particularly in terms of energy density. According to the authors, tuning a linear vibration-based energy harvester to the excitation frequency is practically difficult and it may result in inefficient transduction characteristics outside the laboratory environment. The design of arrays of harvesters, each with a distinct fundamental frequency, has been proposed to allow at least one of the harvesting components to have a matching fundamental frequency such that it harvests energy at least from the corresponding excitation frequency.

Aboulfotoha et al. [27] [2011] have developed a vibratory electromagnetic energy harvester with the facility of the adjustable natural frequency that automatically changes the harvester's natural frequency to get tuned with base excitation frequency. The harvester comprises of a cantilever beam with a magnet as a tip mass that is positioned in

close proximity to another magnet with an opposite polarity that can move axially, allowing mechanical straining to modify the beam's natural frequency. To monitor the output signal from a base-mounted electromagnetic sensor, a microcontroller is used to determine the periodic time of base vibration. The resonant frequency was adjusted from 4.7 Hz to 9 Hz by changing the spacing between two toning magnets from 66 mm to 16.7 mm and producing the voltage per acceleration from 6.3 V/m/s^2 to 1.1 V/m/s^2

Tang and Zuo [28] [2011] have analyzed an energy transducer that is attached between two masses of the transducer subjected to harmonic force and motion excitations. For both dual-mass and single-mass systems, analytical solutions of maximum power harvested were derived, demonstrating that dual-energy harvesters are more efficient than single-degree freedom harvester. The sensitivity of the local and global maximum powers to system factors was examined using simulation. The optimal electrical damping is larger than the mechanical damping for a fixed excitation frequency of force or base motion, except when the excitation occurs at the harvester system's natural frequency.

It has been shown that there are two local maxima and a global maximum for energy harvesting rate. When the excitation is at the natural frequency and the electrical damping is the same as the mechanical damping, the local optimums are reached. When the electrical damping ratio is very high, much more harvesting power may be obtained in the excitation frequency region between the first and second mode natural frequencies.

Niell et al. [29] [2011] have obtained for a single degree of freedom harvester the ideal electric resistive load for maximum power output at both the resonance and off-resonance excitation. The impact of the parasitic effect of the generator coil resistance has been examined. The results demonstrate that at a resonance frequency of 112.25Hz, normalized power densities of 1.7 mW/[(m/s^2)^{2}cm^3] are operating. The analytical findings for an electromagnetic generator have been compared with the experimental data using the derived models, and it is seen that these results are in good agreement. It is shown that the electromagnetic generators can still be useful because they are less expensive than equivalent ceramic-based piezoelectric generators, and their relatively low damping coefficients may lead to significantly higher overall power conversion even when parasitic coil resistance is high.

William et al. [30] [2001] have described the design process for a linear micro-generator as a single degree of freedom system. The process of creating a prototype using commonly accessible micro-fabrication methods is also explained. The prototype has an

upper mass-spring mounted on a substrate connected to a lower pick-up coil and substrate. The inertial mass is a vertically polarized samarium-cobalt permanent magnet (B, = 0.9 T) coupled to a polyimide membrane. Over a frequency range of 0.1- l0 kHz, source vibration amplitudes in the range of 1 nm to 500 nm were produced. At a 4 MHz excitation frequency, the fabricated prototype can generate 0.3 μW. It is shown that the power generated by these devices depends on the cube of the vibration frequency.

Zhang et al. [31] [2020] investigated the performance of the electromagnetic device connected to ohmic resistors, rectifiers, and capacitors. It is shown that the performance of an electromagnetic harvester with a pure resistive load could not be extended beyond a certain limit performance of the electromagnetic harvester is improved by using a big storing capacitor having a low rectifier voltage drop.

Lei and Wen [32] [2014] have tested the output the performance of a vibration-based energy harvester by two different structures developed for the same. They investigated the damping effect on the vibration energy harvester's resonant frequency, output voltage, power, and efficiency. The amplitude of the output voltage increases with the increase in electrical damping, and the value of output voltage is maximum when the electrical damping matches the mechanical damping. The mechanical dampening lowers the micro-vibration energy harvester's output voltage and efficiency.

Yulong Zhang et al. [33] [2020] have developed a rotating electromagnetic energy harvester which consists of a twist drive structure and a ratchet clutch mechanism that collects the mechanical energy of human motion at a low frequency. The structure is fitted to the shoes. From the experimental results, it is seen that the harvester is able to convert mechanical energy at a low frequency (1 Hz) into electrical energy giving a maximum electrical power of 32.2 mW.

2.3 Methods of Enhancement of Power of Electromagnetic Energy Harvesters and Optimization

Lee and Chung [34] [2015] have proposed a method of tuning in which the change in the position of the spring can adjust the harvester's resonant frequency. The spring constant can be modified by changing the relationship to the spring length deformation. The output power of the proposed energy harvester has been calculated at resonance frequencies ranging from 15 to 50 Hz. Using the ANSYS finite element approach, the impacts of magnetic pole orientation, input frequency, acceleration, and load resistance on the output

are measured. It is seen that the developed energy harvester had a maximum power output of 60.3 μW and 0.5 g acceleration. The developed harvester produced a maximum open-circuit voltage of 1.78 V at 700 RPM when it was connected to a car engine.

Dong et al. [35] [2016] have developed a vibration-based energy harvesting device which is tunable in two dimensions and which uses magnetic forces in two dimensions. A cantilever beam with the tuning magnet is free to move in 2D space with respect to the fixed magnet was used to harvest energy. The magnetic tuning forces and axial force are calculated using MATLAB, and the magnetostatics 3D model from COMSOL was used to simulate the results. Finally, an experimental case study has been discussed to validate the 2D tuning model results.

Rahim et al. [36] [2018] have developed a vibration-driven electromagnetic energy harvester with a view to enhancing the output performance of a conventional energy harvester by using the technique of multi-resonance frequencies to widen its low excitation frequency range. The developed harvester has been tested using a vibration exciter and demonstrated its multi-resonant behavior at 4.26 and 8.34 Hz. The harvester produced an RMS voltage of 108 mV. The maximum average power produced across a load resistance of 150 Ω was 78 μW.

Li et al. [37] [2018] have carried out theoretical, experimental, and simulation analysis of vibration-driven energy harvester comprising of both the piezoelectric and electromagnetic types. The effect of strength of coupling between piezoelectric and electromagnetic elements has been studied using simulation and experimental tests. Using ANSYS software, the output voltage of PZT is obtained. Using ANSYS Maxwell software, the value of current through the coil is determined. It has been pointed out that with the increase in the coupling strength at the optimal load resistance, the output power increases and such an energy harvester can enhance power output and efficiency of harvesting when compared to individual piezoelectric and electromagnetic energy harvesters. Finally, the energy storage circuit has been designed and developed to charge the hybrid harvester's batteries.

Ooi et al. [38] [2015] demonstrated how to enhance the operational bandwidth of vibration-driven harvesters based on electromagnetic induction by varying the electrical damping coefficient and by load resistance adjustment within the cycle of oscillation. The fundamental models of a fixed damping system (linear type) and switching damping

system were developed. It is seen that switching the damping can decrease or increase the duration of the oscillation cycle, and resonance frequency can be altered.

Yildirim et al. [39] [2017] have discussed the fundamentals of vibration energy harvesting methods. Various techniques have been presented to widen the operating frequency band and enhance the output power of these harvesters. These techniques include resonance tuning, the inclusion of nonlinearities, etc., the use of multimodal arrays and stiffness tuning, etc. Nonlinear harvester oscillators have the ability to enhance both power and operating frequency range. For real-world operating situations, a bi-stable system is beneficial.

Smilek and Hadas [40] [2017] have shown that the performance enhancement of electromagnetic energy harvester is possible by maximizing electromechanical coupling by optimization of magnetic circuit design, placement of coil and its shape and size. The equal optimization algorithm for optimizing call shape best on greedy search algorithm has been explained. It ensures the cylindrical shape of the coil with uniform distribution of wire laterally and longitudinally. With this optimization, maximum power delivery to the load is ensured for given working conditions.

Wheeler [41] [1928] has shown that the inductor design of energy harvesting with electromagnetic principle becomes key to optimizing output electrical power. To optimize the output electrical power, the formulae for calculating the diameter, longitudinal and latitudinal number of turns and length of the coil have been used.

Tai and Zuo [42] [2017] have studied the condition for optimization for maximum power output from vibration-driven electromagnetic and piezoelectric energy harvester devices. These conditions have been driven by using resistive load, electrical damping ratio, and the normalized excitation frequency. This optimization condition is valid only for constant acceleration amplitude of base vibration excitation and when it is assumed that the mechanical damping is small i.e., less than 2%. The maximum power is achieved at resonance and when the mechanical damping ratio is equal to the electrical damping ratio. When the mechanical damping ratio is greater than the critical value, the optimization condition is no longer valid. The optimal excitation frequency is dependent on the mechanical damping ratio only.

Malaji et al. [43] [2015] have proposed a single degree of freedom system comprising of a pendulum absorber and an electromagnetic energy harvester mechanism to mitigate vibration of the primary structure and simultaneously extract energy from the pendulum

absorber. Using a Genetic Algorithm, the problem was solved. The frequency ratio and pendulum damping are the parameters to be optimized. The objective function of optimization includes both the reduction of vibration and harvested energy maximization. A double peak is shown on the power curve of the pendulum harvester, suggesting that broadband energy harvesting is possible under the condition that maximum electrical damping is equal to the pendulum damping. The topics of influence of pendulum nonlinearity on optimal performance as well as experimental validation of the developed model are the areas in which further research can be carried out.

Ali and Adhikari [44] [2013] have proposed a design of a dynamic vibration absorber to minimize the vibration of the primary system and simultaneously harvest the energy from the absorber mass vibration. The optimal non-dimensional frequency ratio of the decoupled system is obtained using a frequency domain approach and a closed-form formula is derived. For a coupled electromechanical system, analysis of the damping of energy harvesting dynamic vibration harvester, non-dimensional coupling coefficient and non-dimensional time constant has been carried out. For small values of the electrical parameters, it is shown that the fixed-point theory is approximately applicable.

Arroyoa and Badel [45] [2011] have explored the Synchronous Electric Charge Extraction (SECE), an energy harvesting nonlinear approach for piezoelectric generators and applied it to electromagnetic generators. This is termed as Synchronous Magnetic Flux Extraction (SMFE) for this new circuit, which is a dual of the SECE circuit. Its theoretical performance is compared to that of the conventional extraction approach, and tests on an electromagnetic generator are carried out to verify the SMFE technique's operating principle. It is also demonstrated that the electromagnetic harvester's dependency on the load is decreased, and useable DC voltages are produced directly, allowing generator design optimization to be focused only on power maximization.

Kim et al. [46] [2018] have proposed an approach for optimizing voltage and power from three different types of vibration-driven electromagnetic vibration energy harvesters having the same volume. If the magnets, coils, and air gap mesh sizes are 0.5, 0.2, and 0.5 mm, respectively, the finite element analysis may be used to compute magnetic flux density in the radial direction. The output power and voltage are calculated using MATLAB software; when the aspect ratio is between 0.4 and 0.8, the maximization of the output power of vibration-driven electromagnetic energy harvesters is carried out for the same volume.

Cepnik and Wallrabe [47] have discussed the power output of a linear electromagnetic micro-energy harvester, the limitations are limited flux conduction, low volume utilization, and low aspect ratios. The output power may be increased by more than 250 percent by properly designing the magnetic circuit with back iron, an adequate coil aspect ratio, small air gaps, and high volume utilization.

Caruso [48] [2015] has discussed a base excited electromagnetic energy harvester coupled to a resonant electric circuit. Theoretical formulae for the optimal circuit parameters to obtain maximum harvested power are given. The harvester circuit parameters have been optimized by using an alternative objective function. It is shown that under resonant excitation conditions, a constant level of the harvester power can be achieved.

Cohen [49] [2010] has discussed the harvesting of natural vibrations to power up medical and surgical devices. A method for limiting the size of the harvester is described. The optimized harvester comprises a two-degree freedom system operating at a lower frequency, which enables the optimization of an electromagnetic circuit.

Rahim [50] [2018] has discussed the challenges related to bandwidth and linearity of a vibration-driven energy harvester. To widen the bandwidth of this harvester, a dual-mass system resembling a two-degree of freedom system is proposed, fabricated, and investigated here. It presents the architecture mechanism and operation of this system along with mechanical modeling and numerical modeling with MATLAB has been presented. The experimental results of the prototype show two peaks over the operating range of frequency.

Stephen [51] [2006] has discussed the aspects related to maximum power transfer between source and load for electrical, mechanical, and electromechanical systems. For electrical system maximum power transfer is achieved when source impedance and load impedance are equal. For an electromechanical system, maximum power transfer depends on coupling between electrical and mechanical systems. The maximum power transfer in such a case can be achieved at the condition of resonance.

William et al. [52] [1996] present a method for electrical power generation from a vibration-based electromagnetic transducer. The procedure of design, fabrication, and testing of the prototype is explained. To maximizing the power output, the system is designed at resonating frequency. To ensure a good impedance match between the device and the electrical load, the electromagnetic coupling is optimized.

2.4. Miscellaneous types of energy harvesters.

Rajarathinam and Ali [53] [2018] have proposed a novel energy harvester integrating piezoelectric and electromagnetic transducers subjected to simple harmonic base excitation. In comparison to the small operational frequency range, the new energy harvester functions over a wide range of frequencies. A cantilever beam PZT harvester and a magnetic mass hanging through a spring at the free end and cantilever form this new harvester system. The piezoelectric mechanism harvests energy in the PZT beam, while electromagnetic energy oscillates in the copper coil via hanging mass oscillations. The results reveal that when the amplitude of the base excitation grows, the power increases monotonically. The highest power of a harvester was obtained at two frequencies: 2.1 Hz and 14.2 Hz.

Takeya et al. [54] [2016] have developed a Tuned Mass Generator (TMG) with dual-mass system. The performance analysis was carried out using an analogous electric circuit of a linear electromagnetic transducer, which extracts energy from the damper system. TMG was fine-tuned using a multi-domain parameter design approach developed by the authors.

Zhang and Kim [55] [2014] have developed a novel method for mechanical energy to electrical energy conversion, which can acquire mW to W power output from tens to hundreds of micrometers. An array of alternating north and south direction magnets is used to increase the magnetic flux change. The change in flux in this array of magnets is simulated and optimized using COMSOL software. It is compared the change of flux of single magnet. Micro-fabricated and very small electromagnetic energy harvesters with magnet and coil arrays are designed and developed on the basis of this novel concept. The conversion efficiency of this vibration energy harvester is exceptional. Experimental results show that when a micro-fabricated energy harvester is excited at 290 Hz and vibration amplitude is 1.1 micrometer, electromotive force of peak to peak voltage of 30mV is generated and power output of 2.6 μW.

Zuo et al. [56] [2013] have developed a high-efficiency and portable electromagnetic energy harvester. This harvester comprises of super capacitor which transforms the vibrations of train track into electrical energy, which is stored in super capacitor. It is utilized for safety amenities in remote places. It can also be used as a backup power supply for the equipment at the rail side. A rack and gears set amplifiers even the small vibrations of the rails. The rails' bidirectional motion is converted to unidirectional

rotation. The developed harvester's dynamic response was initially obtained by simulations. In bench testing, fifty-point five percent efficiency was recorded. The developed energy harvesting device can be used to capture renewable energy from railroad vibrations.

Harne [57] [2012] has derived the dimension-less governing equation of a mass-spring-damper system to which either a piezoelectric or electromagnetic vibration absorber is connected. For light weight oscillator masses, electromagnetic energy harvesting vibration absorbers (EHVAs) induce high damping. The order of the coupling coefficients of EHVA is generally the same, but for Piezoelectric coupling, terms diverge with high magnitude. The cyclic displacement stroke of the oscillating mass is enhanced to optimize the electrical output of electromagnetic energy harvesters, whereas, in piezoelectric energy harvesters, the electric output is enhanced by increasing the amount of spring deformation. The strength of connection limits electromagnetic energy harvesting efficiency and maximum power output. However, the coupling strength and specific design constraints determine the maximum power and efficiency feasible in piezoelectric harvesters.

Riduan and Foisal [58] [2012] have proposed two variants of an electromagnetic multi-frequency converter array for diverse ambient frequencies. They have tested the performance of these variants. To capture energy from low frequency vibrations, the magnetic spring is taken as a cantilever. The number of turns of the coil, coil width, coil location, and spacing between fixed magnets have been optimized in the single frequency harvester. From the experimental studies, it is seen that models A and B can work in the frequency range of 7 - 10 Hz. Model A and Model B have power densities of 21.92 $\mu W/cm^3$ and 52.02 $\mu W/cm^3$, respectively, when the acceleration of level is 0.5 g.

Mitcheson and Yeatman [59] [2004] have developed three different energy harvesting systems. These are (i) velocity damped resonance generators (VDRGs) (ii) unified analytical structure micro-generator architecture, and (iii) coulomb damped resonant generators (CDRG). In addition, a Coulomb-force parametric generator (CFPG) is also proposed. This generator can work at non-resonant conditions and higher damping. The power output of both CDRG and VDRG is same at resonance; however, the CDRG performs better in the neighborhood of resonance. When the allowable mass frame displacement is small compared to the amplitude of vibration excitation, both the resonant and generator types are not able to function.

Roundy et al. [60] [2003] have asserted that converting vibrations into electricity is the most appropriate method for harvesting ambient power. It is a viable source of power. Different methods of conversion are evaluated from the point of view of optimum design for capacitive MEMS as well as piezoelectric harvester converters. From Piezoelectric harvesters, a power density of 70 mW/cm3 can be achieved with PZT bimorph. In the optimized design of piezoelectric converters, a density of 250 mW/cm^3 from a source of vibration having an amplitude of acceleration of 2.5 m/s^2 at 120 Hz can be achieved. Low- level vibrations appear to have a fundamental mode near to 100 Hz, with a range of maximal acceleration magnitudes of 0.5 - 5 m/s^2.

Mullen and Lee [61] [2017] have studied a linear generator energy harvester based on human motion, in which the hip displacement during human steps serves as the basic excitation for an energy harvesting backpack. The calculation of magnetic flux density and coil inductance is carried out using the ANSYS software, and the power is calculated by plugging these numbers into a MATLAB/Simulink model. A comparison analysis was carried out with a previously published article, as well as an experimental voltage evaluation from a commercially available portable energy harvester, to ensure the Simulink model's accuracy.

Khan et al. [62] [2015] have investigated linear vibration-driven electromagnetic energy harvesters with a non-uniform magnetic field configuration under harmonic base excitations. Using Faraday’s and Lenz’s laws, the non-uniform magnetic flux density for a planner coil and a square magnet is obtained. As the size of the planar coil is small as compared to the size of the magnet, for larger gaps between magnet and coil these models overestimate the performance of the device. This also happens when the size of the coil is larger than the magnet. The results of these models' simulations agreed well with the experimental results. COMSOL Multi-physics 2D magneto-static analysis was performed using the simulations of these models that agreed well with the experimental results. When the gap between the magnet and the coil is 250mm, the simulation result showed an increase in load voltage by 20.5 percent and an increase in harvester power by 42.5 percent.

Davidson and Mo [63] [2014] have discussed recent advancements in systems of energy harvesting suitable for the health monitoring of structures. A detailed review of energy harvesting systems installed at various points is presented for linear and non-linear energy harvesters. It has been pointed out that the research on autonomous, self-powered systems

that harvest energy from the surrounding environment has a lot of scope, and it will continue to grow in tandem with new advancements in electronics.

Shirai [64] [2019] has discussed the design, simulation, experimentation, and results of a multi-degree of freedom system with ferromagnetic material and fluid. It is very difficult to harvest energy using an electromagnetic energy harvester from very low-frequency natural vibration sources such as the motion of creatures or due to ocean waves. To generate electricity from low-frequency vibrations (1 Hz or less), the simulation results were confirmed, using computational fluid dynamics, the working of the newly developed energy harvesting device. A summary of generator characteristics and suitability of search generators for various frequency ranges is given.

Ashraf et al. [66] have discussed an energy pumping frequency increased vibration energy harvester which uses a technique of wide band, resonant and impact based frequency up-conversion, which is particularly useful to harvest energy from low frequency ambient vibration source.

Tao et al. [67] have presented a novel two degree of freedom MEMS electromagnetic vibration energy harvester to address the fundamental issue of these energy harvesters that they give maximum power output in a narrow bandwidth around its resonance frequency of the ambient mechanical vibration sources, which have distributed/multiple frequencies.

Aldraihem and Baz [68] have shown that with proper selection of the design parameters of the dynamic magnifier, the power harvested from a piezoelectric energy harvester can be increased and the effective operational frequency band of the harvester can be broadened.

Zhou et al. [69] have proposed and investigated a new type of vibration based piezoelectric energy harvester with multiple mode dynamic magnifier with a view to enhance the power and extent the operational frequency band over virtually all natural frequencies of the harvesting beam.

2.5 Research Gaps

From this literature review, it is observed that there are some areas in which further research can be carried out. These research areas are as follows.

1. Detailed experimental analysis of the vibration-based electromagnetic energy harvester (VBEH) with special reference to the determination of reliable values of mechanical damping ratio ζ_m and electrical damping ratio ζ_e since these ratios control the power that can be generated from VBEH.
2. Effect of variation of ζ_m and ζ_e on the maximum average power generated from a VBEH at the resonance and off the resonance conditions.
3. To determine experimentally the effect of various types of electrical loads connected on the power harvested from a VBEH and maximization of this power by using the concept of impedance matching.
4. To design and develop a 2DOF system with a view to

    i. Enhance the harvested power of SDOF VBEH
    ii. Widen the operating frequency range
    iii. To study the effect of changing harvester mass to amplifying mass ratio on the harvester power.
5. To determine the global optimal values of power output 2DOF VBEH, when the electrical damping ratio ζ_e and normalized excitation frequency α are varied simultaneously for a set of values of tuning ratio f for given mass ratio μ.

Chapter – 3

SOME EXPERIMENTAL AND ANALYTICAL STUDIES ON MAXIMUM AVERAGE POWER OUTPUT FROM A VIBRATION-BASED ELECTROMAGNETIC ENERGY HARVESTER

3.0 Introduction

In this chapter, the results of a theoretical and experimental investigation on the maximum average power output from a vibration-based electromagnetic energy harvester (VBEH) at resonance and in the neighborhood of resonance are presented. An expression for the maximum average power output of a vibration-based electromagnetic energy harvester (VBEH) has been established. Using the developed experimental setup, the experimental values of electrical and mechanical damping ratios have been obtained.

3.1 Development of a Vibration-Based Electromagnetic Energy Harvester Device

The transformation of vibration energy into electricity takes place in a VBEH as per Faraday's law, $V = -N\frac{d\emptyset}{dt}$. In this equation, V is the electromotive force (EMF), Φ is the magnetic flux through a single loop, and N is the number of coil windings. In a VBEH, under the unidirectional low-frequency base excitation from the vibratory source, a relative displacement between coil and magnet causes variation of the magnetic flux density. This produces an electromotive force (EMF) and thereby voltage E is generated across the coil terminals.

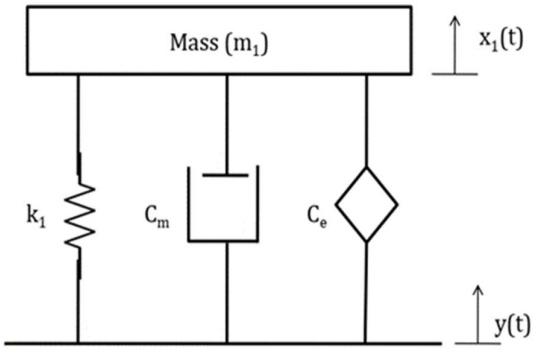

Figure 3.1 Mathematical model of a SDOF VBEH

Figure 3.1 shows the mathematical model of a SDOF VBEH. The system of spring k_1, mass m_1, and damper C_m is subjected to harmonic excitation y(t) at the base.

Let, z (t)= [x(t) – y(t)], the relative motion between the harvester mass and base of the device.

The governing equation of the VBEH is given as

$$\mathbf{m\ddot{z} = -c\dot{z} - kz - m\ddot{y}} \qquad (\mathbf{3.1})$$

Where c is the sum of mechanical damping coefficient c_m and electrical damping coefficient c_e with harmonic base excitation as y(t) = Y sin(ωt), where Y is the amplitude of base excitation and ω is the circular excitation frequency.

The steady-state amplitude as z = Z sin(ωt), one can write,

$$|Z| = \frac{m\omega^2 Y}{\sqrt{(k - m\omega^2)^2 + (c\omega)^2}} \qquad (3.2)$$

Using $\zeta_m = \frac{c}{2\sqrt{mk}}$, $\zeta_e = \frac{c_e}{2\sqrt{mk}}$, $\omega_n = \sqrt{\frac{k_1}{m_1}}$ in equation (3.2) we get,

$$|Z| = \frac{\left(\frac{\omega}{\omega_n}\right)^2 Y}{\sqrt{\left(1 - \left(\frac{\omega}{\omega_n}\right)^2\right)^2 + \left(2(\zeta_e + \zeta_m)\left(\frac{\omega}{\omega_n}\right)\right)^2}} \qquad (3.3)$$

The expression for $\dot{Z}$ is given as

$$\dot{Z} = \frac{\omega \cdot \left(\frac{\omega}{\omega_n}\right)^2 Y}{\sqrt{\left(1 - \left(\frac{\omega}{\omega_n}\right)^2\right)^2 + \left(2(\zeta_e + \zeta_m)\frac{\omega}{\omega_n}\right)^2}} \qquad (3.4)$$

Average Power (P_{ave}) is given as (Willam, Yates [23], Roundy [60])

$$P_{ave} = \frac{1}{2} c_e \dot{z}^2 \qquad (3.5)$$

Using the equation (3.4) and (3.5), P_{ave} is given as

$$P_{ave} = \frac{m\omega^3 Y^2 \zeta_e \left(\frac{\omega}{\omega_n}\right)^3}{\left(1 - \left(\frac{\omega}{\omega_n}\right)^2\right)^2 + \left(2(\zeta_e + \zeta_m)\frac{\omega}{\omega_n}\right)^2} \qquad (3.6)$$

P_{aven}in the non-dimensional form as

$$P_{aven} = \frac{P_{ave}}{m\omega^3 Y^2} = \frac{\zeta_e \left(\frac{\omega}{\omega_n}\right)^3}{\left(1 - \left(\frac{\omega}{\omega_n}\right)^2\right)^2 + \left(2(\zeta_e + \zeta_m)\frac{\omega}{\omega_n}\right)^2} \quad (3.7)$$

3.2 Experimental Setup

On the basis of the schematic model of VBEH shown in figure 3.1, an electromagnetic energy harvester is developed. For this research work, the primary or harvester system is selected as follows. It is seen that most of the practical ambient vibration sources the excitation frequency in the range of 2 to 3 Hz. The excitation frequency $\omega_1 = \frac{2\pi N}{60}$ where, N is the rpm of the motor.

$$\omega_1 = \frac{2\pi \times 185}{60} = 18.45 \frac{rad}{sec}. = 2\pi fn$$

$$f_1 \cong 3Hz$$

The arrangement for the generation of vibrations of the primary mass $m_1$is a simple, frictionless, and smooth in operation with ω_1 = 18.45 rad/sec (185 rpm) obtained by a cam driven by an electrical motor.

3.2.1 Selection of primary mass and primary spring rate

The selected undammed circular natural frequency for the SDOF system is also ω_n = 18.45 rad/ sec (resonant condition, 185 rpm). The height of the basic frame is 450 mm, and the width is 370 mm to ensure the mass will slide vertically in this space.

Taking into account the space available in the frame, a primary mass of about 4.31 Kg is selected.

$$\omega_n = 18.45 \frac{rad}{\text{sec}} = \sqrt{\frac{k_1}{m_1}} = \sqrt{\frac{k_1}{4.31}}$$

Stiffness = K = 1467.13 N/m

Thus harvester mechanical sub-system parameters are m_1 = 4.31 Kg. and $k_1 = 1460$ N/m

Using the standard procedure of design of helical compression spring with the ground and squared ends, the spring is designed for stiffness $k_1 = 1460$ N/m. The specifications of the designed spring are given in Table 3.1

Table 3.1 Specifications of spring for vibration based energy harvester

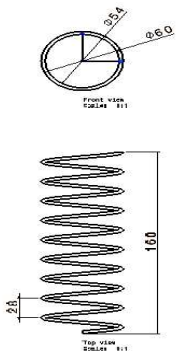

Figure 3.2 Harvester Spring

d_{mean}	54 mm
d_{wire}	3mm
N	Active turns – 6
k_1	spring rate :1460 N/m
L_f	Free length160 mm
L_s	Solid length 48 mm
Material	Spring steel.
Types of ends -ground and squared ends	

The Overall system shown in figure 3.5 consists of a mechanical sub-system, which comprises the harvester mass, suspension spring and magnet, and coil (in-line configuration) electrical system.

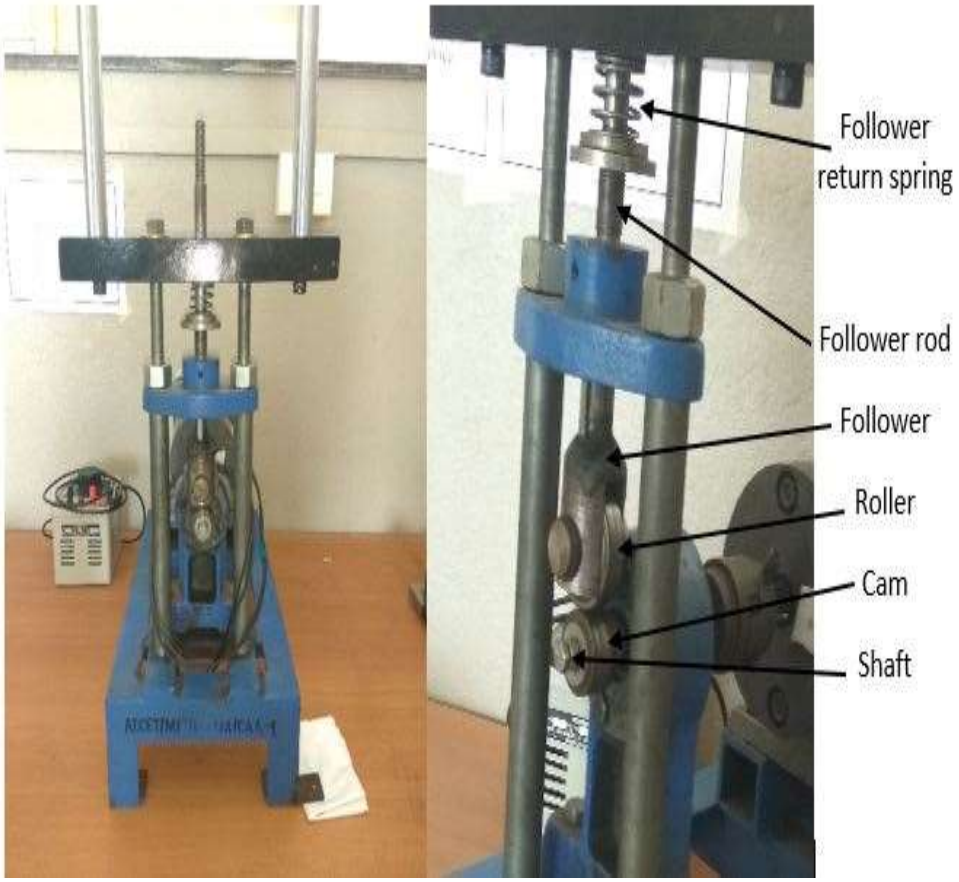

Figure 3.3 Cam and Follower

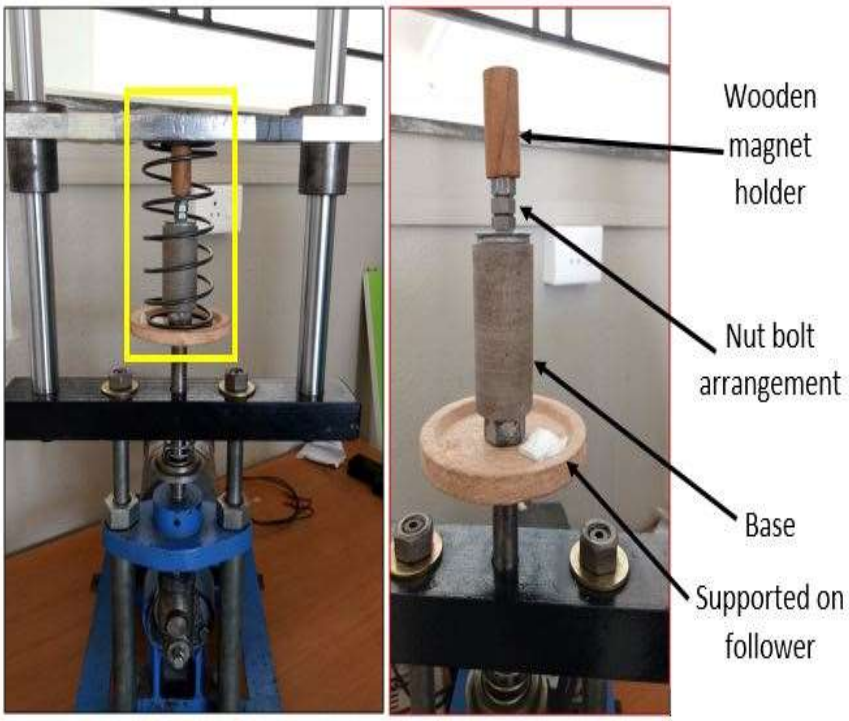

Figure 3.4 Magnet Holding Device

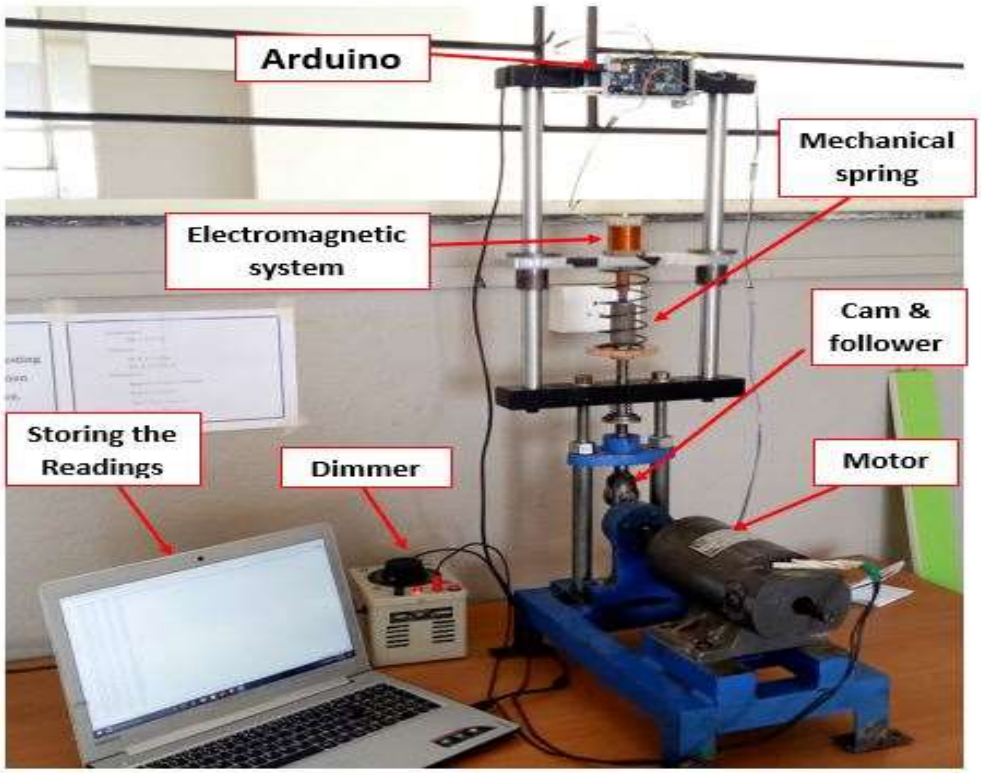

Figure 3.5 Overall Experimental Setup

The base frame on which the electric motor drive is placed has on its front side, and another vertical frame is connected for holding two parallel rods. These rods are held between two supporting plates. The harvester mass moves between two supporting rods with rolling contact bearings.

To convert rotary motion into simple harmonic motion, a cam and follower unit are placed on the drive shaft of the electric motor using the cam eccentricity of ±0.5 mm, base excitation amplitude of 1mm is realized (refer to figure 3.3). A wooden holder insulates the magnet from the steel body. The wooden support is placed on the end of the follower shaft. One end of the suspension spring is connected to a wooden support, and its other end is attached to the harvester mass. The copper coil is fixed to the harvester mass, and the magnet is attached to the end of the follower (refer to figure 3.5) to obtain relative displacement between the permanent magnet and the copper coil.

3.2.2 Design of Electromagnetic Coil

As per the guidelines given by Spreerman and Manoli [65], the number of windings in longitudinal direction N_{Long} and lateral direction N_{Lat} have been calculated. In the design of the copper coil, the copper fill factor k_{co} is taken as 0.6.

Step 1- Calculation of Longitudinal number of turns (N_{long})

$$N_{long} = \frac{2h_{coil}}{d_{co}\sqrt{\frac{\pi}{K_{co}}}} = \frac{2 \times 0.04}{0.000285\sqrt{\frac{\pi}{0.6}}}$$

$$N_{long} = 122.6721 \text{ turns}$$

Step 2- Calculation of Lateral number of turns (N_{lat})

$$N_{lat} = \frac{2(r_o - r_i)}{d_{co}\sqrt{\frac{\pi}{K_{co}}}} = \frac{2 \times (0.019 - 0.0105)}{0.000285\sqrt{\frac{\pi}{0.6}}}$$

$$N_{lat} = 26.0678 \text{ turns}$$

Step 3- Calculation of Total number of turns (N) $N = N_{long} \times N_{lat}$

$$= 122.6721 \times 26.0678$$

$$N = 3197.7945 \text{ turns}$$

$$N \cong 3198 \text{ turns}$$

Step 4- Internal Resistance of coil (R_{coil})

The internal resistance of coil is calculated using the equation

$$R_{coil} = \frac{\rho l}{a}$$

and the length l of copper wire is given as

$$l = circumference\ .N$$

$$l = 2\pi r.N$$

$$R_{coil} = \frac{\rho.2\pi r.N}{a}$$

The internal resistance is estimated as

$$R_{coil} = \frac{1.68 \times 10^{-8} \times 2 \times 3.142 \times 0.015 \times 3198}{3.2 \times 10^{-9}} = 1.58 \times 10^{3}$$

$$R_{coi} = 1.58\ K\Omega$$

Step 5 - Inductance (L_{coil}) of Copper Coil

Using Wheeler's approximation, the inductance of coil is obtained as

$$L_{coil} = \frac{3.15 \times 10^{-5} \times {r_m}^2 \times N^2}{6r_m + 9h_{coil} + 10(r_o - r_i)}$$

Where, the mean middle radius $r_m = \frac{(r_i + ro)}{2}$

$$= \frac{3.15 \times 10^{-5} \times 0.01475^2 \times 3197.7945^2}{6 \times 0.01475 + 9 \times 0.040 + 10 \times (0.019 - 0.0105)}$$

$$L_{coil} = 0.131325\ H$$

The Specifications for designed coil are given in table 3.2

Table 3.2 Specifications of Copper Coil

r_i= Inner radius of coil (mm)	10.5
r_o= Outer radius of coil (mm)	19
r_m=Mean radius of coil (mm)	14.75
h_{coil} = Length of coil (mm)	40
N_{long}= Longitudinal number of turns	122.67
N_{lat} = Lateral number of turns	26.06
N = Total number of turns	3197.79
L_{coil} = Inductance of coil (H)	0.131325
R_{coil}=Resistance of coil (KΩ)	1.58

3.2.3 Type of permanent magnet for copper coil-magnet sub-system

There are four types of rare earth magnetic materials, viz. neodymium iron boron (NdFeB), alnico, ceramic (hard ferrite), and samarium cobalt. Out of these materials, a rare earth magnetic material Neodymium Iron Boron (NdFeB) magnet is selected for the copper coil-magnet sub-system. NdFeB magnetic material has a high coercive force and has a relatively low cost with high residual flux density. It is easy to machine. The properties of NdFeB magnets are retained up to the temperature of 150°C.Therefore, a cylindrical NdFeB magnet with a diameter of 10 mm and 30 mm height is finalized for the copper coil-magnet sub-system.

3.2.4 Plan of instrumentation and measurement system

The measurement system comprises sensors and signal processing devices. At present, a wide variety of these elements and devices are available for the developed experimental setup; a sensor shown in figure 3.7 is used for the displacement measurement of harvester mass and a proximity sensor for speed measurement. These sensors are connected to Arduino (refer to figure 3.6) with the help of jumper wires, as shown in figure 3.9

Refer appendix 1 for Arduino program.

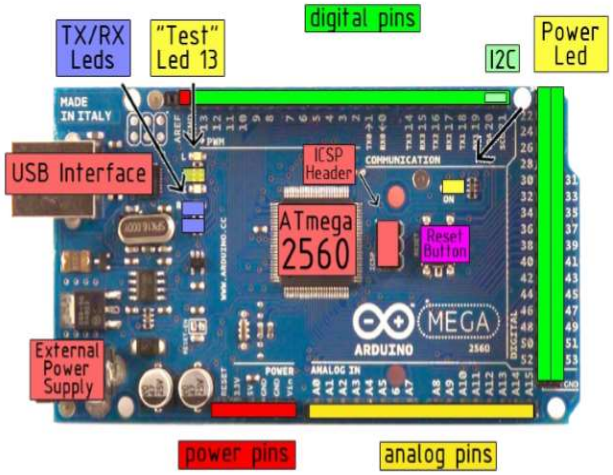

Figure 3.6 Arduino Uno unit

Figure 3.7 Ultrasonic displacement sensor

Figure 3.8 Speed measurement with proximity sensor

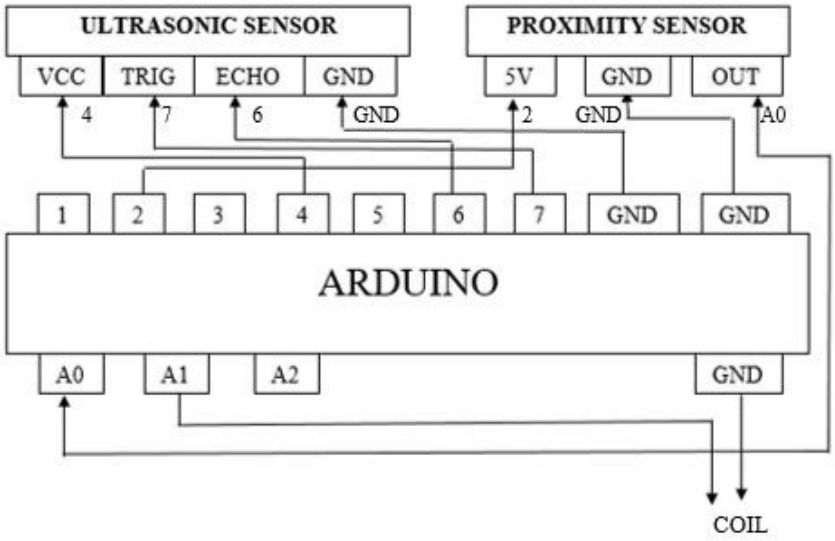

Figure 3.9 Circuit for connecting sensors with Arduino

The ultrasonic sensor having four ports (VCC, TRIG, ECHO, GND) is connected to Arduino (figure 3.9) VCC pin is connected to port number 4 of the Arduino. Trigger pin to port 7 and the ECHO pin to port 6. These port numbers of Arduino are selected according to the developed program. The connection of the ultrasonic sensor is made to the digital ports of the Arduino because the output signal of the sensor is in digital form.

Similarly, a proximity sensor for speed measurement of the motor is also connected with the Arduino. This sensor has 3 pins (5V, GND, OUT). One of them is connected to the A0 port of the Arduino because the output signal of the sensor is coming from the OUT pin, and this signal is in analog form.

The output voltage of the electromagnetic coil E is also measured and the two pins of the coil are connected directly to the Arduino. One of them is connected to the GND, and the other is connected to the A1 port. The output voltage E of the electromagnetic coil is in the analog form, and hence it is connected to the analog port of the Arduino.

3.2.5 Calibration of the Displacement system

The displacement system is calibrated by using the steel rule. The steel rule is placed between mass and sensor base as shown in figure 3.10. The displacement of the mass is recorded by the data acquisition system. It is observed that the value of scale reading and digital value of the ultrasonic sensor, which is connected to the PC, are the same.

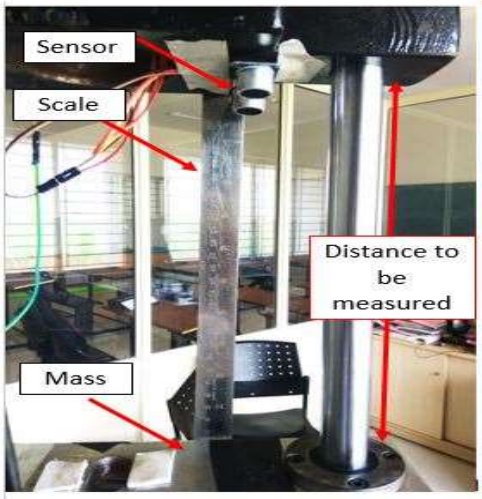

1.53	191.00	489.84	2.88	1411.45
0.51	191.00	420.02	2.47	1037.74
-0.85	191.00	478.03	2.81	1344.18
-1.02	191.00	421.09	2.48	1043.06
2.21	191.00	472.66	2.78	1314.14
-2.38	191.00	431.84	2.54	1096.95
-3.40	191.00	476.95	2.81	1338.14
-3.40	191.00	426.46	2.51	1069.84
-4.93	191.00	469.43	2.76	1296.28
-4.59	191.00	435.06	2.56	1113.39
-4.42	191.00	444.73	2.62	1163.42
-3.91	191.00	454.39	2.67	1214.56
-3.57	191.00	421.09	2.48	1043.06
-2.89	191.00	473.73	2.79	1320.12
-2.38	191.00	403.91	2.38	959.65
-1.87	191.00	475.88	2.80	1332.12
0.00	191.00	416.80	2.45	1021.88
1.02	191.00	473.73	2.79	1320.12
2.04	191.00	423.24	2.49	1053.73
2.55	191.00	467.29	2.75	1284.44
3.74	191.00	417.87	2.46	1027.15
4.59	191.00	466.21	2.74	1278.55
5.10	191.00	430.76	2.53	1091.50
6.12	191.00	441.50	2.60	1146.62

Figure 3.10 Comparison of the displacement sensor reading with scale reading

1.53	191.00	489.84	2.88	1411.45
0.51	191.00	420.02	2.47	1037.74
-0.85	191.00	478.03	2.81	1344.18
-1.02	191.00	421.09	2.48	1043.06
2.21	191.00	472.66	2.78	1314.14
-2.38	191.00	431.84	2.54	1096.95
-3.40	191.00	476.95	2.81	1338.14
-3.40	191.00	426.46	2.51	1069.84
-4.93	191.00	469.43	2.76	1296.28
-4.59	191.00	435.06	2.56	1113.39
-4.42	191.00	444.73	2.62	1163.42
-3.91	191.00	454.39	2.67	1214.56
-3.57	191.00	421.09	2.48	1043.06
-2.89	191.00	473.73	2.79	1320.12
-2.38	191.00	403.91	2.38	959.65
-1.87	191.00	475.88	2.80	1332.12
0.00	191.00	416.80	2.45	1021.88
1.02	191.00	473.73	2.79	1320.12
2.04	191.00	423.24	2.49	1053.73
2.55	191.00	467.29	2.75	1284.44
3.74	191.00	417.87	2.46	1027.15
4.59	191.00	466.21	2.74	1278.55
5.10	191.00	430.76	2.53	1091.50
6.12	191.00	441.50	2.60	1146.62

Figure 3.11 Comparison of speed of the motor reading with the tachometer reading

The speed measurement system is calibrated by using a tachometer. The readings from the sensor and tachometer were taken simultaneously and it is observed that the readings from the sensor and readings from the tachometer are nearly the same with a deviation of 1 or 2 rpm. Figure 3.11 shows the calibration setup of the speed sensor with the tachometer.

3.2.6 Experimental procedure

i) Initially, the motor speed is varied from 0 to 250 rpm. It is observed that the resonance condition occurs in the speed range of 160 to 210 rpm of the motor. Hence, the frequency response readings are taken in this motor speed range.

ii) The motor speed was kept constant at 160 rpm. The readings of displacement of harvester mass, speed of the motor, and the EMF induced in the electromagnetic coil etc., are recorded by the data acquisition system.

iii) The frequency response analysis of the harvester mass-spring sub-system is carried out. Using an ultrasonic displacement sensor to record the relative displacement of harvester mass (m) and the base for different values of frequency of excitation. For this purpose, the speed of the motor is varied from 160 to 210 rpm.

3.2.7 Estimation of mechanical damping ratio ζ_m

Figure 3.5 shows the experimental setup on which the frequency response analysis of the harvester mass-spring sub-system is carried out. In this case, the ultrasonic sensor is used to measure the relative amplitude Z between harvester mass and base. The excitation frequency (ω) is varied in the range of 17.5 to 21.0 rad/sec. From the curve of Z vs.ω, the value of the mechanical damping ratio ζ_m is obtained by using the half-power point method as 0.046 (refer to figure 3.12 and table 3.3).

Table 3.3 Z when Y = 1mm and without coil and magnet system

Ω	ω/ωn	X	Z
18.325	0.946	10	9
18.85	0.973	12	11
19.373	1.00	15	14
19.896	1.027	13	12
20.42	1.054	11	10

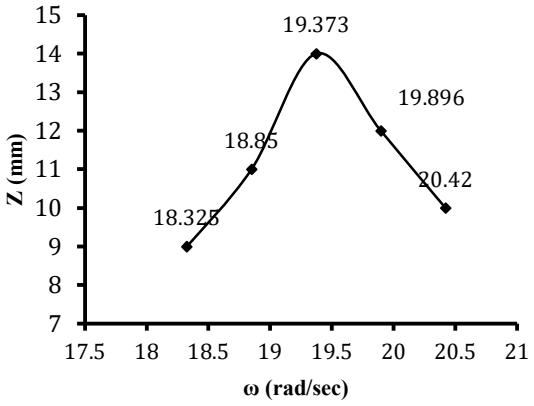

Figure 3.12 Relative amplitude (Z) vs. frequency of excitation (ω)

3.2.8 Voltage E across Copper Coil Terminals

In figure 3.13, the variation of voltage E across copper coil terminals vs. frequency excitation (ω) is shown. Also, the variation of amplitude Z vs. ω is shown in figure 3.14. From this curve, using the half-power point technique, values of the electrical damping ratio ζ_e is determined. It comes out as ζ_e= 0.0516. In table 3.4, the values of relative amplitude Z and Voltage E at different values of ω are given (with the coil-magnet system).

Table 3.4 Amplitude Z and Voltage E (with magnet and coil system) and at Y = 1 mm

ω	ω/ωn	X	Z =X-Y	E (mV)
18.325	0.946	8	7	230
18.85	0.973	10	9	410
19.373	1	11	10	525
19.896	1.027	10	9	430
20.42	1.054	8	7	250

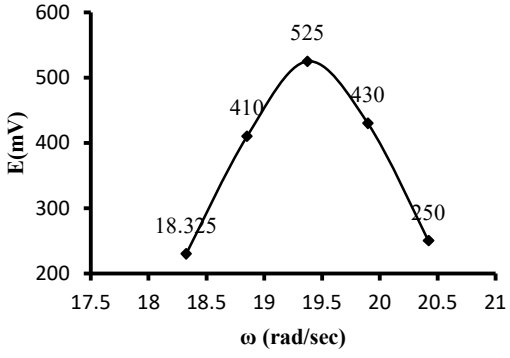

Figure 3. 13 Voltage E vs. ω

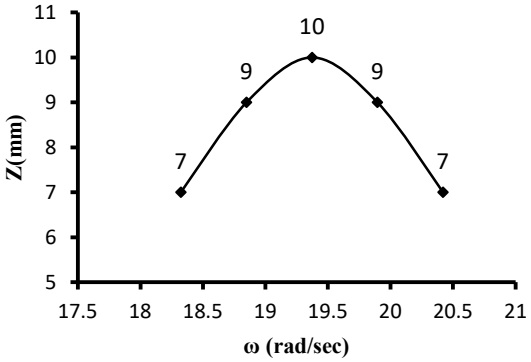

Figure 3.14 Amplitude Z vs. ω

3.2.9 Effect of pure resistive load on the voltage across the load and average power harvested P_{ave}

The pure resistive load R_L is connected across the transducer coil. The effect of R_L on the average power Pave of VBEH is analyzed using the test setup. $V_R$is voltage drops across R_L and the power, $P_{ave} = {V_R^2}/{R_L}$.

The curve of V_R vs. ω (frequency of excitation) and P_{ave} vs. ω for different values of R_L are obtained (refer table 3.5 and figures 3.15, 3.16, and 3.17). In these calculations of natural frequency ω_n is 19.373 rad/sec and amplitude of excitation Y = 1 mm.

Table 3.5 Values of V_R, Z and P_{ave}

R_L =750 Ω						R_L =1000 Ω			
ω	ω/ωn	X	Z	V_R (mV)	P_{ave} (mW)	X	Z	V_R (mV)	P_{ave} (mW)
18.325	0.946	6	5	90	0.0108	6	5	110	0.0121
18.85	0.973	8	7	125	0.0208	8	7	125	0.0156
19.373	1	10	9	130	0.0225	12	11	160	0.0256
19.896	1.027	8	7	120	0.0192	7.5	6.5	130	0.0169
20.42	1.054	7	6	110	0.0161	6.5	5.5	100	0.0100
R_L =1287 Ω						R_L =1500 Ω			
ω	ω/ωn	X	Z	V_R (mV)	P_{ave} (mW)	x	z	V_R (mV)	P_{ave} (mW)
18.325	0.946	7	6	75	0.0044	8	7	138	0.0127
18.85	0.973	11	10	135	0.0142	11	10	250	0.0417
19.373	1	12	11	175	0.0238	13	12	260	0.0451
19.896	1.027	10.5	9.5	160	0.0199	9	8	210	0.0294
20.42	1.054	9	8	150	0.0175	8	7	155	0.0187
R_L =1750 Ω									
ω	ω/ωn	X	Z	V_R (mV)	P_{ave} (mW)				
18.325	0.946	6	5	90	0.0046				
18.85	0.973	9	8	220	0.0277				
19.373	1	11	10	230	0.0302				
19.896	1.027	10	9	225	0.0289				
20.42	1.054	8	7	200	0.0229				

For example, the curves of voltage V_R across resistance R_L vs. excitation frequency ω, relative displacement Z vs. ω and power P vs. ω for the case R_L =1500 Ω have been shown in figures 3.15, 3.16 and 3.17.

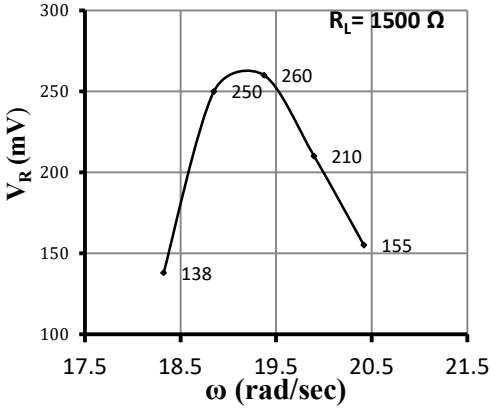

Figure 3. 15 V_R vs. ω

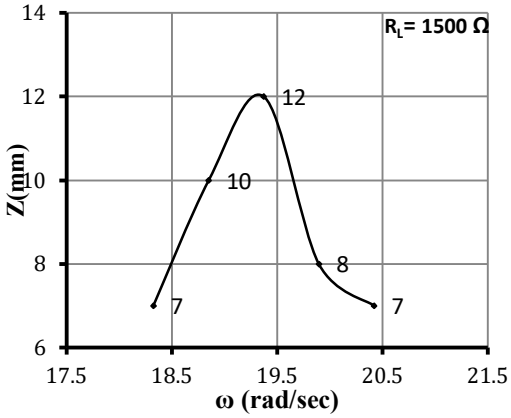

Figure 3. 16 Z vs. ω

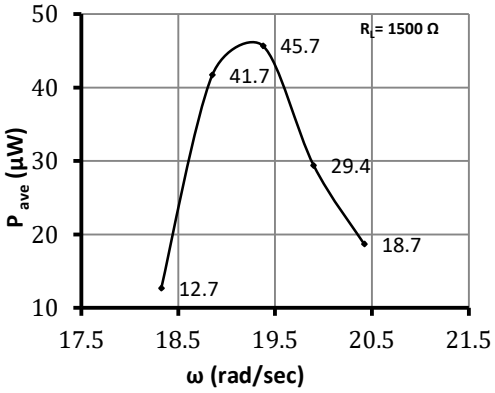

Figure 3. 17 P_{ave} vs. ω

The values of pure resistive load R_L for maximum P_{ave} and corresponding values of electrical damping ratio ξ_e are given in table 3.6

ξ_{ev}, electrical damping ratio is obtained from V_R vs. ω curve

ξ_{ez}, electrical damping ratio is obtained from Z vs. ω curve

Table 3.6 R_L, P_{ave} (maximum) and ξ_{ev} and ξ_{ez}

Sr. no.	R_L	P_{max} (μW)	ξ_{ev}	ξ_{ez}
	0	-	0.038	0.051
1	750	22.5	0.061	0.0474
2	1000	25.6	0.053	0.0490
3	1287	23.8	0.047	0.0495
4	1500	45.1	0.043	0.0340
5	1750	30.2	0.054	0.043

Figure 3.19 shows the curves of maximum P_{ave} vs. R_L. Figure 3.18 shows the curve of ζ_{ev} vs. ω. Figure 3.19 shows the curves of the electrical damping ratio ζ_{ez} vs. R_L. Figure 3.21 shows the curves of the electrical damping ratio ζ_{ev} and ζ_{ez} for various values of resistive load R_L.

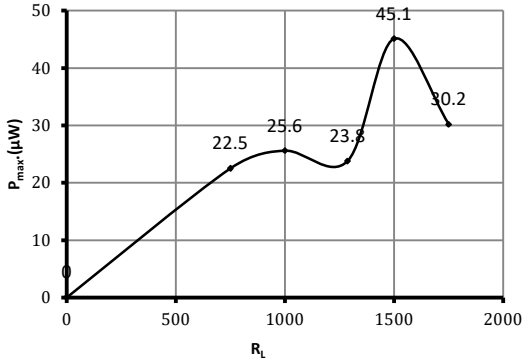

Figure 3. 18 P_{max} (maximum) vs. R_L

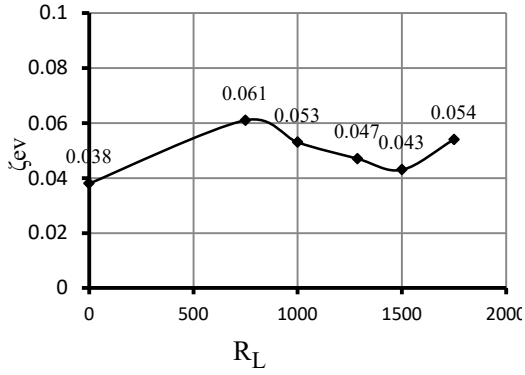

Figure 3. 19 ζ_{ev} vs. Load R_L

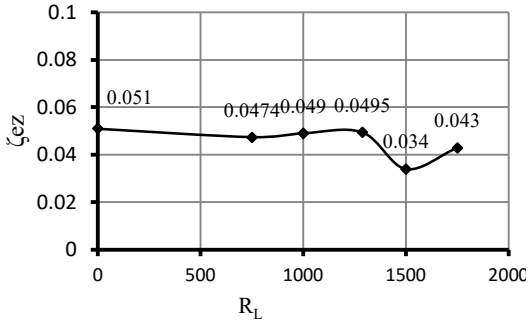

Figure 3. 20 ζ_{ez} vs. Load R_L

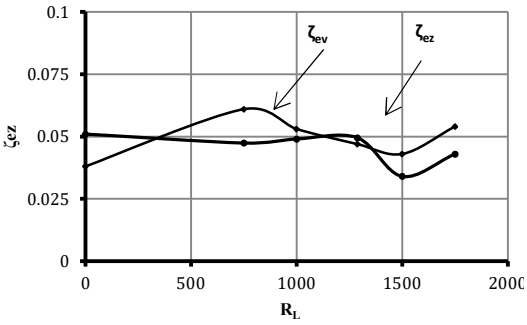

Figure 3. 21 ζ_{ez} vs. Load R_L

3.2.10 Discussion on Results

From the results of experimental analysis, it is observed that the maximum power P_{ave} from VBEH is at the resonant frequency and some power is available in the neighborhood of resonance. The resistive load affects the value of maximum P_{ave} and the electrical damping ratios.

3.3.1 Dimensionless average power P_{aven} for various values of electrical damping ratio ζ_e

At the resonance, the excitation frequency ratio $\left(\frac{\omega}{\omega_n}\right) = 1$.Taking mechanical damping ratio as $\zeta_m = 0.0046$, the values of dimensionless average power P_{aven} for different values of electrical damping ζ_e have been calculated using equation (3.7).

Table 3.7 presents these values and figure 3.22 shows the curve of vibration of P_{aven} vs. ζ_e for $\zeta_m = 0.0046$

$$P_{aven} = \frac{\zeta_e \left(\frac{\omega}{\omega_n}\right)^3}{\left(1 - \left(\frac{\omega}{\omega_n}\right)^2\right)^2 + \left(2(\zeta_e + \zeta_m)\frac{\omega}{\omega_n}\right)^2}$$

Table 3.7 Dimensionless Average Power (P_{aven}) for Different Values of Electrical Damping Ratio for $\zeta_m = 0.0046$

ζ_e	P_{aven}	ζ_e	P_{aven}
0	0.000	0.05	4.193
0.002	11.478	0.07	3.145
0.004	13.521	0.09	2.514
0.006	13.350	0.1	2.285
0.008	12.598	0.3	0.808
0.01	11.728	0.5	0.491
0.03	6.265	0.7	0.352

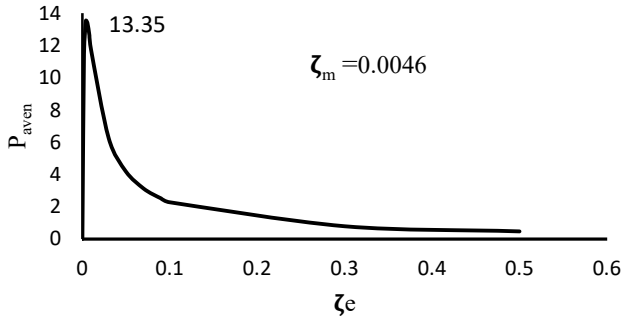

Figure 3.22 Dimensionless Average Power P_{aven} vs. Electrical Damping ratio (ζe) for ξm =0.0046

Similarly, curves of P_{aven} vs. ζ_e are plotted for $\zeta_m = 0.046$, and $\zeta_m = 0.46$ as shown in figure 3.23 and 3.24 and corresponding values of P_{aven} and ζ_e are plotted in Table 3.8 and 3.9

Table 3. 8 Dimensionless Average Power (P_{aven}) for Different Values of Electrical Damping Ratio for $\zeta_m = 0.046$

ζ_e	P_{aven}	ζ_e	P_{aven}
0	0	0.05	1.356
0.002	0.217	0.07	1.300
0.004	0.400	0.09	1.216
0.006	0.554	0.1	1.172
0.008	0.685	0.3	0.688
0.01	0.797	0.5	0.445
0.03	1.298	0.7	0.328

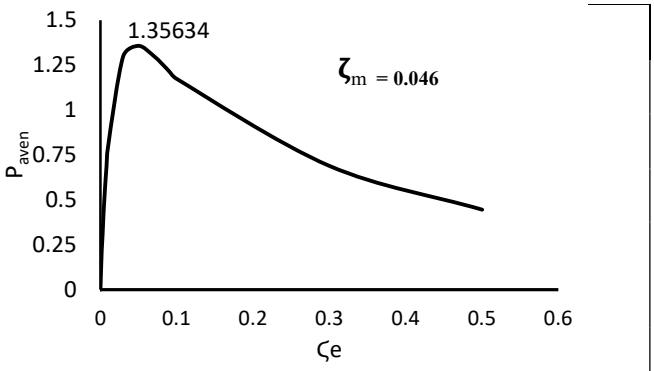

Figure 3. 23 Dimensionless Average Power P_{aven} vs. Electrical Damping ratio (ζ_e) for ζ_m =0.046

Table 3. 9 Dimensionless Average Power (P_{aven}) for Different Values of Electrical Damping Ratio for $\xi_m = 0.46$

ζ_e	P_{aven}	ζ_e	P_{aven}
0	0.000	0.05	0.048
0.002	0.002	0.07	0.062
0.004	0.005	0.09	0.074
0.006	0.007	0.1	0.080
0.008	0.009	0.3	0.130
0.01	0.011	0.5	0.136
0.03	0.031	0.7	0.130

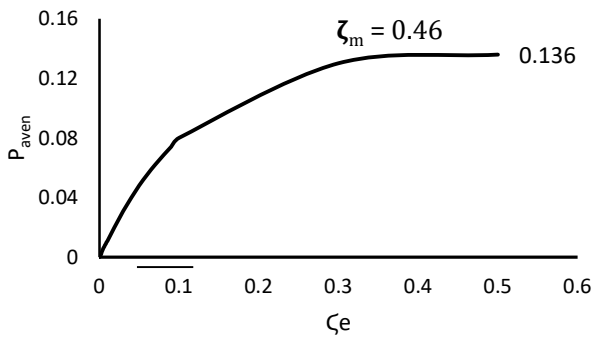

Figure 3. 24 Dimensionless Average Power P_{aven} vs. Electrical Damping ratio (ζ_e) for ζ_m =0.46

3.3.2 Dimensionless average power P_{aven} for different values of mechanical damping ratio ζ_m

At the resonance, the excitation frequency ratio $\left(\frac{\omega}{\omega_n}\right) = 1$, taking the electrical damping ratio as $\zeta_e = 0.0051$, the values of dimensionless average power P_{aven} for different values of the mechanical damping ζ_m have been calculated using equation (3.7).

Table 3.10 gives these values and figure 3.25 gives the curve of P_{aven} vs. ζ_m for ζ_e = 0.0051

Table 3. 10 Dimensionless Average Power (P_{aven}) for various Values of Mechanical Damping Ratio (ζ_m) for ζ_e = 0.0051

ζ_m	P_{aven}	ζ_m	P_{aven}
0	48.450	0.05	0.424
0.002	25.163	0.07	0.228
0.004	15.374	0.09	0.142
0.006	10.358	0.1	0.117
0.008	7.449	0.3	0.014
0.01	5.613	0.5	0.005
0.03	1.043	0.7	0.004

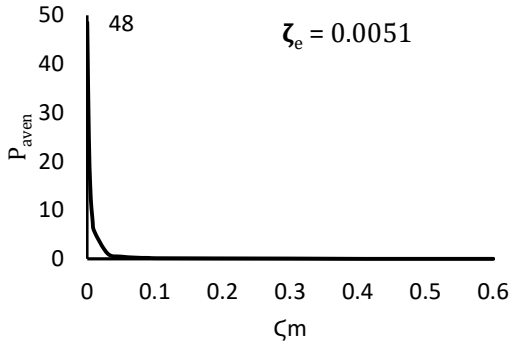

Figure 3.25 Dimensionless Average Power (P_{aven}) vs. Mechanical Damping ratio (ζ_m) for ζ_e = 0.0051

Similarly, curves of P_{aven} vs. ζ_m has been calculated for ζ_e = 0.051, and ζ_e= 0.51

Tables 3.11 and 3.12gives these values P_{aven} respectively for ζ_e = 0.051, and ζ_e= 0.51 and corresponding curves of P_{aven} vs. ζ_m have been plotted respectively in figures 3.26 and 3.27

Table 3. 11 Dimensionless Average Power (P_{aven}) for various Values of Mechanical Damping Ratio (ζ_m) for $\zeta_e = 0.051$

ζ_m	P_{aven}	ζ_m	P_{aven}
0	4.845	0.05	1.250
0.002	4.490	0.07	0.872
0.004	4.173	0.09	0.643
0.006	3.888	0.1	0.561
0.008	3.632	0.3	0.104
0.01	3.400	0.5	0.042
0.03	1.937	0.7	0.030

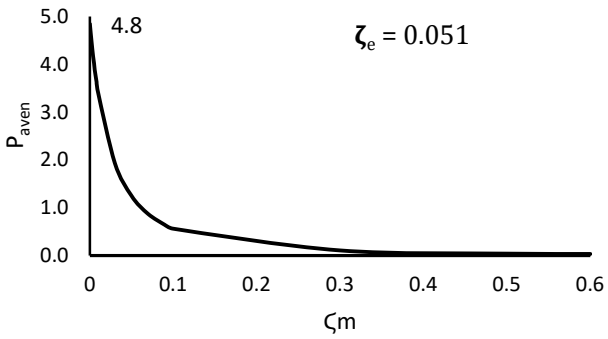

Figure 3. 26 Dimensionless Average Power (P_{aven}) vs. Mechanical Damping ratio (ζ_m) for $\zeta_e = 0.051$

Table 3. 12 Dimensionless Average Power (P_{aven}) for various Values of Mechanical Damping Ratio (ζ_m) for $\zeta_e = 0.051$

ζ_m	P_{aven}	ζ_m	P_{aven}
0	0.484	0.05	0.403
0.002	0.481	0.07	0.376
0.004	0.477	0.09	0.351
0.006	0.473	0.1	0.340
0.008	0.470	0.3	0.194
0.01	0.466	0.5	0.125
0.03	0.433	0.7	0.104

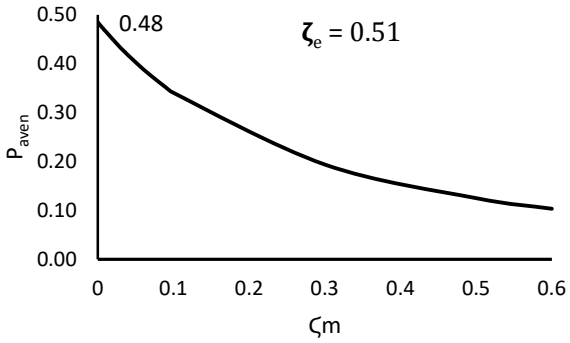

Figure 3. 27 Dimensionless Average Power (P_{aven}) vs. Mechanical Damping ratio (ζ_m) for $\zeta_e = 0.51$

3.3.3 Discussion on Results

From the results of analysis, it is seen from figures 3.22, 3.23, and 3.24 that the value of dimensionless maximum average power obtained is 13.7 for $\zeta_m = 0.0046$, at $\frac{\omega}{\omega_n} = 1$. The results shown in figures 3.25, 3.26, and 3.27 it can be noted that the maximum average power obtained is 48 for $\zeta_e = 0.00516$, at $\frac{\omega}{\omega_n} = 1$. As such, to obtain maximum dimensionless average power from a VBEH, the value of ζ_m should be as small as possible.

3.4 Conclusion

i. It is seen from the theoretical and experimental analysis of the developed VBEH that the values of electrical and mechanical damping ratio affect the maximum average power output of VBEH, especially at resonance conditions.

ii. For the design of a VBEH for maximum average power output, it is necessary that the mechanical damping ratio ζ_m should be as less as possible and the value of the electrical damping ratio ζ_e should be nearly equal to the mechanical damping ratio ζ_m.

iii. The electrical resistive load connected to VBEH influences the maximum average power output at and off-resonance conditions

Chapter – 4

EXPERIMENTAL STUDIES ON THE EFFECT OF ELECTRICAL LOAD IMPEDANCES ON THE POWER OUTPUT OF A VIBRATION-BASED ELECTROMAGNETIC ENERGY HARVESTER

4.0 Introduction

Vibration-based electromagnetic energy harvester (VBEH) power output is of the order of a few microwatts. Therefore, it is required to maximize the power generated from a VBEH to bear electrical load impedances. It is in this context, an experimental set-up has been designed and developed with attendant instrumentation to (i) study the effect of changes in resistive, capacitive and inductive load on the maximum power developed from VBEH and (ii) to determine experimentally the values of ξ_e and ξ_m where ξ_m is the mechanical damping ratio and ξ_e is electrical damping ratio. In this chapter, the results of the above-mentioned studies are presented.

4.1 Vibration-Based Electromagnetic Harvester (VBEH)

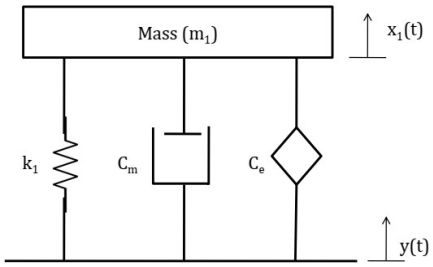

Figure 4.1 Mathematical model of a SDOF VBEH

In this section, some of the basic information regarding SDOF VBEH is recapitulated for continuity of the write-up.

A mathematical model of a single degree of freedom (SDOF) vibration-based electromagnetic harvester (VBEH) is shown in figure 4.1. It consists of a mass (m), spring (k) and damper (c) system subjected to sinusoidal base excitation y(t). If c_m is the mechanical damping coefficient, and c_e is the electrical damping coefficient, then one can write

$$C = C_m + C_e$$

If x(t) is the displacement of harvester mass m and y(t) is the base excitation displacement, then $z(t) = x(t) - y(t)$ is the displacement of mass m relative to the base. Here $y(t) = y \sin \omega t$ where y is the amplitude of base vibration and excitation frequency is ω. The governing equation of motion is

$m\ddot{z} = -c\dot{z} - kz - m\ddot{y}$, or

$$m\ddot{z} + c\dot{z} + kz = -m\ddot{y} \tag{4.1}$$

If P_{ave} is the average generated power from VBEH, it is given by equation 3.7 of chapter 3 as

$$P_{ave} = \frac{m\omega^3 Y^2 \zeta_e \left(\frac{\omega}{\omega_n}\right)^3}{\left(1-\left(\frac{\omega}{\omega_n}\right)^2\right)^2 + \left(2(\zeta_e+\zeta_m)\frac{\omega}{\omega_n}\right)^2} \tag{4.2}$$

Where,

$\zeta_e = \frac{c_e}{c_c}$ = electrical damping ratio

$\zeta_m = \frac{c_m}{c_c}$ = mechanical damping ratio

c_c is the critical damping coefficient and circular natural frequency is ω_n.

4.2 Experimental Setup: VBEH Shunted to Electrical Loads

Figure 4.2 represents a schematic of an SDOF VBEH. An electrical load comprising of resistance R, capacitance C and inductance L is connected across the vibration transducer coil.

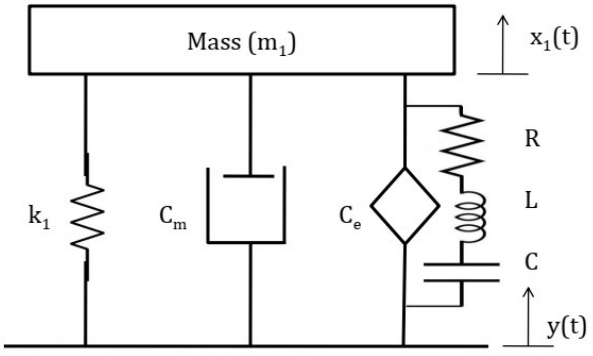

Figure 4.2 Experimental schematic of a SDOF VBEH connected to electrical load

An experimental setup for a SDOF VBEH shown schematically in figure 4.2 has been developed. The mechanical and coil-magnet sub-system and magnet holder are shown in figure 4.3 and figure 4.4 for experimental test setup for the developed VBEH with attendant instrumentation and electrical load circuit is shown in figure 4.3

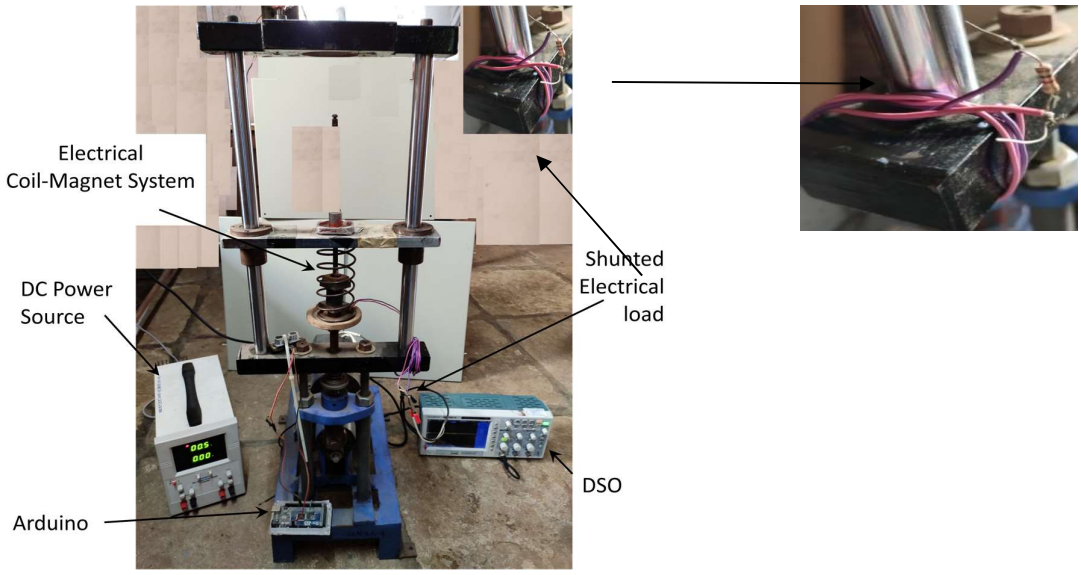

Figure 4.3 Overall Experimental Setup

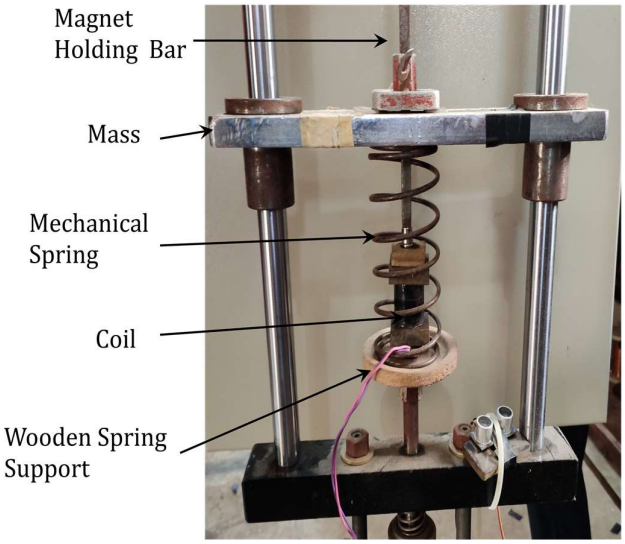

Figure 4.4 The harvester mass - suspension spring and magnet holder

The copper coil is supported on a wooden base. The permanent magnet is connected to the harvester mass to get the relative motion $z(t)$between the copper coil and the permanent cylindrical magnet. To measure the displacement response of the harvester mass an ultrasonic displacement sensor is used and a proximity speed sensor to measure the speed of the DC drive motor. To record displacement and speed signals are measured using a Computer-Arduino system.

4.3 Design of In-Line Architecture of Coil and Permanent Magnet Vibration Transducer

4.3.1 Copper Coil Design

Figure 4.5 shows the arrangement of motion of cylindrical magnet w.r.t. coil in the direction of motion.

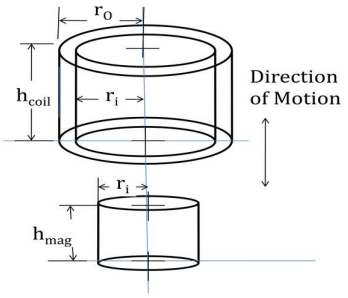

Figure 4.5 In-line configuration of magnet and coil

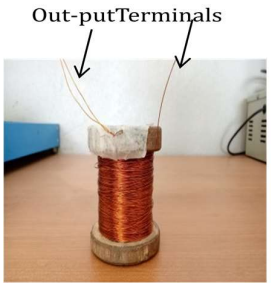

Figure 4.6 Developed coil

For designing the electromagnetic coil, the 41 gauge copper wire of diameter (d_{co}) is 0.08 mm, the height of coil (h_{coil}) is assumed as 30 mm, r_i = inner radius of the coil = 8 mm, and r_o = outer radius of the coil = 10 mm refer figure 4.5. By selecting the inductance of the coil 0.45 Hennery (H), the number of turns can be calculated by wheelers approximation as [41]

$$L_{coil} = \frac{3.15\times10^{-5}\times r_m{}^2\times N^2}{6r_m+9h_{coil}+1\ (r_o-r_i)} \tag{4.3}$$

$$N^2 = \frac{6r_m+9h_{coil}+10(r_o-r_i)\times L_{coil}}{3.15\times10^{-5}\times r_m{}^2} \tag{4.4}$$

Where, r_m denotes the mean radius $= \frac{(r_o+r_i)}{2} = 9\text{mm} = 0.009$ m

$$N^2 = \frac{[(6\times 0.009)+(9\times 0.030)+10(0.01-0.008)]\times 0.45}{3.15\times10^{-5}\times 0.009^2}$$

N =7790 turns

With

$$K_{co} = \frac{\text{overall wire diameter } (A_1)}{\text{cross section of the winding area}(A_w)}$$

Now,

$$A_w = (r_o - r_i).h_{coil} \tag{4.5}$$

Therefore,

$$k_{co} = \frac{A_1}{A_w} = \frac{\pi\cdot d_{co}{}^2\cdot rN}{4\cdot A_w} = \frac{3.14\times0.08^2\times7790}{4\times2\times30} = 0.6522 \tag{4.6}$$

Here, d_{co} is the wire diameter with $K_{co} = 0.6522$

N_{long}= Number of longitudinal turns are given as

$$N_{long} = \frac{2h_{coil}}{d_{co}\sqrt{\frac{\pi}{K_{co}}}} = \frac{2\times30}{0.08\sqrt{\frac{\pi}{0.6522}}} = 341.13 = 342 \text{ Turns} \quad (4.7)$$

And

N_{lat}= Number of Lateral turns are obtained as

$$N_{lat} = \frac{2(r_o - r_i)}{d_{co}\sqrt{\frac{\pi}{K_{co}}}} = \frac{2\times(10-8)}{0.08\sqrt{\frac{\pi}{0.6522}}} = 22.80 \text{ turns} \quad (4.8)$$

Total number of turns (N)

$N = N_{long} \times N_{lat} = 342 \times 22.80 = 7790$ turns

Resistance of coil (R_{coil})

Taking specific resistivity (ρ) of copper as 1.72 x 10^{-8}Ωm and a as cross section area of wire = 6.4 x 10^{-9} m^2 Resistance of the coil is estimated as

$$R_c = \frac{4\rho(r_o^2 - r_i^2)h_{coil}}{a^4} = \frac{4\times1.72\times10^{-8}(0.010^2 - 0.0008^2)0.03}{(6.4\times10^{-9})^2} = 1814\ \Omega \quad (4.9)$$

The measured value of R_c =1620 Ω. The difference between the theoretical and experimental values may be attributed to the method of coil winding and in calculation of N. For specifications of coil design refer Table 4.1.

Table 4.1 Specifications of the designed coil

r_o	Coil outer radius (mm)	10	N_{lat}	Lateral turns of coil	23
r_i	Coil inner radius (mm)	8	N	Total number of turns of coil	7790
h_{coil}	coil height (mm)	30	R_c	The internal resistance of the coil (Ω)	1620
N_{long}	Longitudinal turns of coil	343	L	The internal inductance of coil (H)	0.45

4.3.2 Cylindrical Permanent Magnet Material Selection

The types of magnetic material are ceramic, alnico, neodymium iron boron (NdFeB) samarium cobalt. Neodymium Iron Boron (NdFeB) magnet (rare earth magnetic material) has a high coercive force and strength and is a relatively low cost, easy to machine with low cost. Hence, the selection of cylindrical magnet of NdFeB grade 30 having 10 mm diameter and height 30 mm was finalized for vibration transducer.

4.4 Experimental Studies

The performance analysis of the SDOF VBEH is carried out on the set-up developed for the same. The frequency response analysis of the mechanical sub-system is performed using an ultrasonic sensor to measure the relative displacement Z between base and harvester mass in the band of excitation frequency (ω) from 0 to 21.0 rad/sec. This analysis is carried out on the set-up shown in figure 4.3. The values of Z for various values of ω are given in table 4.2. The results of the analysis are given in table 4.2 (Also refer to figure 4.7).

4.4.1 Relative Amplitude Z for various values of excitation frequency ω

From figure 4.7, it is seen that the value of Z is highest at the resonance (for with and without a coil magnet system) (Refer also Table 4.2).

Table 4. 2 Relative Amplitude (Z) (without magnet and coil)

N	ω	ω/ω_n	X	Y	Z = X-Y
172	18.00	0.945	9	1	8
176	18.42	0.967	12	1	11
180	18.84	0.989	20	1	19
182	19.05	1.000	30	1	29
184	19.26	1.011	28	1	27
188	19.68	1.033	17	1	16
192	20.09	1.055	10	1	9

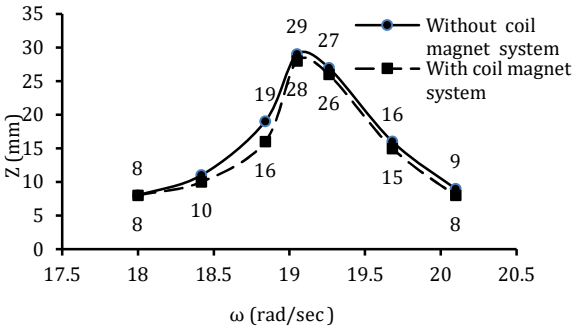

Figure 4.7 Amplitude Z vs. frequency of excitation (ω)

4.4.2 Voltage E across Transducer Coil

Figure 4.8 shows the curve of voltage E vs. frequency of excitation ω. (Also refer to Table 4.3)

Table 4. 3 Values of Voltage (E) generated

N	ω	ωn	X	Y	X-Y= Z	E
172	18.00	0.945	9	1	8	1.2
176	18.42	0.967	11	1	10	2.4
180	18.84	0.989	17	1	16	4.8
182	19.05	1.000	29	1	28	9
184	19.26	1.011	27	1	26	8.6
188	19.68	1.033	16	1	15	4.2
192	20.09	1.055	9	1	8	3

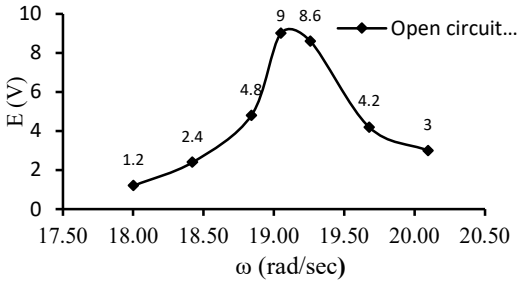

Figure 4.8 Voltage E vs. frequency of excitation ω.

From figure 4.8, it is seen that the peak value of voltage E generated is 9 Volts.

4.4.3 Effect of Electrical Load Impedances on Average Power Output (P_{aveh}) of VBEH

When the electrical load is matched with harvester mechanical system the condition that $\omega_e = \omega_n = {}^{1}/_{\sqrt{LC}}$ has to be fulfilled

Where, $\omega_e \; and \; \omega_n$ are the natural frequencies of electrical load and mechanical sub-system. For a tuned VBEH $\omega_n = \omega$ at resonance or $\omega_e = \omega_n = \omega_R = 19.05 \; rad/sec$

With L= 0.45H, using equation 4.10, the value of C is calculated as 0.0055F (5500 μ F).

Varying the values of L and C around their value, L = 0.45H and C = 5500μF respectively, the effect of variation of load impedances (i.e., variation of R_L, R_L and L and R_L, L and C) on P_{ave} is analysed (Refer 4.10)

4.4.4 Output Voltage V_R across different values of Pure Resistive Load R_L

The pure resistive load R_L in the electrical load circuit is varied (refer table 4.4). A Digital Signal Oscilloscope (DSO) is used to measure V_R. The results are given in Tables 4.4 to 4.9. Also, refer to figure 4.9.

Table 4.4 Harvested Power with R_L = 500 Ω

N (rpm)	ω(rad/sec)	ω/ωn	X (m)	Y (m)	Z (m)	V (V)	P (mW)
172	18.00	0.945	0.009	0.001	0.008	0.600	0.72
176	18.42	0.967	0.010	0.001	0.009	0.700	0.98
180	18.84	0.989	0.017	0.001	0.016	1.200	2.88
182	***19.05***	***1.000***	***0.027***	***0.001***	***0.026***	***2.200***	***9.68***
184	19.26	1.011	0.025	0.001	0.024	2.100	8.82
188	19.68	1.033	0.016	0.001	0.015	1.400	3.92
192	20.096	1.055	0.009	0.001	0.008	0.800	1.28

Table 4.5 Harvested Power with RL = 1000 Ω

N (rpm)	ω (rad/sec)	ω/ωn	X (m)	Y (m)	Z (m)	V (V)	P (mW)
172	18.00	0.945	0.009	0.001	0.008	0.800	0.64
176	18.42	0.967	0.010	0.001	0.009	0.900	0.81
180	18.84	0.989	0.016	0.001	0.015	2.100	4.41
182	**19.05**	**1.000**	**0.027**	**0.001**	**0.026**	**3.600**	**12.96**
184	19.26	1.011	0.025	0.001	0.024	3.500	12.25
188	19.68	1.033	0.011	0.001	0.010	2.000	4.00
192	20.096	1.055	0.009	0.001	0.008	1.200	1.44

Table 4.6 Harvested Power with R_L =1600 Ω

N (rpm)	ω (rad/sec)	ω/ωn	X (m)	Y (m)	Z (m)	V (V)	P (mW)
172	18.00	0.945	0.009	0.001	0.008	1.00	0.63
176	18.42	0.967	0.011	0.001	0.010	1.80	2.02
180	18.84	0.989	0.016	0.001	0.015	3.0	5.6
182	**19.05**	**1.000**	**0.027**	**0.001**	**0.026**	**4.90**	**15**
184	19.26	1.011	0.026	0.001	0.025	4.50	13.22
188	19.68	1.033	0.016	0.001	0.015	2.90	5.56
192	20.096	1.055	0.009	0.001	0.008	1.80	2.0

Table 4.7 Harvested Power with R_L = 2000 Ω

N (rpm)	ω (rad/sec)	ω/ωn	X (m)	Y (m)	Z (m)	V (V)	P (mW)
172	18.00	0.945	0.009	0.001	0.008	1.100	0.61
176	18.42	0.967	0.011	0.001	0.010	1.700	1.45
180	18.84	0.989	0.016	0.001	0.015	2.800	3.92
182	**19.05**	**1.000**	**0.027**	**0.001**	**0.026**	**5.000**	**12.50**
184	19.26	1.011	0.026	0.001	0.025	4.800	11.52
188	19.68	1.033	0.015	0.001	0.014	2.600	3.38
192	20.096	1.055	0.009	0.001	0.008	1.600	1.28

Table 4.8 Harvested Power with R_L = 3000 Ω

N (rpm)	ω (rad/sec)	ω/ωn	X (m)	Y (m)	Z (m)	V (V)	P (mW)
172	18.00	0.945	0.009	0.001	0.008	1.300	0.56
176	18.42	0.967	0.010	0.001	0.009	1.600	0.85
180	18.84	0.989	0.015	0.001	0.014	3.200	3.41
182	**19.05**	**1.000**	**0.026**	**0.001**	**0.025**	**5.600**	**10.45**
184	19.26	1.011	0.026	0.001	0.025	5.500	10.08
188	19.68	1.033	0.016	0.001	0.015	3.000	3.00
192	20.096	1.055	0.009	0.001	0.008	1.700	0.96

Table 4.9 Harvested Power with R_L = 4000 Ω

N (rpm)	ω (rad/sec)	ω/ωn	X (m)	Y (m)	Z (m)	V (V)	P (mW)
172	18.00	0.945	0.009	0.001	0.008	1.300	0.42
176	18.42	0.967	0.011	0.001	0.010	1.600	0.64
180	18.84	0.989	0.016	0.001	0.015	3.600	3.24
182	**19.05**	**1.000**	**0.027**	**0.001**	**0.026**	**6.300**	**9.92**
184	19.26	1.011	0.026	0.001	0.025	6.100	9.30
188	19.68	1.033	0.015	0.001	0.014	3.200	2.56
192	20.096	1.055	0.008	0.001	0.007	2.200	1.21

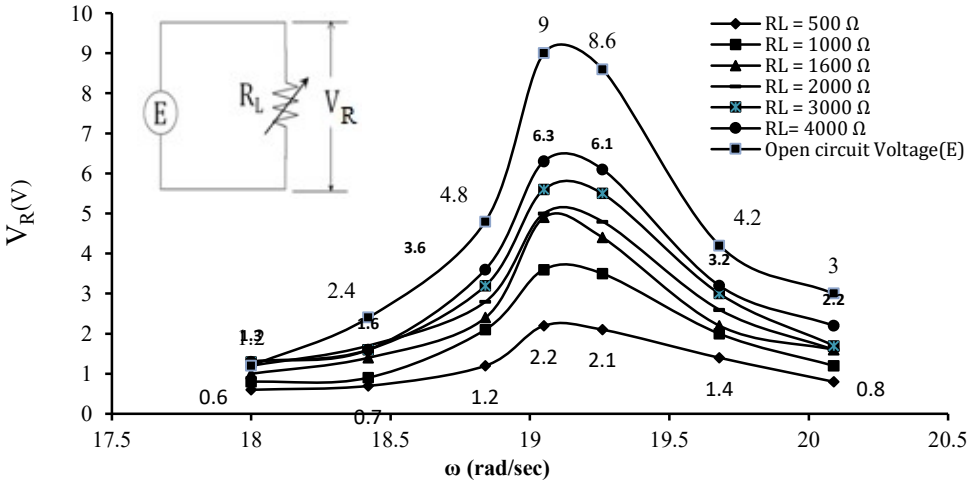

Figure 4.9 Voltage V_R vs. frequency of excitation ω (for different values of load resistances)

4.4.5 Average Harvested Power P_{aveh} at Various Values of Resistive Load R_L

Average harvested power P_{aveh} calculated as $P = V_R^2/R_L$. Using the values of V_R from tables 4.4 to 4.9, the curves of average harvested power P_{aveh} vs. excitation frequency ω for various R_L are plotted as shown in Figure 4.10.

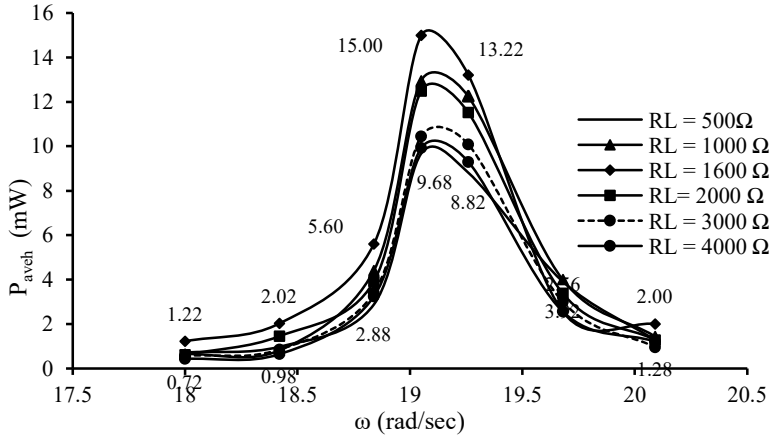

Figure 4. 10 Average Harvested Power P_{aveh} vs. frequency of excitation ω (for different values of load resistances)

Figures 4.11 and 4.12 respectively show the curves of peak values of V_R and P_{aveh} at resonance for various values of resistive load R_L.

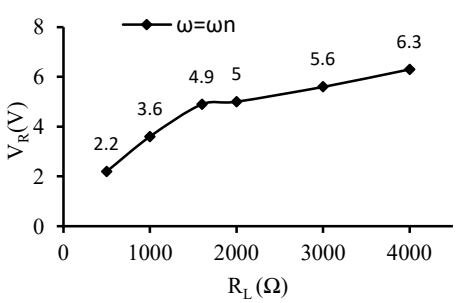

Figure 4. 11 V_R vs. Resistive Load R_L, at $\omega = \omega_n$

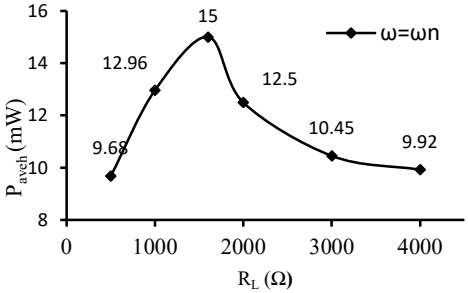

Figure 4. 12 P_{aveh} vs. Pure Resistive Load R_L, at resonance

It is seen from figure 4.11 that V_R increases with an increase in R_L and from figure 4.12 it is observed that P_{aveh} reaches to the maximum value at R_L = 1600 Ω, and the corresponding value of power is 15 mW.

4.4.6 Effect of Resistive and Inductive Load on Voltage V_R

Figure 4.13 shows the R – L load circuit connected to the VBEH.

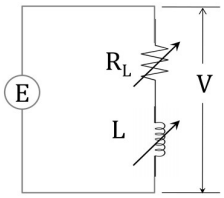

Figure 4. 13 Electrical load circuit

Figure 4.14(a)Variable Inductance coil

(b) Resister

Here, the resistive and inductive load impedance

$$Z_1 = \sqrt{{R_c}^2 + {x_L}^2}$$

Where, the resistive load is R_L and x_L is the inductance reactance. x_L is $x_L = \omega_e L$

In figure 4.14 (a) the developed variable inductance coil is shown and in figure 4.14 (b) resister used is shown.

Resistance of the coil (R_c)= 400 ,Inducatnace of the coil(L_{coil}) $= 0.310\ H$, Frequency (f) = 3Hz. Then, x_L = Inductance Reactance(Ω) =$2\pi f L_{coil}$

$$x_L = 2 \times \pi \times 0.31 = 5.652\ \Omega$$

$$Z_1 = \sqrt{{R_c}^2 + {x_L}^2} = \sqrt{400^2 + 5.625^2} \cong 400\Omega$$

Using above equation, the values of Z_1 for different values of R_L and L are estimated and are given in table 4.10. For these values of load impedances (z_1), the values of power harvested P_{aveh} at various values of excitation frequency are obtained. Table 4.10 to 4.12 shows these values of P_{aveh}.

Table 4.10 Values of load impedance Z_1

Sr. No.	Resistive Load $R_L(\Omega)$	Inductance L(H)	Reactance $x_L(\Omega)$	Load impedance Z_1 (Ω)
1	400	0.310	5.625	400.3
2	900	0.310	5.625	900.01
3	1600	0.510	9.608	1600
4	2100	0.510	9.608	2100.02
5	2800	0.700	13.188	2800.03

Table 4.11 Harvested power (P_{aveh}) with R-L Circuit for load Impedance (Z_1) 400Ω and 900Ω

N (rpm)	ω(rad/sec)	ω/ωn	Load Impedance (Z_1) 400Ω		Load Impedance (Z_1) 900Ω	
			V_R (V)	P_{aveh} (mW)	V_R (V)	P_{aveh}(mW)
172	18.00	0.945	0.700	1.23	0.800	0.71
176	18.42	0.967	1.000	2.50	1.200	1.60
180	18.84	0.989	1.300	4.23	2.200	5.38
182	***19.05***	***1.000***	***2.100***	***11.03***	***3.500***	***13.61***
184	19.26	1.011	2.000	10.00	3.300	12.10
188	19.68	1.033	1.200	3.60	1.600	2.84
192	20.096	1.055	0.600	0.90	1.200	1.60

Table 4. 12 Harvested power (P_{aveh}) with R-L Circuit for load Impedance (Z_1) 1600 Ω, 2100 Ω and 2800 Ω

N (rpm)	ω (rad/sec)	ω/ωn	Load Impedance (Z_1) 1600Ω		Load Impedance (Z_1) 2100Ω		Load Impedance (Z_1) 2800Ω	
			V (V)	P (mW)	V (V)	P (mW)	V (V)	P_{aveh} (mW)
172	18.00	0.945	1.000	0.63	1.200	0.69	1.200	0.51
176	18.42	0.967	1.200	0.90	1.500	1.07	1.600	0.91
180	18.84	0.989	2.200	3.03	2.700	3.47	3.700	4.89
182	**19.05**	**1.000**	**4.800**	**14.40**	**5.100**	**12.39**	**5.700**	**11.60**
184	19.26	1.011	4.500	12.66	4.900	11.43	5.100	9.29
188	19.68	1.033	2.400	3.60	2.500	2.98	2.700	2.60
192	20.096	1.055	1.600	1.60	1.800	1.54	1.800	1.16

Figure 4.15 shows curves of V_R vs. frequency of excitation for different values of Z_1

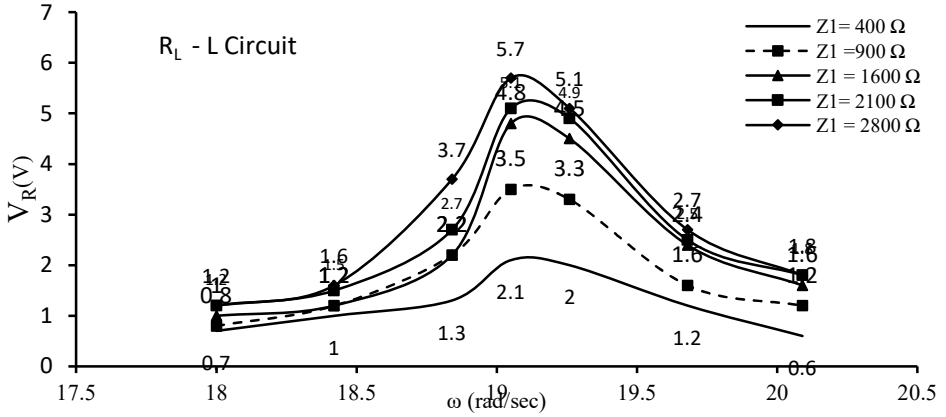

Figure 4.15 Voltage V_R vs. Excitation frequency ω

4.4.7 Average Harvested Power P_{aveh} of VBEH for Different Values of Z_1

Figure 4.16 shows curves of P_{aveh} vs. ω for different values of Z_1.

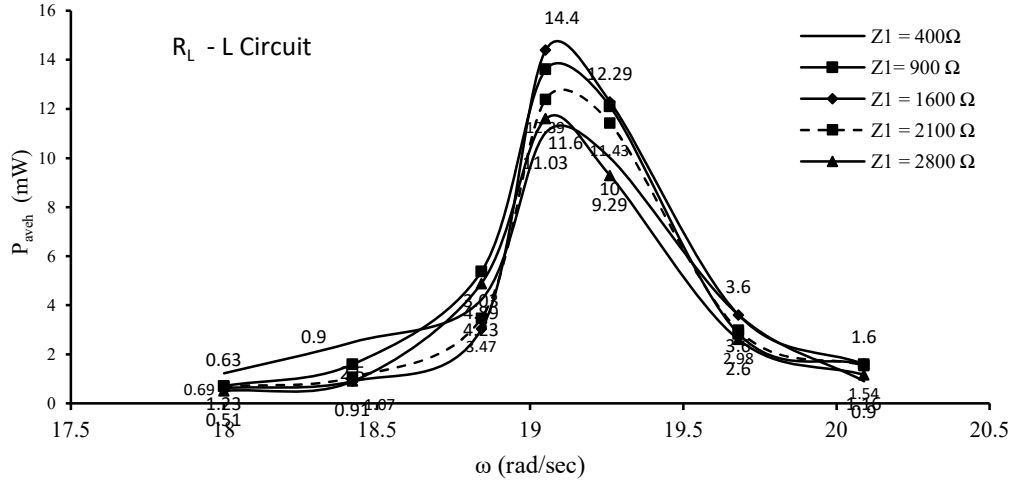

Figure 4.16 P_{aveh} vs. ω for various values of Z_1

Figure 4.17 shows the curve of peak values of V_R vs. Z_1. Figure 4.18 shows the curve of values of P_{aveh} vs. Z_1 at resonance. The curves of the peak value of V_R at different values of Z_1 are shown in figure 4.17. The curves of P_{aveh} vs. Z_1 at resonance are shown in figure 4.18.

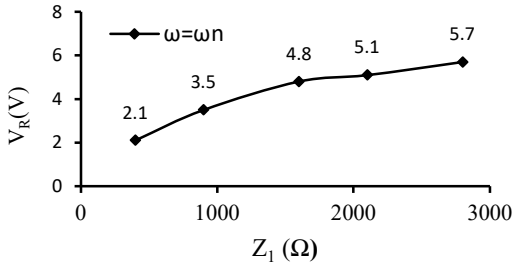

Figure 4. 17 Peak values of V_R vs. Z_1, at resonance

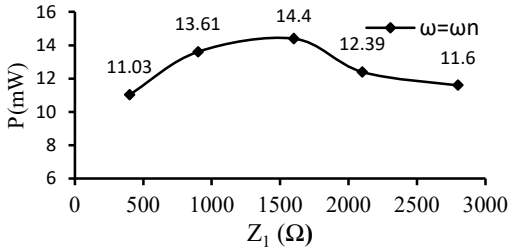

Figure 4. 18 P_{aveh} vs. Z_1, at resonance

Figure 4.17 shows that with the increase in the Z_1, the voltage V_R increases. Figure 4.18shows that the P_{aveh} is maximum at Z_1 = 1600 Ω, and its value is 14.40 mW. It is seen from figure 4.17 that the peak value of V_R increases with the increase in Z_1 and figure 4.18 shows that the maximum value of P_{aveh} is 14.340 mW at resonance.

4.4.8. Effect of Combined Resistive, Inductive and Capacitive Load (R_L – L – C) on Voltage V_R

The combined R_L – L – C load circuit connected to VBEH is shown in figure 4.19 and figure 4.20 shows R_L, L and C elements of the circuit of figure 4.19.

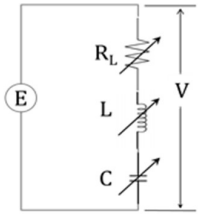

Figure 4.19 Electrical load circuit

(a)

(b)

(c)

Figure 4. 20 (a) Resister (b) Variable Inductance coil (c) capacitors

In this case, the combined R_L – L – C load impedance Z_2 is given as

$$Z_2 = \sqrt{{R_L}^2 + (x_L - x_c)^2}$$

Where, the resistive load is R_L, inductance reactance is $x_L = \omega_e$ Land capacitive reactance $x_c = \frac{1}{\omega_e C}$ .Where C is capacitance. A resistor is shown in figure 4.20 (a), a developed variable inductor in figure 4.20 (b) and capacitor C is shown in figure 4.20 (c).

In this case, the resistance of the coil (R_C) = 400Ω ,Inducatnace of the coil(L_c) = 0.310 Henry(H), Resonance frequency (f) is 3Hz.

Inductive Reactance (x_L) =2π f L_c= $2 \times \pi \times 3 \times 0.31$ =5.652Ω

Capacitive Reactance (x_c) = $\frac{1}{2\pi f C} = \frac{1}{2\pi \times 3 \times 0.0032}$ = 16.58Ω

The combined impedance of the coil is given as $Z_2 =$

$\sqrt{{R_c}^2 + (x_L - x_c)^2} = \sqrt{400^2 + (5.652 - 16.58)^2} = \sqrt{400^2 + (-10.92)^2}$

$Z_2 \cong 400\ \Omega$

Using the above equation for Z_2, the values of load impedance Z_2 for different values of R_L, L and Care obtained. Table 4.13 gives the results of the analysis. The harvested power P_{aveh} for various values of load impedance Z_2 have been obtained at different values of excitation frequency ω. Tables 4.14.and 4.15 give these results.

Table 4.13 Combined load impedance Z_2

Sr. No.	$R_L(\Omega)$	L(H)	C (F)	Z_2 (Ω)
1	400	0.310	0.0032	400.14
2	900	0.310	0.0044	900.01
3	1600	0.510	0.0054	1600
4	2100	0.510	0.0064	2100.12
5	2800	0.700	0.0069	2800.03

Table 4.14 Power harvested P_{aveh} for Z_2 = 400 Ω and 900 Ω

N (rpm)	ω (rad/sec)	ω/ωn	Load Impedance (Z_2) 400Ω		Load Impedance (Z_2) 900Ω	
			V (V)	P (mW)	V (V)	P (mW)
172	18.00	0.945	0.400	0.40	0.900	0.90
176	18.42	0.967	0.500	0.63	1.500	2.50
180	18.84	0.989	1.700	7.23	2.100	4.90
182	***19.05***	***1.000***	***2.000***	***10.00***	***3.500***	***13.61***
184	19.26	1.011	1.800	8.10	3.200	11.38
188	19.68	1.033	1.100	3.03	1.700	3.21
192	20.096	1.055	0.800	1.60	1.200	1.60

Table 4. 15 Power harvested P_{aveh} for Z_2 = 1600Ω, 2100Ω and 2800Ω

N (rpm)	ω (rad/sec)	ω/ωn	Load Impedance (Z_2) 1600Ω		Load Impedance (Z_2) 2100Ω		Load Impedance (Z_2) 2800Ω	
			V (V)	P (mW)	V (V)	P (mW)	V (V)	P (mW)
172	18.00	0.945	0.900	0.51	1.100	0.58	1.100	0.43
176	18.42	0.967	1.800	2.03	1.400	0.93	1.700	1.03
180	18.84	0.989	2.600	4.23	3.700	6.52	3.600	4.63
182	19.05	1.000	4.700	13.81	5.300	13.38	5.500	10.80
184	19.26	1.011	4.200	11.03	4.700	10.52	5.200	9.66
188	19.68	1.033	1.600	1.60	2.400	2.74	2.800	2.80
192	20.096	1.055	1.400	1.23	1.600	1.22	1.700	1.03

Figure 4.21 shows the curves of V_R vs. ω for different values of z_2

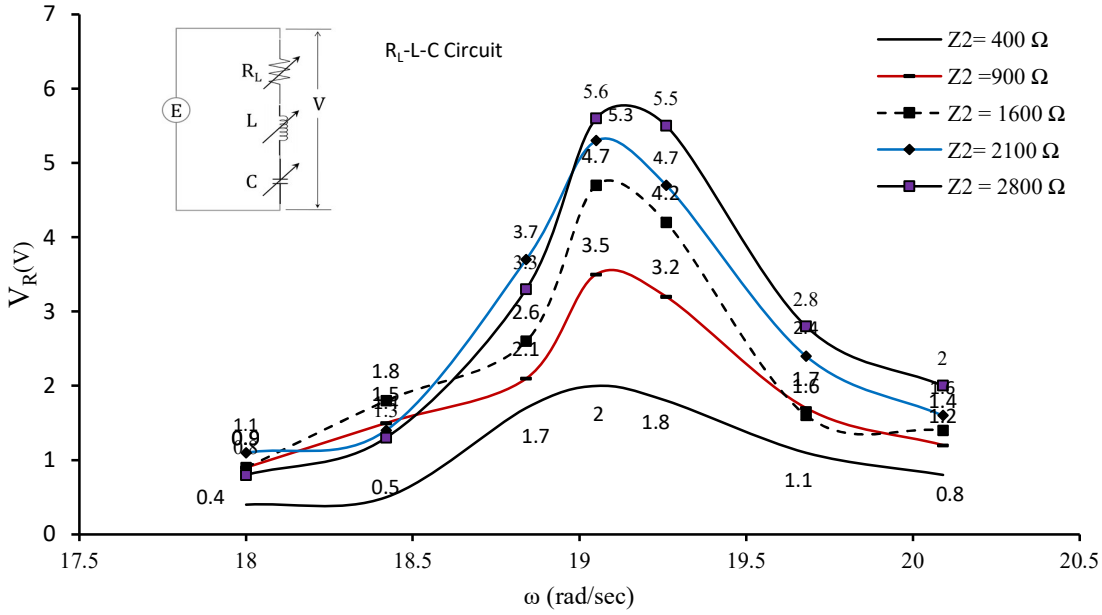

Figure 4.21 Voltage V_R vs.ω

4.4.9 Harvested Power P_{aveh} for Different Values of Z_2

Figure 4.22 shows the curves of P_{aveh} vs. ω for different values of Z_2.

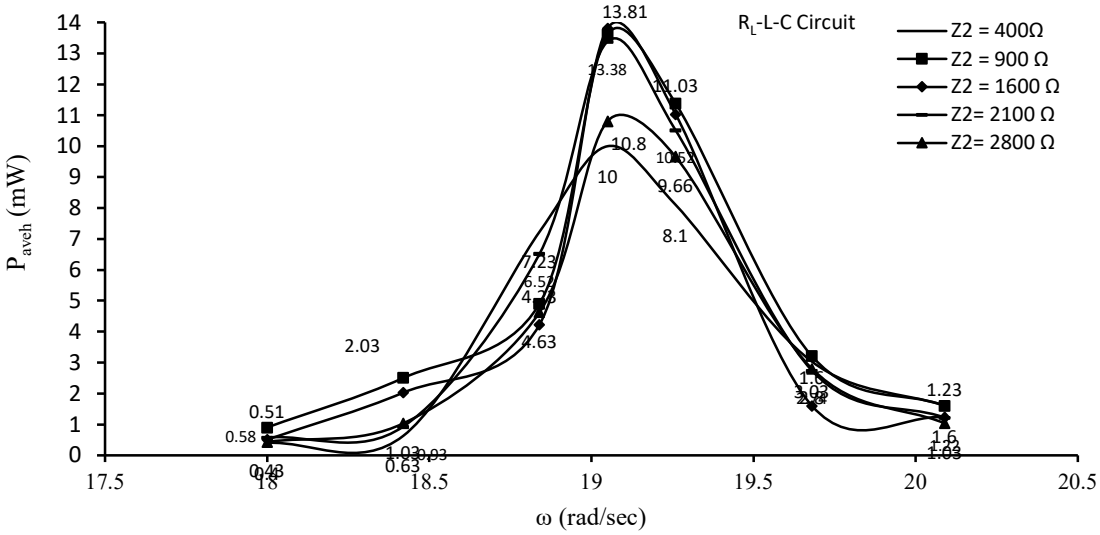

Figure 4.22 Power Harvested P_{aveh} vs. ω for different values of Z_2

The peak value of voltage $V_R$vs.Z_2 are shown in the figure 4.23 and the value of P_{aveh} vs. Z_2 at the resonance are shown in figure 4.24

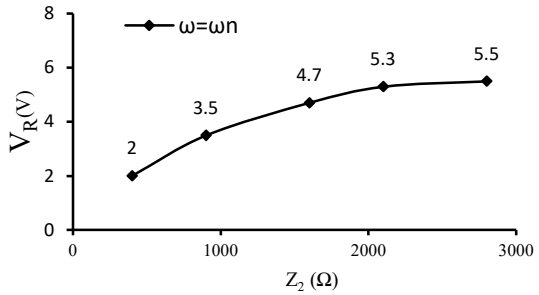

Figure 4. 23 V_R vs. Load Impedance Z_2, at $\omega=\omega_n$

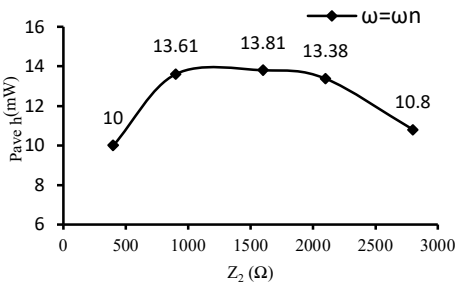

Figure 4. 24 P_{aveh} vs. Load Impedance Z_2, at $\omega=\omega_n$

From figure 4.23, it can be seen that with the increases in the Z_2, the voltage V_R increases and from figure 4.24, it is observed that the value of P_{aveh} is maximum at Z_2 = 1600 **Ω**, and the corresponding P_{aveh} value is 13.81 mW.

4.5 Estimation of Average Power P_{ave} From SDOF VBEH

As per the equation (4.2) of section 4.1, the average power output P_{ave} is given as

$$P_{ave} = \frac{m\zeta_e\left(\frac{\omega}{\omega_n}\right)^3 \omega^3 Y^2}{\left(1-\left(\frac{\omega}{\omega_n}\right)^2\right)^2 + \left(2(\zeta_e+\zeta_m)\frac{\omega}{\omega_n}\right)^2} \quad (4.10)$$

Where the harvester mass is m, excitation frequency is ω, the circular natural frequency of the harvester mass-spring system is ω_n, the amplitude of excitation is Y, the mechanical and electrical damping ratios are ζ_m and ζ_e respectively. Since P_{ave} is controlled by ζ_e the determination of ζ_e is carried out experimentally as per the procedure outlined in section 4.5.1.

4.5.1 Determination of Mechanical Damping Ratio ζ_m

From the experimental setup removing electrical loaf circuit, open circuit voltage E generated vs. time t is obtained (refer to figure 4.25)

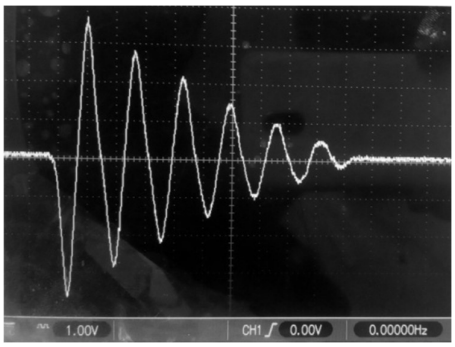

Figure 4.25 Open circuit voltage E vs. time t

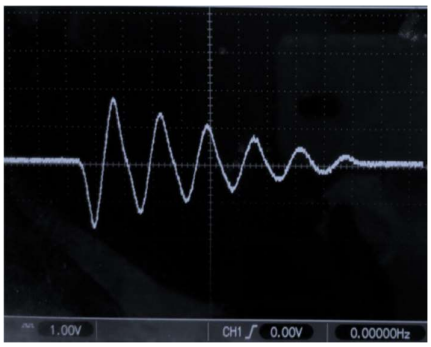

Figure 4.26 Voltage V_R vs. time t

The value of ζ_m was calculated from the transient response curve by logarithmic decrement method as

$$\zeta_m = \frac{\ln\left(\frac{a_1}{a_2}\right)}{\sqrt{(2\pi)^2+\left(\ln\left(\frac{a_1}{a_2}\right)\right)^2}} = \frac{\ln\left(\frac{3.4}{2.9}\right)}{\sqrt{(2\pi)^2+\left(\ln\left(\frac{3.4}{2.9}\right)\right)^2}} = 0.025 \qquad (4.11)$$

Here, a_1 and a_2 are the amplitudes of two successive cycles for the open-circuit voltage vs. time response record.

Now the harvester is connected across the pure resistive impedance of 1600 Ω and the transient curve of voltage across a resistance of 1600 Ω was obtained. From this curve, the total damping ratio ζ was obtained as

$$\text{Total damping ratio}(\zeta) = \frac{\ln\left(\frac{1.8}{1.5}\right)}{\sqrt{(2\pi)^2+\left(\ln\left(\frac{1.8}{1.5}\right)\right)^2}} = \frac{\ln\left(\frac{1.8}{1.5}\right)}{\sqrt{(2\pi)^2+\left(\ln\left(\frac{1.8}{1.5}\right)\right)^2}} = 0.03 \qquad (4.12)$$

4.5.2 Determination of the Electrical Damping Ratio ζ_e by Experimental Analysis (Method 1)

With the help of an experimental setup for testing VBEH connected to a purely resistive load of 1600 Ω, the transient response of VBEH V_R vs. time t is obtained (refer to figure

4.26), where V_R is the voltage across the resistive load. From this graph, using the logarithmic decrement technique, the total damping ratio ζ was estimated as 0.03. Now, total damping ratio $\zeta = \zeta_m + \zeta_e$ has been estimated as 0.025, hence

$$\zeta_e = \zeta - \zeta_m = 0.03 - 0.025 = 0.005$$

4.5.3 Method of Determination of ζ_e from Theoretical Formula (Method 2)

The electrical damping ratio ζ_e is given as [25]

$$\zeta_e = \frac{(NBL)^2}{2\omega_n m\,(R_c+R_L)} \tag{4.13}$$

Where, the total number of turns is N, m is the mass, the circular natural frequency is ω_n,the resistance of the coil is R_C, the resistive load R_L, and the magnetic flux density in the direction of the axis of the magnet is B.

The expression for B is given as [25]

$$B = \frac{B_r}{2}\left[\frac{h_{mag}+x}{\sqrt{R^2+(h_{mag}+x)^2}} - \frac{x}{\sqrt{R^2+x^2}}\right] \tag{4.14}$$

At the point near the magnet pole i.e., x = 0, B is maximum. In the developed vibration transducer, a Neodymium Iron Boron (NdFeB) magnet was selected. Its specifications are height h_{mag}= 0.03m, radius R= 0.005m, and residual magnetic flux density B_r = 0.8T. Using these values of h_{mag}, R, and Br. in equation4.14, the value of B at x=0 is obtained as 0.388T.

Another method used to determine B is by Tesla meter setup (refer to figure 4.27). Two magnets were considered for experimental testing i.e., R = 4 mm and R = 5 mm. Experimental results are given in figure 4.28 (B vs x curves) where 'x' is the distance from the magnet pole face.

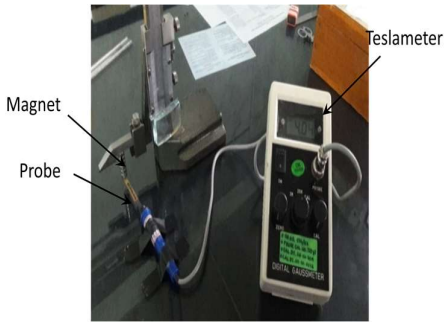

Figure 4. 27 Tesla meter setup

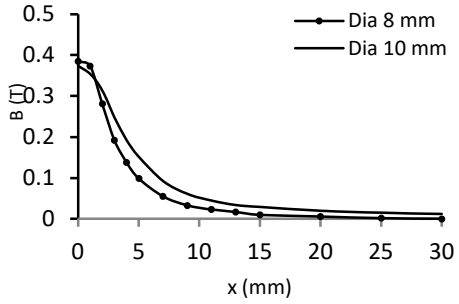

Figure 4. 28 Flux density B vs. Distance x from pole face

For NdFeB (10 mm diameter) magnet B is obtained using Tesla meter setup was 0.390T. It is in close agreement with that obtained from the theoretical formula. Now with B= 0.390T, N= 7790, L= 0.019, m = 4.31 kg,$\omega_n = 19.05\,\text{rad/sec}$, R_c = 1620Ω, and R_L=1600 Ω and substituting in equation 4.14, The value of ζ_e from the method 2 gives the value as 0.008 and it is denoted as ζ_{e2}

4.6 Average Power Output P_{ave} from VBEH

In equation 4.2, the values m = 4.31kg, $\omega_n = 19.05\,\text{rad/sec}$, ζ_m= 0.025, Y=0.001m and $\zeta_e = \zeta_{e1} = 0.005$ are substituted and frequency of excitation ω is varied (in the range of 17.50 to 20.50 rad/sec.). Then the values of power output P_{ave} is obtained as

$$P_{ave} = \frac{m\zeta_e\left(\frac{\omega}{\omega_n}\right)^3\omega^3 Y^2}{\left(1-\left(\frac{\omega}{\omega_n}\right)^2\right)^2+\left(2(\zeta_e+\zeta_m)\frac{\omega}{\omega_n}\right)^2} \quad (4.15)$$

$$P_{ave} = \frac{4.31\times0.005\ x(1)^3\times(19.05)^3\times0.001^2}{(1-(1)^2)^2+(2(0.005+\ .025)\times1))^2}$$

$P_{ave} = \frac{0.000148}{0.0036}$=0.04135 W(at resonance ω = ω_n= 19.03 rad/sec.)

P_{ave} = 41.35 mW

The values of P_{ave} for different values of ω in the range 18 to 20 rad/sec have been calculated and the results are given in table 4.16

Table 4.16 Theoretical and experimental Power output

N (rpm)	ω (rad/sec)	ω/ωn	V (V)	Expt. harvested Power (mW)	Theoretical harvested Power(mW) $\zeta_e = \zeta_{e1}$	Theoretical harvested Power(mW) $\zeta_e = \zeta_{e2}$
172	18.00	0.945	1.00	0.63	7.21	11.03
176	18.42	0.967	1.80	2.02	16.03	23.46
180	18.84	0.989	3.0	5.6	34.83	47.04
182	**19.05**	**1.000**	**4.90**	15	**41.38**	54.72
184	19.26	1.011	4.50	13.22	38.14	51.49
188	19.68	1.033	2.90	5.56	21.66	31.6
192	20.096	1.055	1.80	2.0	12.27	18.82

The plot of P_{ave} vs. ω is, obtained, as shown in figure 4.29**.** The plot of P_{ave} vs. ω is also obtained for the case $\zeta_e = \zeta_{e2}$ = 0.008, and is also shown in figure 4.29.

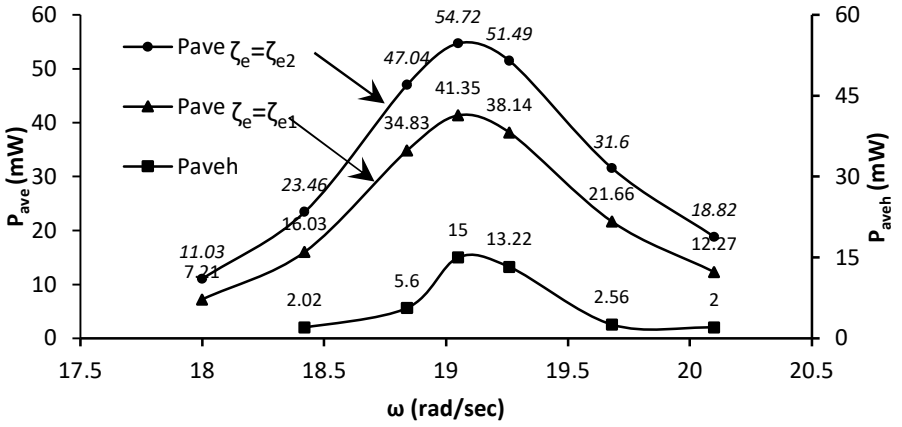

Figure 4. 29 (i) Average power output P_{ave} vs. excitation frequency ω for case $\zeta e = \zeta e_1$, (ii) Average power output P_{ave} vs. excitation frequency ω for case $\zeta e = \zeta e_2$, (iii) Average harvested power output P_{aveh} vs. excitation frequency ω when resistive load is1600Ω

4.7 Discussion on Results

The curves of P_{ave} vs. excitation frequency ω, for $\zeta_e = \zeta_{e1} = 0.005$ and of P_{ave} vs. excitation frequency ω, for $\zeta_e = \zeta_{e2} = 0.008$ and with the resistive load of 1600 Ω (which is approximately equal to the internal resistance of the coil) are shown in figure 4.29. It is seen that the value of P_{ave} based on the electrical damping ratio ζ_{e1} is less than that determined using the theoretical expression for ζ_e (method 2). From the curve of P_{aveh} vs. ω, it can be seen that the average harvested power P_{aveh} is maximum at the resonant frequency when the resistive load is 1600Ω. The value of the average harvested power output is very less than the average generated power output of VBEH.

4.8 Conclusions

1. The influence of variation of resistive, inductive and capacitive impedances of the R – L – C electrical circuit connected on the harvested power output P_{aveh} has been analysed at a various frequency of base excitation of VBEH. It is seen that P_{aveh} has the maximum value at the resonant frequency and it decreases with increase in the electrical load impedance. Hence a judicious choice has to be made for the values of R, L and C in the electrical circuit. Keeping in mind that the undamped electrical natural frequency is to be made equal to the undamped natural frequency of the mechanical sub-system of VBEH.

2. It is observed that P_{aveh} is at maximum at a resistive load of 1600 Ω, which is very close to the internal resistance of the vibration transducer coil. This result is found to be consistent with those published in the literature.
3. From the results of experimental determination of mechanical damping ratio ζ_m and electrical damping ratio ζ_e it is seen that the value of $\zeta_e = \zeta_{e1}$ estimated by method 1 is less than that obtained from method 2 in which analytical expression for ζ_e was used. Hence for accurate prediction of P_{aveh} of VBEH devices, experimental determination of ζ_e is essential. For this purpose, resistive load impedance should be nearly equal to the internal resistance of the transducer coil. This finding will definitely be beneficial in the design of SDOF VBEH.
4. It is observed that the values of P_{ave} based on $\zeta_e = \zeta_{e1}$ (experimental), is less than that obtained using $\zeta_e = \zeta_{e2}$ (using the theoretical formula for ζ_e). Hence the calculation for P_{aveh} should be based on the value of $\zeta_e = \zeta_{e1.}$ Also it is seen that values of both P_{ave} and P_{aveh} are maximum at the resonant frequency. Thus these results are significant and useful for maximization of the harvested power output of SDOF vibration-based electromagnetic energy harvesters (VBEHs).

Chapter – 5

ENHANCING THE POWER OUTPUT AND WIDENING OPERATIONAL BANDWIDTH OF VIBARTION-BASED ELECTROMAGNETIC ENERGY HARVESTER

5.0 Introduction

From the studies on a single degree of freedom vibration-based electromagnetic energy harvester (SDOF VBEH) devices, it is seen that the output power of an SDOF VBEH is low mainly because of its narrow operating frequency range (most of the power output is at resonance condition). The power output falls sharply at off the resonance condition. To overcome this problem, the researchers have worked on various techniques either to increase the power output of SDOF VBEH or to widen the operating range of base excitation frequency or both.

Yildirim et al. [39] have presented an excellent review paper on the techniques of enhancing the power output and widening of the operating frequency range. The prominent among these techniques are mechanical amplification techniques and the method of using nonlinearities. These techniques are useful for increasing the power output as well as for widening the useful excitation frequency range of SDOF VBEH devices.

Tang and Zuo [28] have discussed the method of enhancing the power output and increasing the operating frequency range of SDOF VBEH devices using a dual-mass system.

Therefore, in this chapter, the results of the theoretical and experimental analysis of two degree of freedom (2DOF) VBEH device is carried out in the approach of Tang and Zuo, with a view to increase its power output and to widen the operating frequency range. For this purpose, an SDOF VBEH system has been transformed into a 2DOF VBEH system by adding a mechanical spring-mass system in series with the SDOF VBEH system. Analytical expressions are obtained for the power output of both the SDOF and transformed 2DOF system VBEH devices. The effect of (i) varying the mass ratio, i.e., the ratio of harvester mass to the mass of the amplifier system, on the maximum power output is studied. (ii) also, the effect of tuning ratio and mass ratio on the useful operating range and shunted electrical resistive load on the maximum power has been analyzed. The

tuning ratio is defined as the ratio of the natural frequency of the harvester system to the natural frequency of the amplifier system when considered separately.

5.1 SDOF VBEH Transformed into 2DOF VBEH

The schematic representation of SDOF and 2DOF VBEH taken up for analysis is shown in figure 5.1(a) and figure 5.1(b).

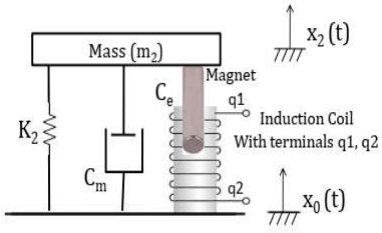

Figure 5.1 Schematic of SDOF VBEH

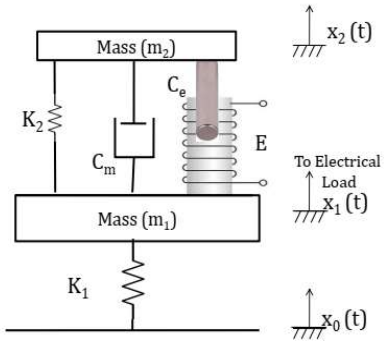

Figure 5.2 Schematic of 2DOF VBEH

In figure 5.1 SDOF harvester system is shown. It is subjected to base excitation $x_0(t) = X_0\, sin\omega t$. where ω is circular excitation frequency. Figure 5.2 shows a 2DOF system in which the harvester system (m_2, k_2, c_m, c_e) is mounted on the mechanical amplifier system (m_1, k_1). It is base excited by $x_0(t) = X_0\, sin\omega t$. In the SDOF system, a cylindrical magnet is connected to harvester mass m_2 and an electrical coil is connected to base plate which is excited by a cam driven by an electrical motor. In the 2DOF system magnet is connected to harvester mass m_2 and electrical coil is connected to mechanical amplifier mass m_1. The relative motion between magnet and coil, in-line configuration produces an electromotive force (EMF), which gives rise to open circuit voltage E between the terminals q_1 and q_2 of the electrical coil to which the electrical load is connected. c_m is the mechanical damping coefficient and c_e is electrical damping coefficient.

5.1.1 Average Power Output Pave of a SDOF VBEH

The average power output P_{ave} of SDOF VBEH is given as refer section 3.4 in chapter 3.

$$P_{ave} = \frac{m_2 \omega^3 X_1 \zeta_e \left(\frac{\omega}{\omega_2}\right)^3}{\left(1 - \left(\frac{\omega}{\omega_2}\right)^2\right)^2 + \left(2(\zeta_e + \zeta_m)\frac{\omega}{\omega_2}\right)^2} \tag{5.1}$$

Where, m_2 is harvester mass, X_0 is amplitude of base excitation, ζ_e is the electrical damping ratio, ζ_m is the mechanical damping ratio, ω_2 is natural frequency of the harvester system,

ω is base excitation frequency.

The non-dimensional average power output P_{aven} is obtained from equation 5.1

$$P_{aven} = \frac{P_{ave}}{m_2 \omega^3 X_1} = \frac{\zeta_e \left(\frac{\omega}{\omega_2}\right)^3}{\left(1 - \left(\frac{\omega}{\omega_2}\right)^2\right)^2 + \left(2(\zeta_e + \zeta_m)\frac{\omega}{\omega_2}\right)^2} \quad (5.2)$$

5.1.2 Design Development and Analysis of 2DOF VBEH Device

In the paper by Tang and Zuo [28], an expression for non-dimensional power output of a 2DOF vibration energy harvester has been given without its derivation. As such, the expression for non-dimensional power output P_{aven} has been derived from the first principles. A schematic of a 2DOF VBEH is shown in figure 5.2.

Referring figure 2, one can write equations of motion of mass m_2 and m_1 respectively as,

$$m_2 \ddot{x_2} \uparrow = -k_2(x_2 - x_1) \downarrow - c\,(\dot{x_2} - \dot{x_1}) \downarrow \quad (5.3)$$

$$m_1 \ddot{x_1} \uparrow = -k_2(x_1 - x_2) \downarrow - c(\dot{x_1} - \dot{x_2}) \downarrow - k_1(x_1 - x_0) \downarrow \quad (5.4)$$

Where $c = c_m + c_e$, the relative displacement z between mass m_2 and mass m_1 is $z = x_2 - x_1$, hence, $\dot{z} = \dot{x_2} - \dot{x_1}$ and $\ddot{z} = \ddot{x_2} - \ddot{x_1}$ Substituting these values in equations (5.3) and (5.4) and after simplification we get,

$$m_2 \ddot{z} + k_2 z + c\dot{z} = -m_2 \ddot{x_1} \qquad and \quad (5.5)$$

$$m_1 \ddot{x_1} + k_1 x_1 - k_2 z - c\dot{z} - k_1 x_0 = 0 \quad (5.6)$$

Take complex forms of variables as $z = Ze^{j\omega t}$, $x_1 = X_1 e^{j\omega t}$, and $x_0 = X_0 e^{j\omega t}$

then $\dot{z} = j\omega Z e^{j\omega t}$ and $\ddot{z} = -\omega^2 Z e^{j\omega t}$, $\dot{x_1} = j\omega X_1 e^{j\omega t}$ and $\ddot{x_1} = -\omega^2 X_1 e^{j\omega t}$

Substituting these values in equation (5.5) and (5.6). we get equation (5.5) in the form

$$m_2 \omega^2 Z + k_2 Z + c(j\omega Z) = + m_2 \omega^2 X_1 \qquad or$$

$[(k_2 - m_2 \omega^2) + jc\omega]Z = m_2 \omega^2 X_1$ then

$$X_1 = \frac{[(k_2 - m_2 \omega^2) + jc\omega]Z}{m_2 \omega^2} \quad (5.7)$$

Similarly, we get the equation (5.6) in the form

$$-m_1 \omega^2 X_1 + k_1 X_1 - k_2 Z - cj\omega Z - k_1 X_0 = 0$$

$$(k_1 - m_1 \omega^2) X_1 - (k_2 + cj\omega) Z = k_1 X_0 \quad (5.8)$$

Substituting value of X_1, from equation (5.7) in equation (5.8) we get,

$$\left\{(k_1-m_1\ \omega^2)\left[\frac{(k_2-m_2\ \omega^2)+jc\omega}{m_2\,\omega^2}\right]-(k_2+cj\omega)\right\}Z=k_1X_0,\quad \text{or}$$

$$[(k_1-m_1\ \omega^2)(k_2-m_2\ \omega^2)+jc\omega(k_1-m_1\ \omega^2)-(k_2+cj\omega)m_2\,\omega^2]$$

$$=m_2\,\omega^2k_1X_0 \qquad (5.9)$$

$$[k_1k_2-k_1\,m_2\omega^2-k_2m_1\omega^2+m_1m_2\,\omega^4+jc\omega k_1-jc\omega m_1\omega^2-k_2m_2\,\omega^2-cj\omega^3m_2\,]Z=k_1m_2\,\omega^2X_0$$

$$\{[k_1k_2-(k_1\,m_2+k_2m_1+k_2m_2)\omega^2+\ m_1m_2\,\omega^4]+jc[\omega k_1-(m_1+m_2\,)\omega^3]\}Z$$

$$=k_1m_2\,\omega^2X_0 \qquad (5.10)$$

Putting

$a_1=[k_1k_2-(k_1\,m_2+k_2m_1+k_2m_2)\omega^2+\ m_1m_2\,\omega^4]$

$a_2=c[\omega k_1-(m_1+m_2\,)\omega^3]=(k_1-(m_1+m_2\,)\omega^2)c\omega$, and

$a_3=k_1m_2\omega^{2``}$

we can rewrite equation (5.10) in the form as,

$$\mathrm{Z}=\left(\frac{\mathrm{a_3}}{\mathrm{a_1+ja_2}}\right)\mathrm{X_0}\quad\text{or}\quad \mathrm{Z^2}=\left(\frac{{\mathrm{a_3}}^2}{{\mathrm{a_1}}^2+{\mathrm{a_2}}^2}\right){\mathrm{X_0}}^2 \qquad (5.11)$$

Now, the average harvested power output P of 2DOF VBEH is defined as

$$\mathrm{P}=\text{Power output}=\int_0^{\mathrm{v}}\mathrm{f}\,\mathrm{dv}$$

Where f is electromagnetic force induced in copper coil and magnet due to their relative velocity. We have $\dot{z}=(\dot{x}_2-\dot{x_1})$ hence$f=\mathrm{c_e}\,\dot{z}=\mathrm{c_e}\,(\dot{x}_2-\dot{x_1})$

using, this relation, the equation of the average power output $\mathrm{P_{ave}}$ is obtained as

$$\mathrm{P_{ave}}=\int_0^z\dot{z}\,\mathrm{dz}=\frac{1}{2}\mathrm{c_e}\,\lfloor\dot{z}^2\rfloor \quad \text{or} \quad \mathrm{P_{ave}}=\frac{1}{2}\mathrm{c_e}\,(\dot{x}_2-\dot{x_1})^2 \qquad (5.12)$$

Maximum Average Power output $\mathrm{P_{ave}}$ is given as,

$$\mathrm{P_{ave}}=\frac{1}{2}\mathrm{c_e}\,(\omega\mathrm{X_2}-\omega\mathrm{X_1})^2 \qquad \text{or}$$

$$\mathrm{P_{ave}}=\frac{1}{2}\mathrm{c_e}\,\omega^2(\mathrm{X_2}-\mathrm{X_1})^2 \qquad (5.13)$$

Where, $\mathrm{X_2}$ and $\mathrm{X_1}$ are amplitudes of $x_2(t)$ and $x_1(t)$ respectively

Substituting $\mathrm{Z}=(\mathrm{X_2}-\mathrm{X_1})$ in equation (5.11) and using the values of a_1,a_2, *and* a_3 just defined

We can write,

$$\mathrm{Z^2}=(\mathrm{X_2}-\mathrm{X_1})^2$$

$$=\left[\frac{\left({k_1}^2{m_2}^2\omega^4\right){\mathrm{X_0}}^2}{\left(k_1k_2-(k_1\,m_2+k_2m_1+k_2m_2)\omega^2+\ m_1m_2\,\omega^4\right)^2+\left[(k_1-(m_1+m_2\,)\omega^2)\right]^2c^2\omega^2}\right] \qquad (5.14)$$

Substituting equation (5.14) in equation (5.13), we get maximum average power output $\mathrm{P_{ave}}$ as

$$\mathrm{P_{ave}}=\left[\frac{\frac{1}{2}\mathrm{c_e}\,\omega^2\left({k_1}^2{m_2}^2\omega^4\right){\mathrm{X_0}}^2}{\left(k_1k_2-(k_1\,m_2+k_2m_1+k_2m_2)\omega^2+\ m_1m_2\,\omega^4\right)^2+\left[(k_1-(m_1+m_2\,)\omega^2)\right]^2c^2\omega^2}\right] \qquad (5.15)$$

We have $c = c_m + c_e$, where $c_m = 2\,\zeta_m\, m_2\, \omega_2$ and $c_e = 2\,\zeta_e\, m_2\, \omega_2$ hence

$c = 2(\zeta_m + \zeta_e) m_2\, \omega_2$ and $c^2 = 4(\zeta_m + \zeta_e)^2 m_2{}^2 \omega_2{}^2$

Using the value of c^2 and c_e just defined, in equation (5.15), we can write,

$$P_{ave} = \left[\frac{\frac{1}{2} \times 2\,\zeta_e m_2\, \omega_2 \omega^2 \left(k_1{}^2 m_2{}^2 \omega^4\right) X_0{}^2}{\left(k_1 k_2 - (k_1 m_2 + k_2 m_1 + k_2 m_2)\omega^2 + m_1 m_2\, \omega^4\right)^2 + \left[(k_1 - (m_1 + m_2)\omega^2)\right]^2 4(\zeta_m + \zeta_e)^2 m_2{}^2 \omega_2{}^2 \omega^2} \right] \quad (5.16)$$

The non-dimensional average power output P_{aven} can be written as,

$$P_{aven} = \frac{P_{ave}}{X_0{}^2 \omega_1{}^3 m_1} \quad (5.17)$$

Where the term $X_0{}^2 \omega_1{}^3 m_1$ has the dimensions of the power

Substituting equation (5.15) in equation (5.17), we get,

$$P_{aven} = \left[\frac{\frac{\zeta_e m_2\, \omega_2 \omega^2 k_1{}^2 m_2{}^2 \omega^4}{\omega_1{}^3 m_1}}{\left(k_1 k_2 - (k_1 m_2 + k_2 m_1 + k_2 m_2)\omega^2 + m_1 m_2\, \omega^4\right)^2 + \left[(k_1 - (m_1 + m_2)\omega^2)\right]^2 4(\zeta_m + \zeta_e)^2 m_2{}^2 \omega_2{}^2 \omega^2} \right] \quad (5.18)$$

Consider the Numerator N of equation (5.18)

$$N = \frac{\zeta_e m_2\, \omega_2 \omega^2 k_1{}^2 m_2{}^2 \omega^4}{\omega_1{}^3 m_1}$$

$$N = \frac{\zeta_e m_2}{m_1} \times \left(\frac{\omega_2}{\omega_1}\right)\left(\frac{\omega^2}{\omega_1{}^2}\right)\left(k_1{}^2 m_2{}^2 \omega^4\right)$$

$$N = \zeta_e\, \mu\, f\, \alpha^2 \left(k_1{}^2 m_2{}^2 \omega^4\right)$$

$$N = \zeta_e\, \mu\, f\, \alpha^2 \left(k_1{}^2 m_2{}^2 \omega^4\right)\left(\frac{\omega_1{}^4}{\omega_1{}^4}\right)$$

$$N = \zeta_e\, \mu\, f\, \alpha^2 \left(k_1{}^2 m_2{}^2\right)\alpha^4 \omega_1{}^4$$

$$N = \zeta_e\, \mu\, f\, \alpha^6 k_1{}^2 m_2{}^2 \omega_1{}^4$$

Where $\mu = \frac{m_2}{m_1}$ is the mass ratio, $f = \frac{\omega_2}{\omega_1}$ is the tuning ratio and $\alpha = \frac{\omega}{\omega_1}$ is the frequency ratio.

Using the above value of numerator N of the equation (5.18) we get,

$$P_{aven} = \left[\frac{\zeta_e\, \mu\, f\, \alpha^6 k_1{}^2 m_2{}^2 \omega_1{}^4}{\left(k_1 k_2 - (k_1 m_2 + k_2 m_1 + k_2 m_2)\omega^2 + m_1 m_2\, \omega^4\right)^2 + \left[(k_1 - (m_1 + m_2)\omega^2)\right]^2 4(\zeta_m + \zeta_e)^2 m_2{}^2 \omega_2{}^2 \omega^2} \right]$$

$$P_{aven} = \left[\frac{\zeta_e\, \mu\, f\, \alpha^6}{\frac{\left(k_1 k_2 - (k_1 m_2 + k_2 m_1 + k_2 m_2)\omega^2 + m_1 m_2\, \omega^4\right)^2}{k_1{}^2 m_2{}^2 \omega_1{}^4} + \frac{\left[(k_1 - (m_1 + m_2)\omega^2)\right]^2 4(\zeta_m + \zeta_e)^2 m_2{}^2 \omega_2{}^2 \omega^2}{k_1{}^2 m_2{}^2 \omega_1{}^4}} \right]$$

$$= \frac{\zeta_e \mu f \alpha^6}{\left[\frac{k_1 k_2}{k_1 m_2 {\omega_1}^2} - \left(\frac{k_1 m_2 + k_2 m_1 + k_2 m_2}{k_1 m_2 {\omega_1}^2}\right)\omega^2 + \left(\frac{m_1 m_2 \omega^4}{k_1 m_2 {\omega_1}^2}\right)\right]^2 + \left[\frac{k_1}{k_1 m_2 {\omega_1}^2} - \frac{(m_1+m_2)\omega^2}{k_1 m_2 {\omega_1}^2}\right]^2 4(\zeta_m + \zeta_e)^2 m_2{}^2 \omega_2{}^2 \omega^2}$$

$$= \frac{\zeta_e \mu f \alpha^6}{D_1 + D_2} \tag{5.19}$$

We have

$$D_1 = \left[\frac{k_1 k_2}{{\omega_1}^2 k_1 m_2} - \left(\frac{k_1 m_2 + k_2 m_1 + k_2 m_2}{{\omega_1}^2 k_1 m_2}\right)\omega^2 + \left(\frac{m_1 m_2 \omega^4}{{\omega_1}^2 k_1 m_2}\right)\right]^2$$

$$= \left[\left(\frac{\omega_2}{\omega_1}\right)^2 - \left(\frac{1}{{\omega_1}^2} + \frac{\mu f^2}{\mu {\omega_1}^2} + \frac{\mu f^2}{{\omega_1}^2}\right)\omega^2 + \frac{1}{{\omega_1}^2}\frac{1}{{\omega_1}^2}(\omega)^4\right]^2$$

$$= \left[f^2 - (1 + f^2 + \mu f^2)\frac{\omega^2}{{\omega_1}^2} + \frac{\omega^4}{{\omega_1}^4}\right]^2$$

$$= [f^2 - (1 + f^2 + \mu f^2)\alpha^2 + \alpha^4]^2$$

$$= [\alpha^4 + f^2 - (1 + (1 + \mu)f^2)\alpha^2]^2 \tag{5.20}$$

$$D_2 = \left[\frac{k_1}{k_1 m_2 {\omega_1}^2} - \frac{(m_1 + m_2)\omega^2}{k_1 m_{2{\omega_1}^2}}\right]^2 4(\zeta_m + \zeta_e)^2 m_2{}^2 \omega_2{}^2 \omega^2$$

$$= 4(\zeta_m + \zeta_e)^2 \left[\frac{k_1}{k_1 m_2 {\omega_1}^2} - \frac{(m_1 + m_2)\omega^2}{k_1 m_2 {\omega_1}^2}\right]^2 m_2{}^2 \omega_2{}^2 \omega^2$$

$$= 4(\zeta_m + \zeta_e)^2 \left[\frac{k_1 m_2 \omega_2 \omega}{k_1 m_2 {\omega_1}^2} - \frac{(m_1 m_2 \omega_2 \omega + m_2 m_2 \omega_2 \omega)\omega^2}{k_1 m_2 {\omega_1}^2}\right]^2$$

$$= 4(\zeta_m + \zeta_e)^2 \left[\frac{k_1 m_2 \omega_2 \omega}{k_1 m_2 {\omega_1}^2} - \left[\frac{m_1 m_2 \omega_2 \omega}{k_1 m_2 {\omega_1}^2} + \frac{(m_2 m_2 \omega_2 \omega)}{k_1 m_2 {\omega_1}^2}\right]\omega^2\right]^2$$

$$= 4(\zeta_m + \zeta_e)^2 \left[\frac{\omega_2}{\omega_1}\frac{\omega}{\omega_1} - \left[\frac{1}{{\omega_1}^2}\frac{\omega_2 \omega^3}{{\omega_1}^2} + \frac{m_2}{k_2}\frac{k_2}{k_1}\frac{(\omega_2 \omega^3)}{{\omega_1}^2}\right]\right]^2$$

$$= 4(\zeta_m + \zeta_e)^2 \left[f\alpha - \left[\frac{\omega_2}{\omega_1}\left(\frac{\omega}{\omega_1}\right)^3 + \frac{1}{{\omega_2}^2}\mu f^2 \frac{(\omega_2 \omega^3)}{{\omega_1}^2}\right]\right]^2$$

$$= 4(\zeta_m + \zeta_e)^2 \left[f\alpha - \left[f\alpha^3 + \mu f^2 \frac{\omega}{\omega_2}\left(\frac{\omega}{\omega_1}\right)^2\right]\right]^2$$

$$= 4(\zeta_m + \zeta_e)^2 \left[f\alpha - \left[f\alpha^3 + \mu f^2 \frac{\omega}{\omega_1}\frac{\omega_1}{\omega_2}\alpha^2\right]\right]^2$$

$$= 4(\zeta_m + \zeta_e)^2 \left[f\alpha - \left[f\alpha^3 + \mu f^2 \alpha \frac{1}{f}\alpha^2\right]\right]^2$$

$$= 4(\zeta_m + \zeta_e)^2 [f\alpha - [f\alpha^3 + \mu f \alpha^3]]^2$$

$$= 4(\zeta_m + \zeta_e)^2 [f\alpha - (1 + \mu)f\alpha^3]^2 \tag{5.21}$$

Putting the values of D_1 and D_2, just obtained, in equation (5.19),

we can write the non-dimensional output power P_{aven} of 2DOF VBEH as

$$P_{aven} = \frac{\zeta_e \mu f \alpha^6}{\left[\alpha^4 + f^2 - \left(1 + (1+\mu)f^2\right)\alpha^2\right]^2 + 4(\zeta_e + \zeta_m)^2[f\alpha - (1+\mu)f\alpha^3]^2} \quad (5.22)$$

From equation 5.22 it is seen that P_{aven} depends on

i. Electrical damping ratio ζ_e and mechanical damping ratio ζ_m

ii. Harvester mass m_2 to amplification mass m_1 i.e., mass ratio μ

iii. Tuning ratio $f = = \frac{\omega_2}{\omega_1}$

iv. Frequency ratio $\alpha = = \frac{\omega}{\omega_1}$

5.3. Effective Non-Dimensional Frequency Band $\overline{b_e}$ of a 2DOF VBEH

If we remove electrical sub system from 2DOF VBEH and assume that the mechanical damping and electrical damping as zero i.e., $\zeta_m = \zeta_e = 0$, an undamped 2 DOF vibrating system results as shown in figure 5.2

Using well founded theory of vibration, we can write the equation of motion of mass m_2 as,

$$m_2\ddot{x}_2 = -k_2(x_2 - x_1) \quad \text{or}$$
$$m_2\ddot{x}_2 + k_2(x_2 - x_1) = 0 \quad (5.23)$$

Equation of motion of mass m_1 as

$$m_1\ddot{x}_1 = -k_2((x_1 - x_2) - k_1(x_1 - x_0)$$
$$m_1\ddot{x}_1 + k_1(x_1 - x_0) + k_2(x_1 - x_2) = 0$$

For free vibration, set $x_0 = 0$, then equation of mass m_1 is

$$m_1\ddot{x}_1 + k_1x_1 + k_2(x_1 - x_2) = 0 \quad (5.24)$$

Setting $x_1 = X_1 \sin\omega_n t$ and $x_2 = X_2 \sin\omega_n t$ Where,$X_1$and X_2 are respectively the amplitudes of free vibration of mass m_1 and m_2, ω_n is the circular natural frequency. Substitute x_1 (t) and x_2 (t) in equation (5.23) and (5.24). Solving the equation (5.23) and (5.24) for X_1 and X_2. The frequency equation is obtained as

$$\omega_n{}^4 - \left[\frac{k_2}{m_2} + \frac{k_1}{m_1} + \frac{k_2}{m_1}\right]\omega_n{}^2 + \frac{k_1 k_2}{m_1 m_2} = 0 \quad (5.25)$$

Setting, Mass ratio$= \mu = \frac{m_2}{m_1}$, $\omega_2 = \sqrt{\frac{k_2}{m_2}}$, $\omega_1 = \sqrt{\frac{k_1}{m_1}}$, Tuning ratio $= f = \frac{\omega_2}{\omega_1}$ and

substituting in equation (5.25), and after simplifying, we get

$$\frac{\omega_n{}^4}{\omega_1{}^4} - [1 + (1+\mu)f^2]\frac{\omega_n{}^2}{\omega_1{}^2} + f^2 = 0 \quad (5.26)$$

Setting, $\frac{\omega_n{}^2}{\omega_1{}^2} = \overline{\omega_n}^2$ in non-dimensional form and solving the equation (5.26) for $\overline{\omega_n}^2$, we get the dimensionless undamped natural frequency equation as

$$\overline{\omega_n}^2 = \frac{[1+(1+\mu)f^2]}{2} \pm \sqrt{\left[\frac{1+(1+\mu)f^2}{2}\right]^2 - f^2} \tag{5.27}$$

From the equation (5.27), we get, non-dimensional first mode frequency $\overline{\omega_{n_1}}$,as

$$\overline{\omega_{n_1}} = \sqrt{\frac{[1+(1+\mu)f^2]}{2} - \sqrt{\left[\frac{1+(1+\mu)f^2}{2}\right]^2 - f^2}} \tag{5.28}$$

Non-dimensional second mode frequency $\overline{\omega_{n_2}}$, as

$$\overline{\omega_{n_2}} = \sqrt{\frac{[1+(1+\mu)f^2]}{2} + \sqrt{\left[\frac{1+(1+\mu)f^2}{2}\right]^2 - f^2}} \tag{5.29}$$

One can define now the effective or operational non-dimensional band width $\overline{b_e}$ as

$$\overline{b_e} = \overline{(\omega_{n_2} - \omega_{n_1})} \tag{5.30}$$

It is seen from equations (5.28) and (5.29) that the non-dimensional bandwidth $\overline{b_e}$ of the 2DOF system depends on the mass ratio μ and tuning ratio f.

5.3.1 Effect of mass ratio μ on undamped circular natural frequencies $\overline{\omega_{n1}}$ and $\overline{\omega_{n2}}$

Using, equation (5.28) and (5.29) curves of undamped natural frequencies $\overline{\omega_{n_1}}$ and $\overline{\omega_{n_2}}$ vs. μ for cases f = 1.0, 0.8 and 1.2 are obtained as shown respectively in figures 5.3, 5.4 and 5.5 shown in table 5.1,5.2, and 5.3 where μ is varied from 0 to 1.0. In each case the effective non-dimensional bandwidth $\overline{b_e}$ is calculated as $\overline{b_e} = \overline{\omega_{n_2}} - \overline{\omega_{n_1}}$. The summary of these results is given in figure 5.6 as curves of $\overline{b_e}$ vs. μ

Table 5. 1 Effect of μ on b for f=1

μ	$\overline{\omega_{n1}}$	$\overline{\omega_{n2}}$	$\overline{b_e}$
0	1.000	1.000	0.000
0.1	0.854	1.171	0.316
0.2	0.801	1.248	0.447
0.3	0.763	1.311	0.548
0.4	0.733	1.365	0.632
0.5	0.707	1.414	0.707
0.6	0.685	1.460	0.775
0.7	0.666	1.502	0.837
0.8	0.648	1.543	0.894
0.9	0.632	1.581	0.949
1.0	0.618	1.618	1.000

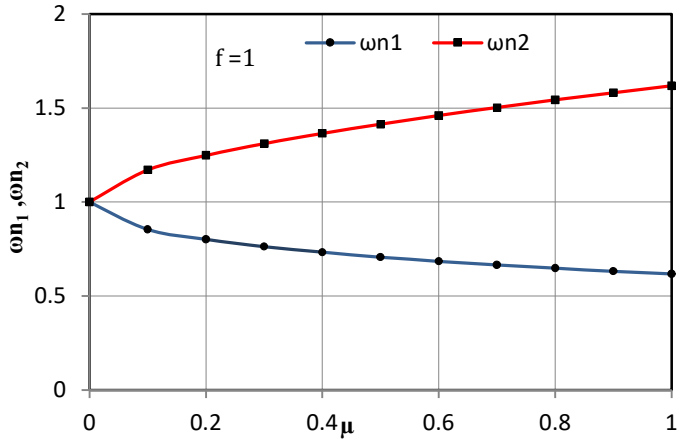

Figure 5. 3 Undamped natural frequencies $\overline{\omega_{n1}}$ and $\overline{\omega_{n2}}$ vs. μ for f = 1

Table 5. 2 Effect of μ on b for f= 0.8

μ	$\overline{\omega_{n1}}$	$\overline{\omega_{n2}}$	$\overline{b_e}$
0	0.800	1.000	0.200
0.1	0.748	1.070	0.322
0.2	0.713	1.123	0.410
0.3	0.685	1.167	0.482
0.4	0.663	1.207	0.544
0.6	0.626	1.277	0.651
0.7	0.611	1.309	0.699
0.8	0.597	1.340	0.743
0.9	0.584	1.369	0.785
1.0	0.573	1.397	0.825
0.6	0.626	1.277	0.651

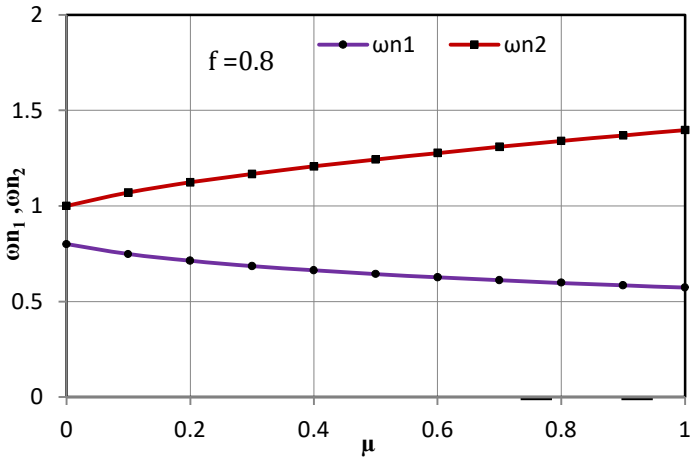

Figure 5. 4 Undamped natural frequencies $\overline{\omega_{n1}}$ and $\overline{\omega_{n2}}$ vs. μ for f = 0.8

Table 5. 3 Effect of μ on b for f=1.2

μ	$\overline{\omega_{n1}}$	$\overline{\omega_{n2}}$	$\overline{b_e}$
0	1.000	1.200	0.200
0.1	0.902	1.331	0.429
0.2	0.846	1.419	0.573
0.3	0.805	1.492	0.687
0.4	0.771	1.556	0.785
0.6	0.719	1.670	0.951
0.7	0.697	1.721	1.024
0.8	0.678	1.770	1.092
0.9	0.661	1.816	1.156
1.0	0.645	1.861	1.217

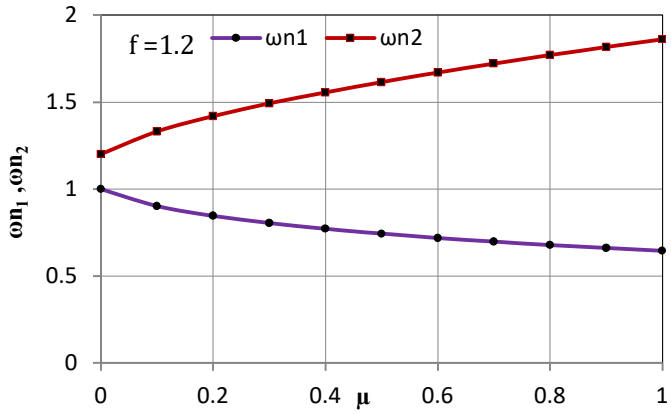

Figure 5. 5 Undamped natural frequencies $\overline{\omega_{n1}}$ and $\overline{\omega n2}$ vs. μ for f = 1.2

Table 5. 4 Effect of Band width b on mass ratio μ for f = 0.8, 1.0, 1.2

Using table 5.1, 5.2, 5.3, and equation 5.30 for '$\overline{b_e}$', we get

μ	$\overline{b_e}$ (f=0.8)	$\overline{b_e}$ (f=1)	$\overline{b_e}$ (f=1.2)
0	0.200	0.000	0.200
0.1	0.322	0.316	0.429
0.2	0.410	0.447	0.573
0.3	0.482	0.548	0.687
0.4	0.544	0.632	0.785
0.5	0.600	0.707	0.872
0.6	0.651	0.775	0.951
0.7	0.699	0.837	1.024
0.8	0.743	0.894	1.092
0.9	0.785	0.949	1.156
1.0	0.825	1.000	1.217

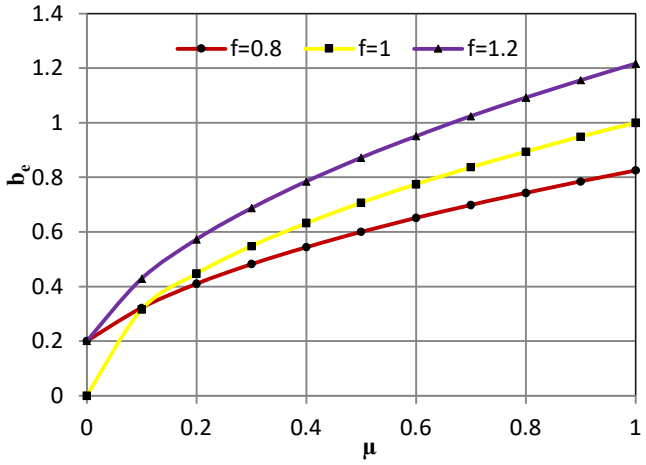

Figure 5.6 Band width b_e vs. mass ratio μ for f = 0.8, 1 and 1.2

5.3.2 Effect of Tuning Ratio f on Undammed Circular Natural Frequency $\overline{\omega_{n1}}$ and $\overline{\omega_{n2}}$

Spread or bandwidth, b = $(\overline{\omega_{n_2}} - \overline{\omega_{n_1}})$ for mass ratio μ = 0.2, 0.3, 0.4, 0.5, 0.6, and 0.7 for various values of tuning ratio μ, are calculated using equation (5.6) and (5.7) The result of analysis are given in Tables 5.5 and 5.6 and curves of figure 5.7, 5.8 and 5.9

Table 5.5 Effect of f on b for μ=0.2, 0.3, 0.4, 0.5, 0.6, and 0.7

f	μ= 0.2			μ= 0.3			μ= 0.4		
	$\overline{\omega_{n1}}$	$\overline{\omega_{n2}}$	$\overline{b_e}$	$\overline{\omega_{n1}}$	$\overline{\omega_{n2}}$	$\overline{b_e}$	$\overline{\omega_{n1}}$	$\overline{\omega_{n2}}$	$\overline{b_e}$
0	0.000	1.000	1.000	0.000	1.000	1.000	0.000	1.000	1.000
0.2	0.199	1.004	0.805	0.199	1.006	0.807	0.198	1.008	0.810
0.4	0.393	1.019	0.626	0.389	1.028	0.639	0.386	1.037	0.651
0.6	0.570	1.052	0.482	0.558	1.076	0.518	0.547	1.098	0.551
0.8	0.713	1.123	0.410	0.685	1.167	0.482	0.663	1.207	0.544
1.0	0.801	1.248	0.447	0.763	1.311	0.548	0.733	1.365	0.632
1.2	0.846	1.419	0.573	0.805	1.492	0.687	0.771	1.556	0.785
f	**μ= 0.5**			**μ= 0.6**			**μ= 0.7**		
	$\overline{\omega_{n1}}$	$\overline{\omega_{n2}}$	$\overline{b_e}$	$\overline{\omega_{n1}}$	$\overline{\omega_{n2}}$	$\overline{b_e}$	$\overline{\omega_{n1}}$	$\overline{\omega_{n2}}$	$\overline{b_e}$
0	0.000	1.000	1.000	0.000	1.000	1.000	0.000	1.000	1.000
0.2	0.198	1.010	0.812	0.198	1.012	0.815	0.197	1.014	0.817
0.4	0.382	1.046	0.663	0.379	1.055	0.675	0.376	1.063	0.687
0.6	0.536	1.119	0.583	0.526	1.140	0.613	0.518	1.159	0.642
0.8	0.643	1.243	0.600	0.626	1.277	0.651	0.611	1.309	0.699
1.0	0.707	1.414	0.707	0.685	1.460	0.775	0.666	1.502	0.837
1.2	0.743	1.615	0.872	0.719	1.670	0.951	0.697	1.721	1.024

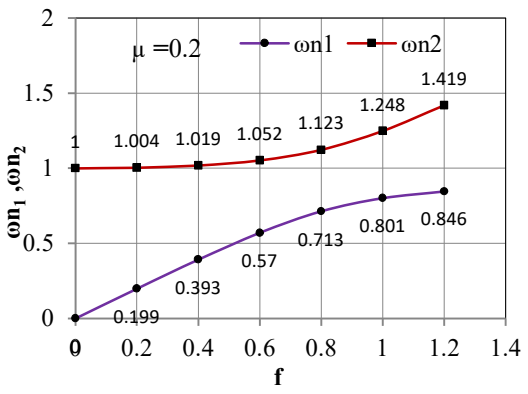

Figure 5.7(a)

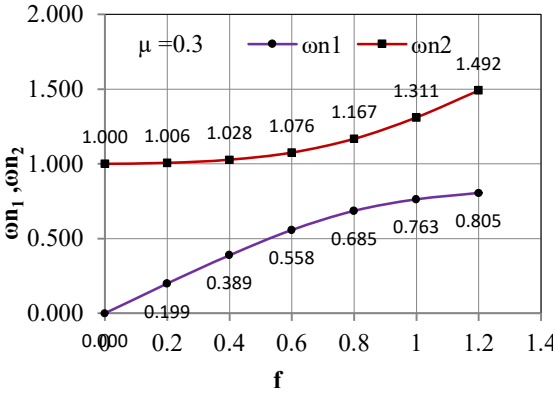

Figure 5.7(b)

Figure 5. 7 Undamped natural frequency ω_{n1} and ω_{n2} vs. Tuning ratio f for μ= 0.2, 0.3

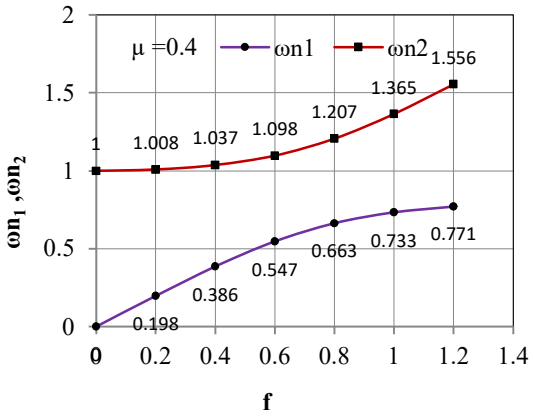

Figure 5.8(a)

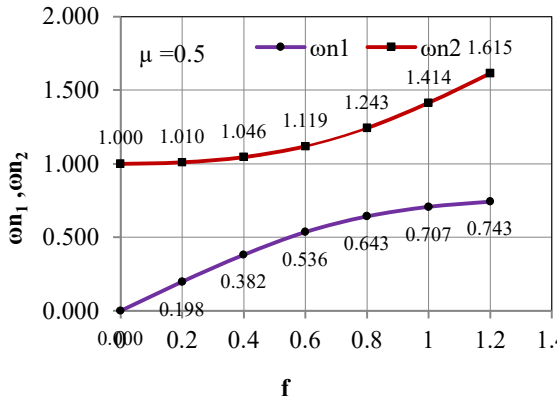

Figure 5.8(b)

Figure 5.8 Undamped natural frequency $\overline{\omega_{n1}}$ and $\overline{\omega_{n2}}$ vs. Tuning ratio f for μ= 0.4, 0.5

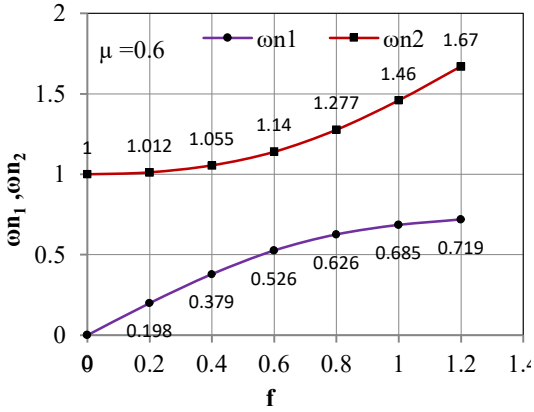

Figure 5.9(a)

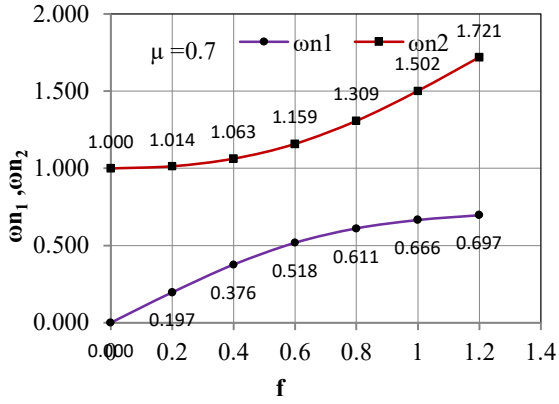

Figure 5.9(b)

Figure 5.9 Undamped natural frequency $\overline{\omega_{n1}}$ and $\overline{\omega_{n2}}$ vs. Tuning ratio f for μ= 0.6, 0.7

5.3.3. Effect of tuning ratio f on band width $\overline{b_e}$ for different values of mass ratio μ

Using the equation (5.8) the curves of the figures are obtained (Refer table 5.6)

Table 5.6 Effect of f on b for μ=0.2, 0.3, 0.4, 0.5, and 0.6

F	$\overline{b_e}$ (μ=0.2)	$\overline{b_e}$ (μ=0.3)	$\overline{b_e}$ (μ=0.4)	$\overline{b_e}$ (μ=0.5)	$\overline{b_e}$ (μ=0.6)	$\overline{b_e}$ (μ=0.7)
0	1.000	1.000	1.000	1.000	1.000	1.000
0.2	0.805	0.807	0.810	0.812	0.815	0.817
0.4	0.626	0.639	0.651	0.663	0.675	0.687
0.6	0.482	0.518	0.551	0.583	0.613	0.642
0.8	0.410	0.482	0.544	0.600	0.651	0.699
1.0	0.447	0.548	0.632	0.707	0.775	0.837
1.2	0.573	0.687	0.785	0.872	0.951	1.024

Undamped natural frequency $\overline{\omega_{n_1}}, \overline{\omega_{n_2}}$, and band width $\overline{b_e}$ vs. Tuning ratio f for μ = 0.2, 0.3, 0.4, 0.5, and 0.6the curves of the figures 5.10, 5.11, 5.12, 5.13, and 5.14 are obtained

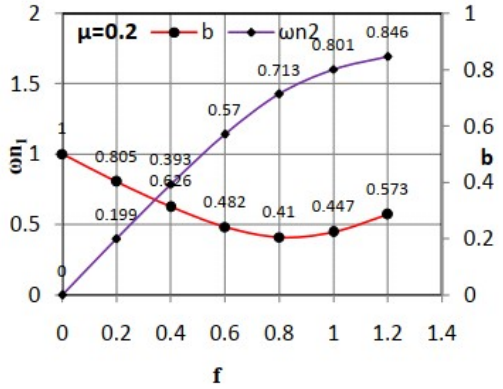

Figure 5. 10 (a) $\overline{\omega_{n_1}}$ vs. f and $\overline{b_e}$ vs. f

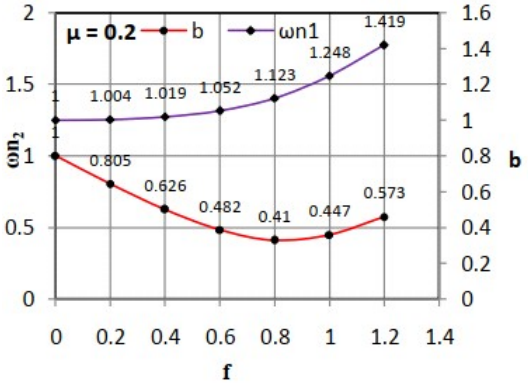

Figure 5.10 (b) $\overline{\omega_{n_2}}$ vs. f and $\overline{b_e}$ vs. f

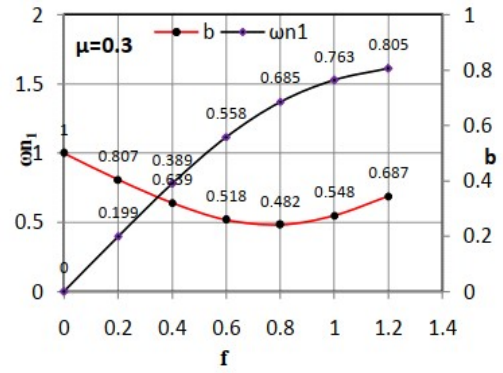

Figure 5. 11 (a) ω_{n1} vs. f and $\overline{\boldsymbol{b_e}}$ vs. f

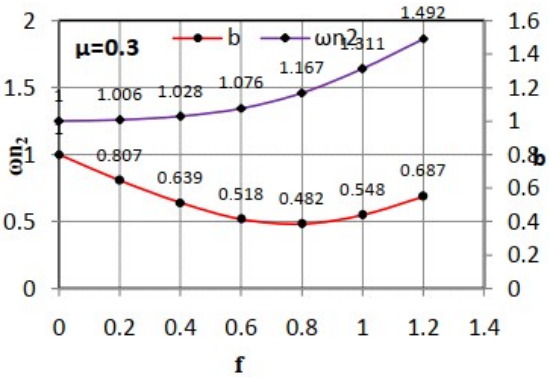

Figure 5.11(b) $\overline{\omega_{n_2}}$ vs. f and $\overline{b_e}$ vs. f

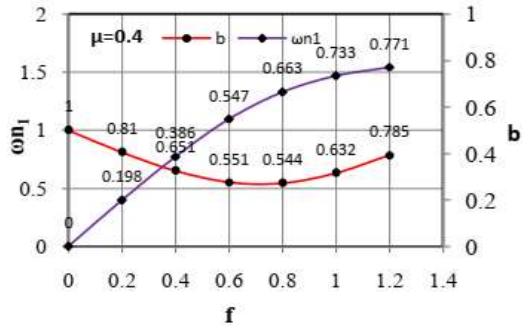

Figure 5. 12 (a) $\overline{\omega_{n1}}$ vs. f and $\overline{\boldsymbol{b_e}}$ vs. f

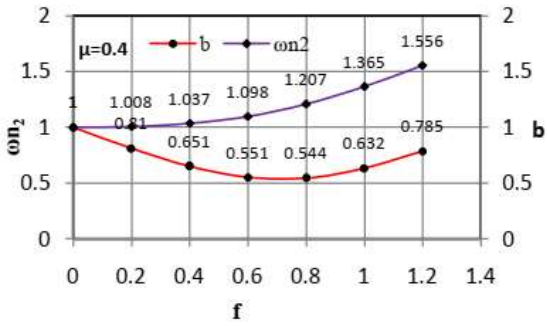

Figure 5.12(b) $\overline{\omega_{n_2}}$ vs. f and $\overline{b_e}$ vs. f

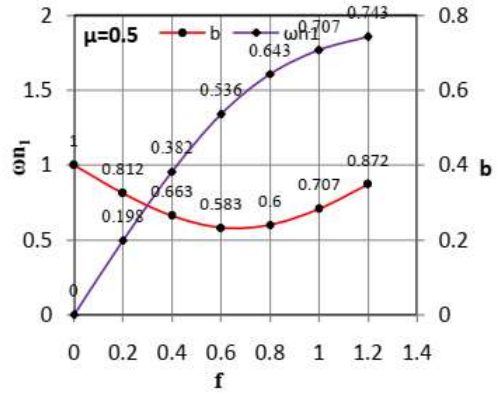

Figure 5. 13 (a) $\overline{\omega_{n1}}$ vs. f and $\overline{b_e}$ vs. f

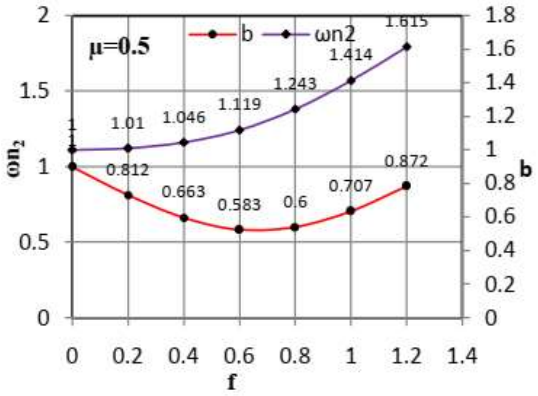

Figure 5.13(b) $\overline{\omega_{n_2}}$ vs. f and $\overline{b_e}$ vs. f

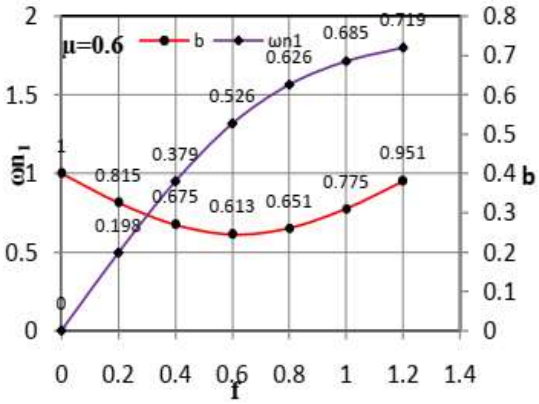

Figure 5. 14 (a) $\overline{\omega_{n1}}$ vs. f and $\overline{b_e}$ vs. f

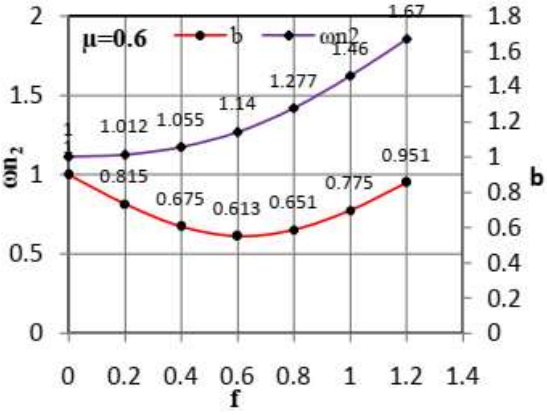

Figure 5.14(b) $\overline{\omega_{n_2}}$ vs. f and $\overline{b_e}$ vs. f

5.3.4. Discussion on Results

i. From figure 5.3, 5.4, 5.5 and 5.6, it is seen that, the values of useful bandwidth b increases with increases in mass ratio μ. For f = 1.2 the value of bandwidth are more for given value of μ this is clearly seen in figure 5.6.

ii. From figure 5.7, 5.8, and 5.9, it is observed that, for f = 0.8 the band width is minimum for all values of mass ratio μ considered, at f = 1, bandwidth '$\overline{b_e}$' is wide enough from the point of design of 2DOF VBEH.

iii. From figures 5.10,5.11,5.12,5.13, and 5.14 as the values of tuning ratio f increases, the first mode of natural frequency $\overline{\omega_{n_1}}$ decreases up to the f = 0.8 and increases thereafter till f = 1.4. Same trend is followed by the second mode of natural frequency $\overline{\omega_{n_2}}$. It is suggested that the design of 2DOF VBEH should be near the value of f = 1

5.4 Experimental Analysis

In this section, the effect of the mass ratio μ on the power output of a 2 DOF VBEH has been analyzed using experimental setup designed and developed for the same.

5.4.1 Experimental Setup and Instrumentation

The Experimental setup has been designed in such a way that the SDOF VBEH system is converted to a 2DOF VBEH with a little bit of a change in the setup

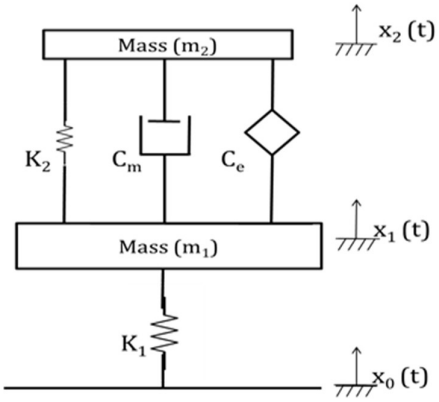

Figure 5.15 Schematic of a 2 DOF VBEH

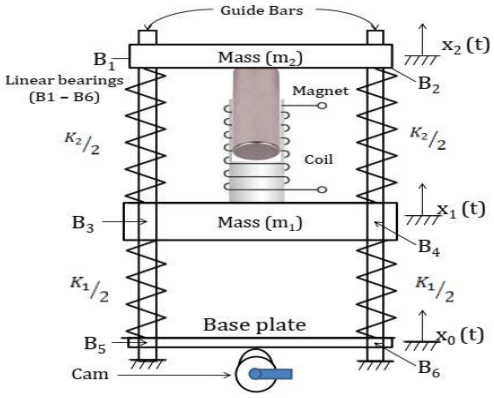

Figure 5.16 2DOF VBEH Experimental Setup

The schematic of a 2 DOF VBEH system is shown in figure 5.15. The experimental setup designed and developed for 2 DOF VBEH is shown in figure 5.16.

The system (m_2, k_2, c_m, c_e) is the energy harvester. The helical compression spring of stiffness k_2 is split into two springs of equal stiffness $\frac{k_2}{2}$ and these springs are placed in parallel to support the harvester mass m_2. The system (m_1, k_1) is the amplifier system. The mass m_2 is supported by helical compression springs each of stiffness $\frac{k_1}{2}$ and are placed in parallel as shown in figure 5.16.

The rectangular plates of appropriate size are selected to represent harvester mass m_2, amplifier mass m_1, and the base plate. The base plate supports the amplifier system. All the plates are equipped with rolling contact bearings to ensure frictionless movement of these plates in the vertical direction in the two vertical parallel guide bars. The cam is driven by an electrical drive motor and is mounted at the end of the electrical drive motor shaft. The guide bars are mounted firmly in the foundation.

5.4.2 Electromagnetic Sub-system

The coil magnet system comprises of a 'Magnet-in-line' type configuration in which a cylindrical magnet moves in the vertical direction in an electrical coil of copper material. Figure 5.17 shows the magnet to be fixed to the harvester mass plate and the copper coil to be fixed to the amplifier mass plate with proper alignment in vertical direction. The relative movement between magnet and coil provides a magnetic field which when cut gives rise to an electromotive force

5.4.3 Selection of Magnet and Coil Design

i) Typically, four types of permanent magnets suitable for the coil-magnet system of a VBEH are: Alnico, Ceramic, Samarium cobalt, and Neodymium Iron Boron (NdFeB). The properties such as high flux density and high magnetic field strength of NdFeB make it suitable for the coil-magnet system of VBEH.

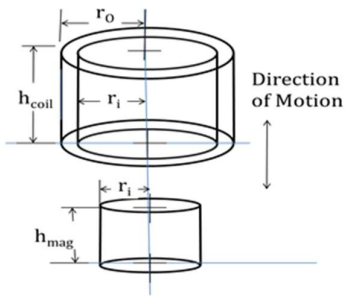

Figure 5. 17 Magnet and coil in-line combination

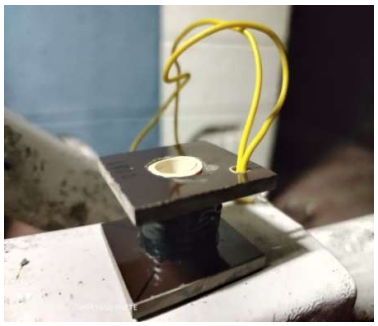

Figure 5. 18 Developed coil

The dimensions of cylindrical NdFeB magnet selected for magnet-coil system are: diameter of magnet 10 mm and the height h_{mag} 30mm and residual flux density B_r = 1.4 Tesla.

ii) The design of the coil is carried out as follows

The inner diameter d_i of the coil is selected as 16 mm such that the cylindrical magnet can move freely during the relative displacement between coil and magnet. The height of the coil h_{coil} is selected as 30 mm, keeping in mind that the magnet should remain inside the coil even during the large amplitude of their relative motion at resonant condition. The outer diameter d_o of the coil is taken as 20 mm, to accommodate the required number of turns of coil. The values of the total number of turns (N) of the coil, internal resistance of the coil (R_c), and internal inductance of the coil (L) are estimated using the standard formulae [65]. These values are given in Table 5.7. Figure 5.18 shows the photograph of developed coil.

Table 5. 7 Specifications of the designed coil

r_o	Coil outer radius (mm)	10	N_{lat}	Lateral turns of coil	23
r_i	Coil inner radius (mm)	8	N	Total number of turns of coil	7790
h_{coil}	Coil height (mm)	30	R_c	The internal resistance of the coil (Ω)	1620
N_{long}	Longitudinal turns of coil	343	L	The internal inductance of coil (H)	0.45

5.4.4 Design Calculations

i) To increase the power output and to extend the effective operational frequency range of 2DOF VBEH device, and to keep its weight low, a reasonable choice for the mass ratio μ is in the range 0.3 to 0.4, hence for the analysis the reasonable values of mass ratio μ are taken as 0.3 and 0.36.

ii) The VBEH is designed essentially for low frequency excitation. Hence, the excitation frequency f_w is taken as 5.5 Hz, therefore the circular excitation frequency is $\omega = 2\pi f_w = 34.54\, rad/sec$, for tuning ratio f = 1, hence, $\omega_1 = \sqrt{\frac{k_1}{m_1}} = \omega_2 = \sqrt{\frac{k_2}{m_2}} = \omega = 34.54\, rad/sec$

5.4.5 Sample calculations for the case μ = 0.36

With the harvester mass $m_2 = 2.4kg$, the amplifier mass m_1 is $m_1 = \frac{m_2}{\mu} = \frac{2.4}{0.36} = 6.67kg$. Using equations $\omega_1 = \sqrt{\frac{k_1}{m_1}}$ and $\omega_2 = \sqrt{\frac{k_2}{m_2}}$ and $\omega_2 = \omega_1$ for f = 1, the values of amplifier spring stiffness k_1 and harvester system spring stiffness k_1 and k_2 are calculated as $k_1 = 7957.38\, N/m$ and $k_2 = 2863.22$ N/m. For harvester system, two helical compression springs of stiffness $\frac{k_2}{2}$ are used in parallel. Therefore each of these two springs is designed for stiffness $\frac{k_2}{2} = 1431.6$ N/m, using standard spring design procedure. Amplifier mass is supported by two springs of stiffness $\frac{k_1}{2}$ in parallel, hence each of these springs is designed for stiffness $\frac{k_1}{2} = 3978.7\, N/m$ using standard spring design procedure. Design specifications of these springs are given in Table 5.8

Table 5.8 Specifications of the Amplifier and Harvester Springs

Spring system	Material of the Spring	Length of spring (mm)	Wire dia. d (mm)	Mean dia. D (mm)	No. of turns (N)
Amplifier	Spring steel	116	4.5	65	7
Harvester	Spring steel	192	4.5	65	11

iii) Rectangular M.S. plate of size 325 x 75 x 15 mm is selected as the harvester mass m_2. Refer figures 5.19 and 5.20. The amplifier mass m_1 is made up of 3rectangular plates of sizes 325 x 75 x 13. Refer figures 5.21 and 5.22.

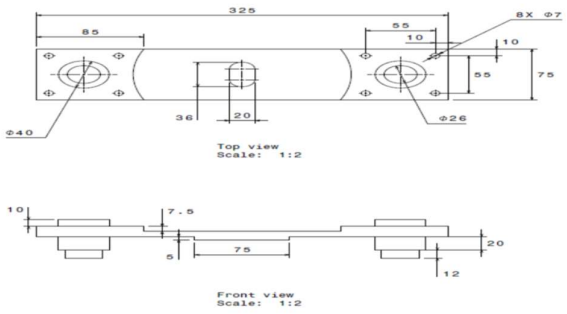

Figure 5.19 Harvester mass

Figure 5.20 Developed harvester mass

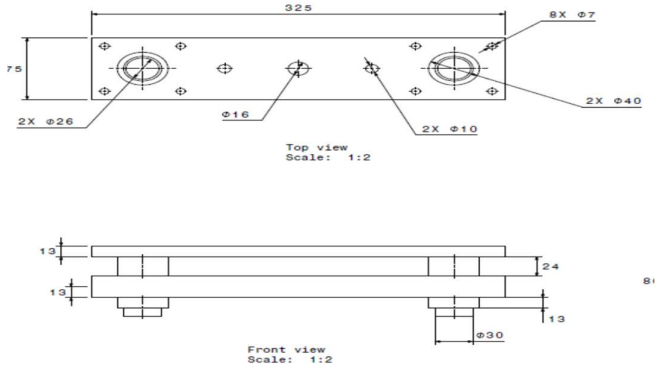

Figure 5.21 Amplifier mass

Figure 5.22 Developed amplifier mass

iv) A suitable M.S. plate is selected as a base plate to support amplifier spring-mass system. The base plate receives sinusoidal excitation by a cam driven by variable speed electric motor.

5.5 Experimental Analysis

The entire experimental setup with attendant instrumentation is shown in figure 5.21

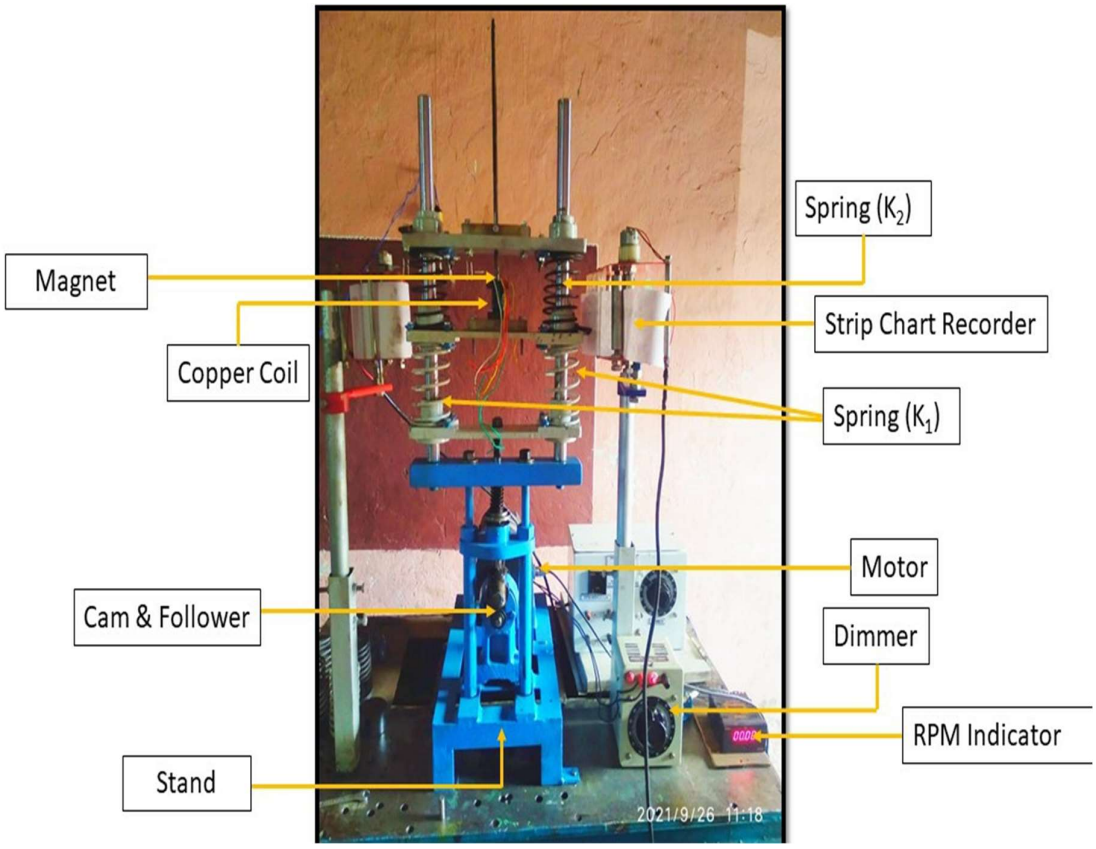

Figure 5. 23 Photograph of 2 DOF VBEH system

On this set-up following experiments have been carried out.

5.5.1 Experimental analysis of SDOF system (m_2, k_2, c_m, c_e)

On this setup following experiments have been carried out.

By removing amplifier (m_1, k_1) system from the 2DOF VBEH set-up the SDOF (m_2, k_2, c_m, c_e) VBEH system is obtained. This SDOF VBEH system is subjected to base harmonic excitation $x_0 = X_0\, sin\omega t$. Base excitation amplitudex_0 is provided by cam eccentricity and excitation frequency is varied by the change in the speed of the electrical drive motor. The response of $x_2(t)$ harvester mass m_2 is measured using a strip chart recorder. The amplitude Z of the relative displacement between harvester mass and base plate is obtained as $Z = [X_2 - X_0]$, at various values of excitation frequency ω.

The curves of Z vs. ω are plotted as shown in figure 5.22. The open circuit voltage E is measured across the copper coil terminals of SDOF VBEH, at various excitation

frequencies ω. The plot of E vs ω is shown in figure 5.23. The corresponding observations are recorded in table 5.10.

Table 5. 9 Amplitude Z of the Relative displacement without magnet and coil

without magnet and coil			
Eccentricity X_0 = 1			
N (rpm)	ω (rad/sec)	X_1 (mm)	$Z = X_1 - X_0$ (mm)
305	31.92	12	11
310	32.45	15	14
315	32.97	22	21
320	***33.49***	***42***	***41***
325	34.02	30	29
330	34.54	21	20
335	35.06	12	11
340	35.59	8	7

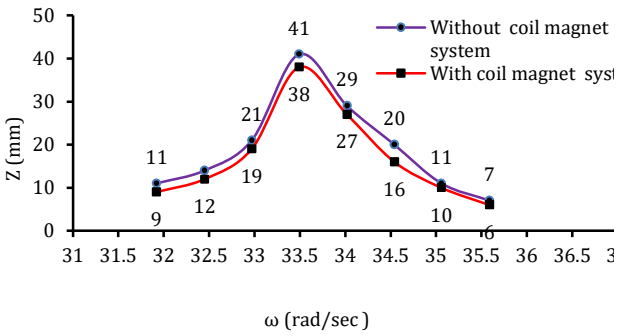

Figure 5.24 Relative amplitude Z vs. Excitation frequency ω

Table 5. 10 Open circuit voltage E with magnet and coil

Eccentricity X_0 = 1				
N (rpm)	ω (rad/sec)	X_1 (mm)	$Z = X_1 - X_0$	E (V)
305	31.92	10	9	2.9
310	32.45	13	12	3.2
315	32.97	20	19	8.2
320	***33.49***	***39***	***38***	**16**
325	34.02	28	27	12
330	34.54	17	16	4.0
335	35.06	11	10	3.1
340	35.59	7	6	2.4

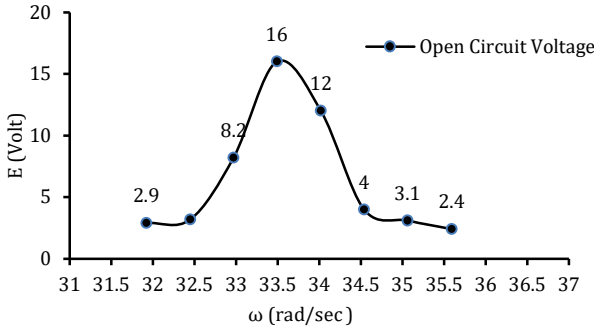

Figure 5.25 Open circuit voltage E vs. Excitation frequency ω

iii) The resistive electrical load R_L is connected across the copper coil terminals, and the voltage V_R across the load R_L is measured at different values of excitation frequency ω. R_L is varied from R_L =1000 Ω to R_L =2000 Ω using a resistive load bank developed for the same. The plots of V_R vs. ω are shown in figure 5.24. (refer table 5.11)

Table 5.11 Voltage V_R at different value of RL

Voltage V_R at different value of R_L				
Eccentricity X_0 = 1				
N (rpm)	ω (rad/sec)	1000 Ω	1500 Ω	2000 Ω
305	31.92	1.5	2	2.3
310	32.45	2	2.8	3.2
315	32.97	4.1	5.2	5.9
320	***33.49***	**6.5**	**8.2**	**9.2**
325	34.02	5.2	6.1	7
330	34.54	2.9	4.2	4.7
335	35.06	2.1	3.2	3.4
340	35.59	1.9	2.5	2.8

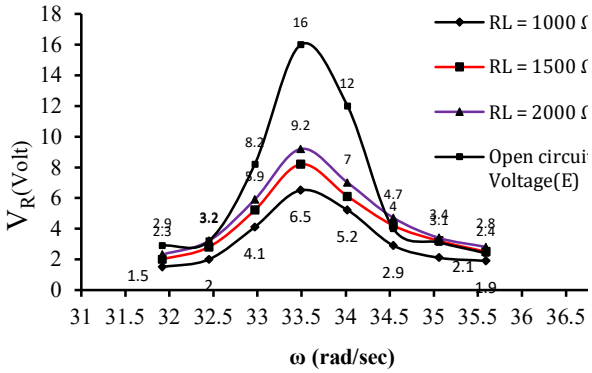

Figure 5. 26 Voltage V_R vs. Excitation frequency ω for various R_L

iv) The power P_{aveh} that can be harvested from the SDOF VBEH is estimated using the formula$P_{aveh} = V_R \times i_R$ where i_R is the current in the electrical load circuit and $i_R = \frac{V_R}{R_L}$. Therefore average power harvested is $P_{aveh} = \frac{{V_R}^2}{R_L}$, neglecting the internal resistance of theelectrical copper coil. R_L is varied as R_L =1000 Ω, R_L =1500 Ω, and R_L = 2000 Ω. The plots of P_{aveh}vs. ω are obtained as shown in figure 5.25. (refer table 5.12) From figures 5.22, 5.23, 5.24, and 5.25, it can be seen that values Z, E, V_R, and P_{aveh} are maximum at resonant frequency ω = 33.5 rad/sec. These values fall sharply at off-resonance frequencies. As such, it is necessary to modify the SDOF VBEH in such a way that increased harvested power can be made available over a wide operational frequency band.

Table 5.12 Harvested Power P_{aveh} for different value of R_L

Power P_{aveh} for different value of R_L				
Eccentricity X_0 = 1				
N (rpm)	ω (rad/sec)	1000 Ω	1500 Ω	2000 Ω
305	31.92	2.25	2.67	2.65
310	32.45	4.00	5.23	5.12
315	32.97	16.81	18.03	17.41
320	***33.49***	**42.25**	**44.83**	**42.32**
325	34.02	27.04	24.81	24.50
330	34.54	8.41	11.76	11.05
335	35.06	4.41	6.83	5.78
340	35.59	3.61	4.17	3.92

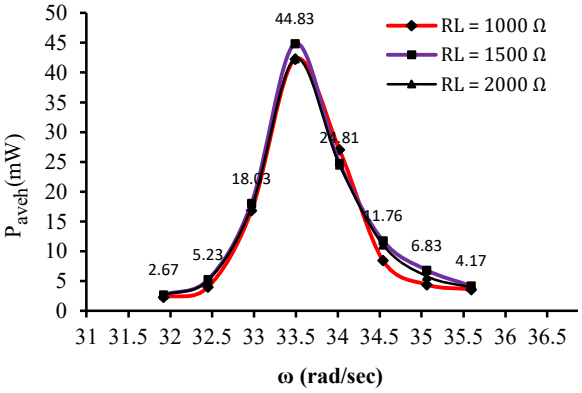

Figure 5. 27 Harvested Power P_{aveh} vs. Excitation frequency ω for various R_L

5.5.2 Experimental Analysis of developed 2DOF VBEH device.

For this purpose, harvester system (m_2, k_2, c_m, c_e) is mounted on the amplifier system (m_1, k_1). Now this set-up is ready for experimental analysis of the developed 2DOF VBEH device.

i) The developed 2 DOF VBEH device is subjected to the base harmonic excitation $x_0(t) = X_0\, sin\omega t$ by the cam driven by an electric motor. The responses $x_2(t) = X_2\, sin\omega t$ of the harvester mass m_2 and $x_1(t) = X_1\, sin\omega t$ of the amplifier mass m_1, at different frequencies of excitation, have been recorded using the strip chart recorder. The curves of relative displacement amplitude Z of harvested mass m_2 and amplifier mass m_1 are plotted as $Z = [X_2 - X_1]$ vs. ω shown in figure 5.26. (refer table 5.13)

Table 5. 13 Amplitude Z of the Relative displacement (with and without magnet and coil)

without magnet and coil									
Eccentricity X_0 = 1									
N (rpm)	ω (rad/sec)	X1 (mm)	X_2 (mm)	$Z = X_1 - X_0$ (mm)	N (rpm)	ω (rad/sec)	X1 (mm)	X2 (mm)	Z= X1 -X0 (mm)
210	21.98	3	8	5	300	31.40	10	17	7
220	23.03	3	12	9	330	34.54	8	12	4
230	24.07	7	22	15	360	37.68	12	10	2
240	25.12	7	36	29	390	40.82	13	10	3
245	**25.64**	**10**	**50**	**40**	400	41.87	15	8	7
250	26.17	10	40	30	410	42.91	20	7	13
260	27.21	8	25	17	**415**	**43.44**	**30**	**8**	**22**
270	28.26	7	23	16	420	43.96	20	5	15
					430	45.01	10	3	7

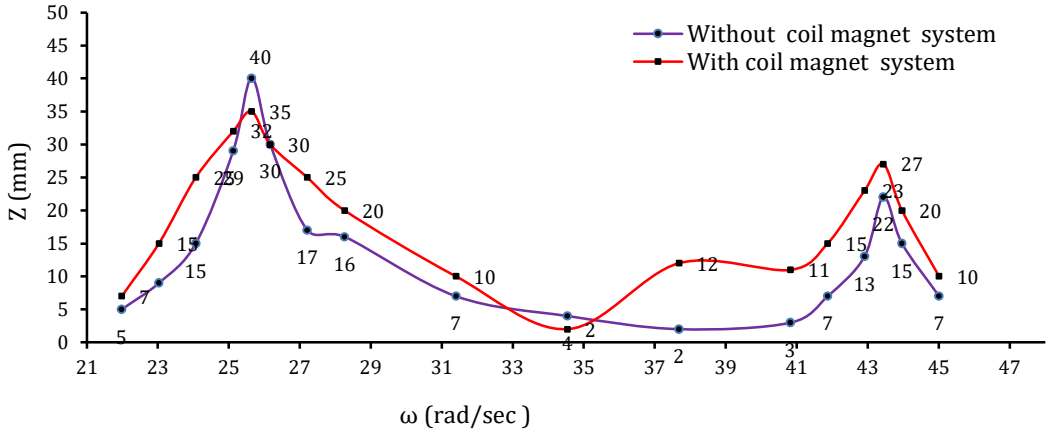

Figure 5. 28 Relative amplitude Z vs. Excitation frequency ω

ii) The open circuit voltage E across the induction coil terminals of 2DOF VBEH is measured at various frequencies of base excitation. Refer table 5.13. The curves of E vs. ω id plotted as shown in figure 5.27.The corresponding observations are recorded in table 5.14.

Table 5.14 Open circuit voltage E for various values of excitation frequency of 2DOF

Eccentricity X_0 = 1 (with magnet and coil)											
N rpm	ω rad/sec	X1 mm	X_2 mm	Z mm	E (V)	N rpm	ω rad/sec	X1 mm	X_2 mm	Z mm	E (V)
210	21.98	4	11	7	5.2	300	31.40	12	15	10	8.2
220	23.03	5	20	15	7.8	330	34.54	12	10	2	3.2
230	24.07	6	31	25	10.8	360	37.68	13	2	12	4.4
240	25.12	6	38	32	15.3	390	40.82	15	4	11	6.3
245	**25.64**	**8**	**43**	**35**	**19.8**	400	41.87	16	1	15	8.1
250	26.17	10	40	30	15.4	410	42.91	27	4	23	12.2
260	27.21	11	37	25	12.2	**415**	**43.44**	**30**	**3**	**27**	**15**
270	28.26	8	25	20	11.8	420	43.96	23	3	20	11.2
						430	45.01	12	2	10	6

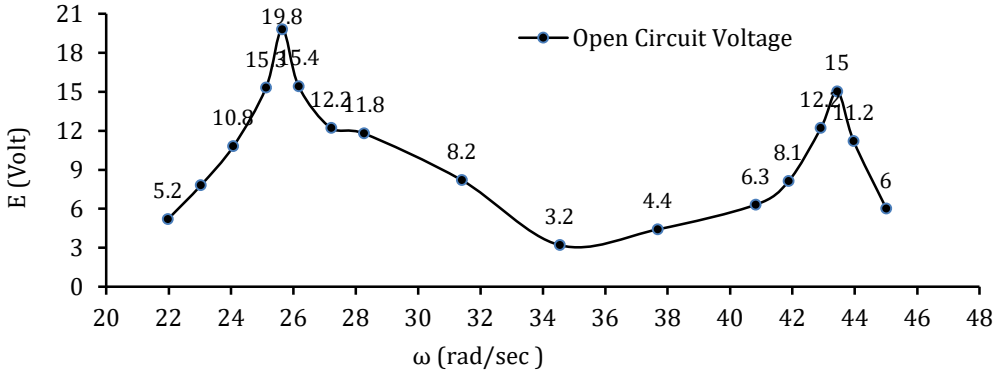

Figure 5.29 Open circuit voltage E vs. Excitation frequency ω

iii) The electrical load i.e., pure resistive load R_L is connected to 2DOF harvester and voltage V_R across the resistance is measured at various values of frequencies of base excitation. R_L is varied as R_L =1000 Ω, R_L =1500 Ω, and R_L =2000 Ω. The curves of V_R vs. ω at above mentioned values of R_L are plotted is shown in figure 5.28. The corresponding observations are recorded in table 5.15.

Table 5. 15 Voltage V_R at different value of R_L

Voltage V_R at different value of R_L						Voltage V_R at different value of R_L				
N rpm	ω rad/sec	1000 Ω	1500 Ω	2000 Ω	1000 Ω	N Rpm	ω rad/sec	1000 Ω	1500 Ω	2000 Ω
210	21.98	2.3	3	3.3	2.3	300	31.40	4.6	6.2	6.5
220	23.03	3.9	4.8	5.2	3.9	330	34.54	2.2	4.2	4.6
230	24.07	6.2	7.6	8	6.2	360	37.68	3	4	4.5
240	25.12	7.2	8.9	9.5	7.2	390	40.82	3.6	4.5	4.8
245	**25.64**	**8.1**	**10.2**	**11**	**8.1**	400	41.87	3.6	4.8	5
250	26.17	7.6	9.4	10.2	7.6	410	42.91	4.2	5.8	6
260	27.21	6.3	7.9	8	6.3	**415**	**43.44**	**6.2**	**8.2**	**8.9**
270	28.26	5.7	7.2	7.8	5.7	420	43.96	4.2	5.6	6.5
						430	45.01	2.2	3.3	4.3

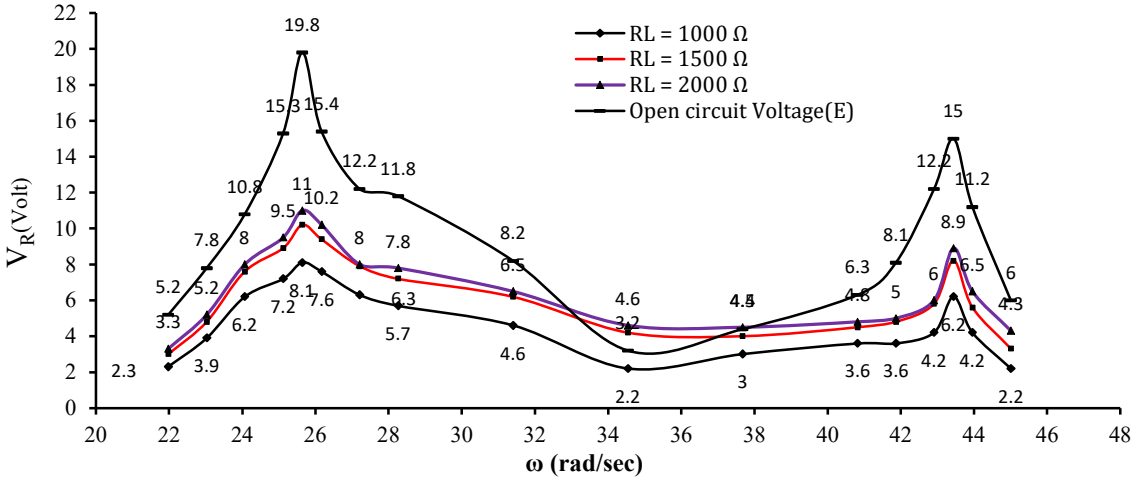

Figure 5. 30 Voltage V_R vs. Excitation frequency ω for various R_L

iv) The power P_{aveh} that can be harvested across resistive load R_L is calculated as $P_{aveh} = \frac{{V_R}^2}{R_L}$, at R_L =1000 Ω, R_L =1500 Ω, and R_L = 2000 Ω for various excitation frequencies. The plot of P_{aveh}vs. ω is shown in figure 5.29. The corresponding observations are recorded in table 5.16

Table 5.16 Average harvested power P_{aveh} at different values of R_L

Average harvested power P_{aveh} at different value of R_L						Average Harvested Power P_{aveh} at different value of R_L				
N rpm	ω rad/sec	1000 Ω	1500 Ω	2000 Ω	1000 Ω	N Rpm	ω rad/sec	1000 Ω	1500 Ω	2000 Ω
210	21.98	5.29	6.00	5.45	5.29	300	31.40	21.16	25.63	21.13
220	23.03	15.21	15.36	13.52	15.21	330	34.54	4.84	11.76	10.58
230	24.07	38.44	38.51	32.00	38.44	360	37.68	9.00	10.67	10.13
240	25.12	51.84	52.81	45.13	51.84	390	40.82	12.96	13.50	11.52
245	**25.64**	**65.61**	**69.36**	**60.50**	**65.61**	400	41.87	12.96	15.36	12.50
250	26.17	57.76	58.91	52.02	57.76	410	42.91	17.64	22.43	18.00
260	27.21	39.69	41.61	32.00	39.69	**415**	**43.44**	**38.44**	**44.83**	**39.61**
270	28.26	32.49	34.56	30.42	32.49	420	43.96	17.64	20.91	21.13
						430	45.01	4.84	7.26	9.25

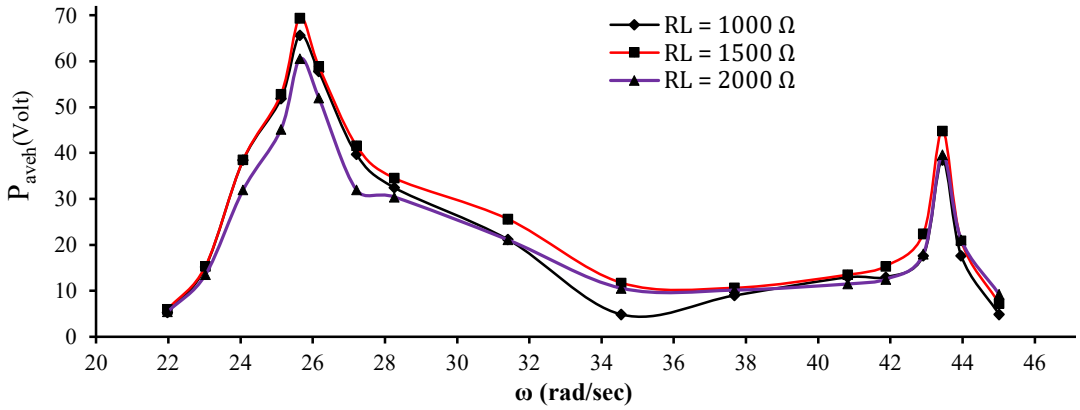

Figure 5. 31 Average harvested power P_{aveh} vs. ω at different value of R_L

5.5.3 Mass Ratio μ = 0.3

Using the procedure outlined in section 3.3.1, the experimental analysis of 2 DOF VBEH for the case μ = 0.3 has also been carried out. The change in mass ratio from μ = 0.36 to μ = 0.3 is achieved by changing the value of harvester mass m_2. Therefore, the design of springs supporting harvester mass is modified to maintain the condition that tuning ratio be unity. The new value of mass m_2 is 2.0 kg and new stiffness $\frac{k_2}{2}$ of each spring supporting harvester mass m_2 is 1193 N/m

i) Figure 5.30 shows the plots of Z vs. ω for the case μ = 0.3 with and without coil-magnet system refer table 5.17

Table 5.17 Amplitude Z of the Relative displacement (with and without magnet and coil)

without magnet and coil									
Eccentricity X_0 = 1									
N (rpm)	ω (rad/sec)	X1 (mm)	X_2 (mm)	Z= X_1 -X_0 (mm)	N (rpm)	ω (rad/sec)	X1 (mm)	X_2 (mm)	Z= X_1 -X_0 (mm)
210	21.98	3	8	5	360	37.68	8	12	4
220	23.03	3	12	9	380	39.77	12	10	2
240	25.12	7	22	15	410	42.91	13	10	3
250	26.17	7	36	29	420	43.96	15	8	7
255	**26.69**	**11**	**50**	**39**	430	45.01	20	7	13
260	27.21	9	42	33	**435**	**45.53**	**30**	**8**	**22**
270	28.26	8	25	17	440	46.05	20	5	15
300	31.40	7	23	16	455	47.62	10	3	7
340	35.59	10	17	7					

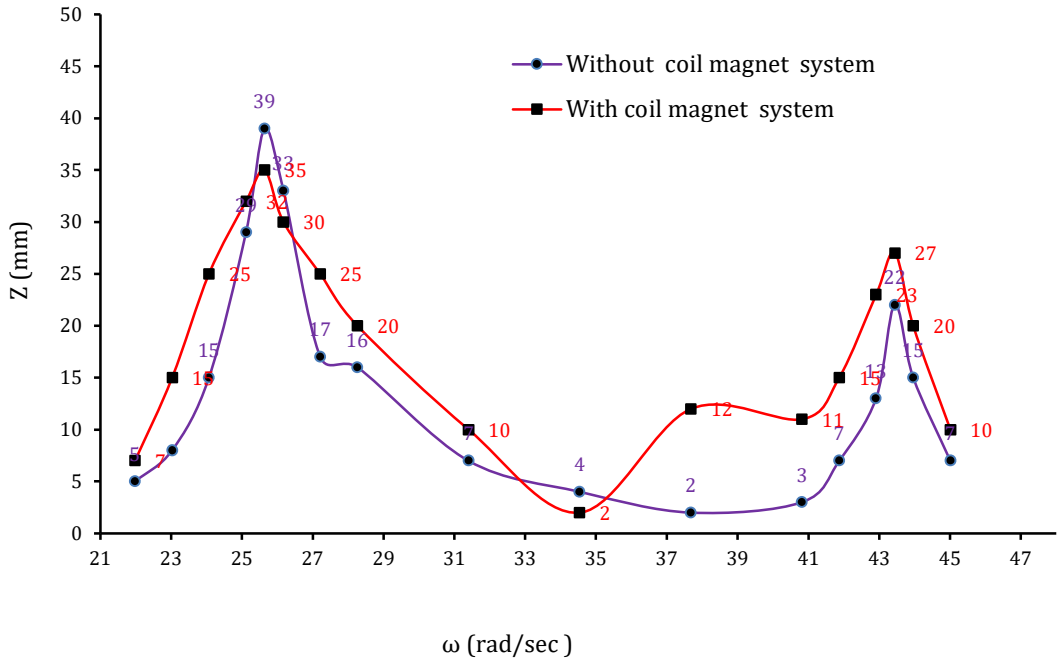

Figure 5. 32 Relative amplitude Z vs. Excitation frequency ω

ii) The open circuit voltage E across the induction coil terminals of 2DOF VBEH is measured at various frequencies of base excitation. The curves of E vs. ω are plotted as shown in figure 5.31 (refer table 5.18).

Table 5. 18 Open circuit voltage E for various values of excitation frequency of 2DOF

Eccentricity X_0 = 1 (with magnet and coil)											
N (rpm)	ω (rad/sec)	X1 (mm)	X_2 (mm)	Z (mm)	E (V)	N (rpm)	ω (rad/sec)	X1 (mm)	X_2 (mm)	Z (mm)	E (V)
210	21.98	4	11	7	5.2	360	37.68	12	10	2	3.2
220	23.03	5	20	15	7.8	380	39.77	13	2	12	4.4
240	25.12	6	31	25	10.8	410	42.91	15	4	11	6.3
250	26.17	6	38	32	15.3	420	43.96	16	1	15	8.1
255	**26.69**	**8**	**43**	**35**	**17**	430	45.01	27	4	23	17
260	27.21	10	40	30	15.4	**435**	**45.53**	**30**	**3**	**27**	**19**
270	28.26	11	37	25	12.2	440	46.05	23	3	20	16
300	31.40	8	25	20	11.8	455	47.62	12	2	10	6
340	35.59	12	15	10	8.2						

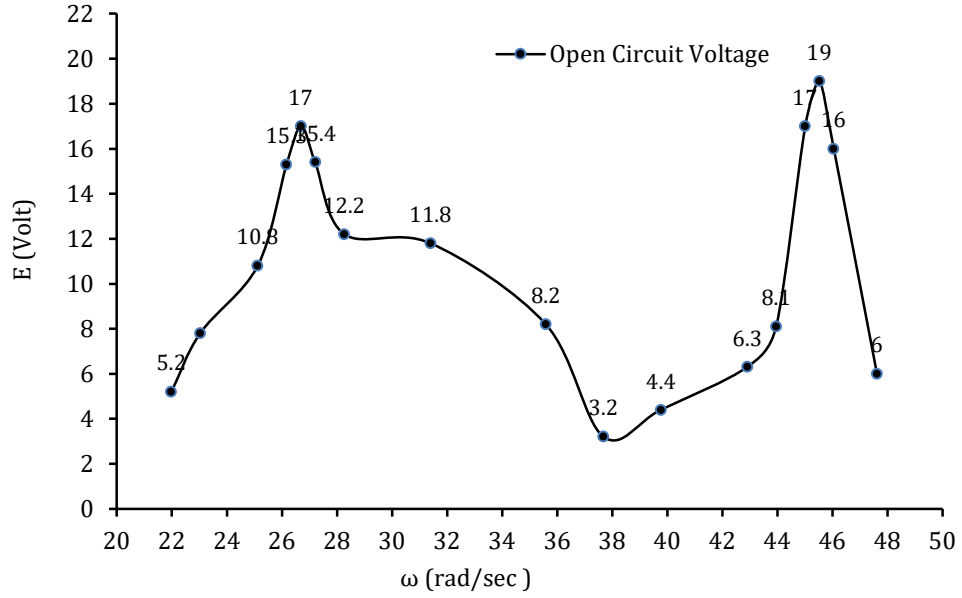

Figure 5. 33 Open circuit voltage E vs. Excitation frequency ω

iii) The pure resistive load R_L is connected to 2DOF VBEH and voltage V_R across the resistance is measured at various values of frequencies ω of base excitation. R_L is varied as R_L =1000 **Ω**, R_L =1500 **Ω**, and R_L = 2000 **Ω**. The curves of V_R vs. ω for above mentioned values of R_L are plotted in figure 5.32 (refer table 5.19).

Table 5.19 Voltage V_R at different value of R_L

Eccentricity X_0 = 1 (with magnet and coil)					Voltage V_R at different value of R_L				
N (rpm)	ω (rad/sec)	1000 Ω	1500 Ω	2000 Ω	N (rpm)	ω (rad/sec)	1000 Ω	1500 Ω	2000 Ω
210	21.98	2.3	3	3.3	360	37.68	2.2	4.2	4.6
220	23.03	3.9	4.8	5.2	380	39.77	3	4	4.5
240	25.12	4.9	6.4	7.5	410	42.91	3.6	4.5	4.8
250	26.17	6.2	7.7	8	420	43.96	3.6	4.8	5
255	**26.69**	**7.2**	**8.9**	**9.5**	430	45.01	6.3	7.9	8.1
260	27.21	7.6	9.4	10.2	**435**	**45.53**	**8.2**	**10.3**	**11.4**
270	28.26	6.3	7.9	8	440	46.05	7.1	9.1	9.8
300	31.40	5.7	7.2	7.8	455	47.62	2.2	3.3	4.3
340	35.59	4.6	6.2	6.5					

=

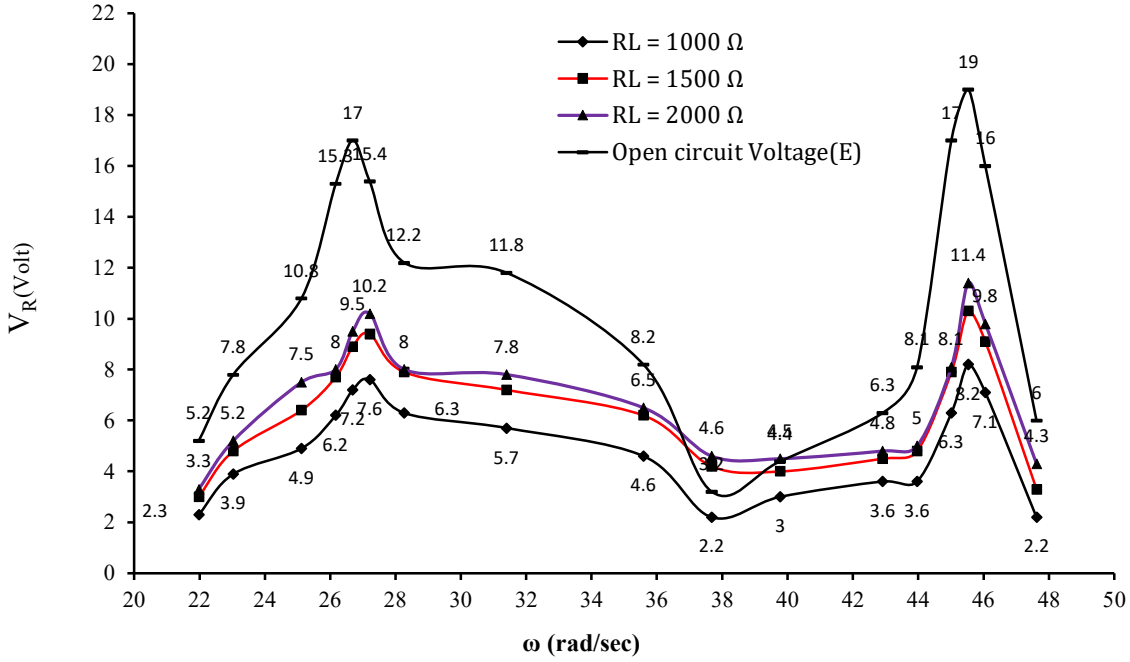

Figure 5. 34 Voltage V_R vs. Excitation frequency ω for various R_L

The power P_{aveh} that can be harvested across the resistive load R_L is calculated as $P_{aveh} = \frac{{V_R}^2}{R_L}$, for R_L =1000 Ω, R_L = 1500 Ω, and R_L = 2000 Ω at various excitation frequencies ω. The plots of P_{aveh} vs. ω are shown in figure 5.33 (refer table 5.20).

Table 5.20 Average harvested power P_{aveh} vs. excitation frequency ω at various values of R_L

N (rpm)	ω (rad/ sec)	Average Harvested Power P_{aveh} at different value of R_L			N (rpm) 1000 Ω	ω (rad/sec)	Average Harvested Power P_{aveh} at different value of R_L		
		1000 Ω	1500 Ω	2000 Ω			1000 Ω	1500 Ω	2000 Ω
210	21.98	5.29	6.00	5.45	360	37.68	4.84	11.76	10.58
220	23.03	15.21	15.36	13.52	380	39.77	9.00	10.67	10.13
240	25.12	24.01	27.31	28.13	410	42.91	12.96	13.50	11.52
250	26.17	38.44	39.53	32.00	420	43.96	12.96	15.36	12.50
255	**26.69**	**51.84**	**52.81**	**45.13**	430	45.01	39.69	41.61	32.81
260	27.21	57.76	58.91	52.02	**435**	**45.53**	**67.24**	**70.73**	**64.98**
270	28.26	39.69	41.61	32.00	440	46.05	50.41	55.21	48.02
300	31.40	32.49	34.56	30.42	455	47.62	4.84	7.26	9.25
340	35.59	21.16	25.63	21.13					

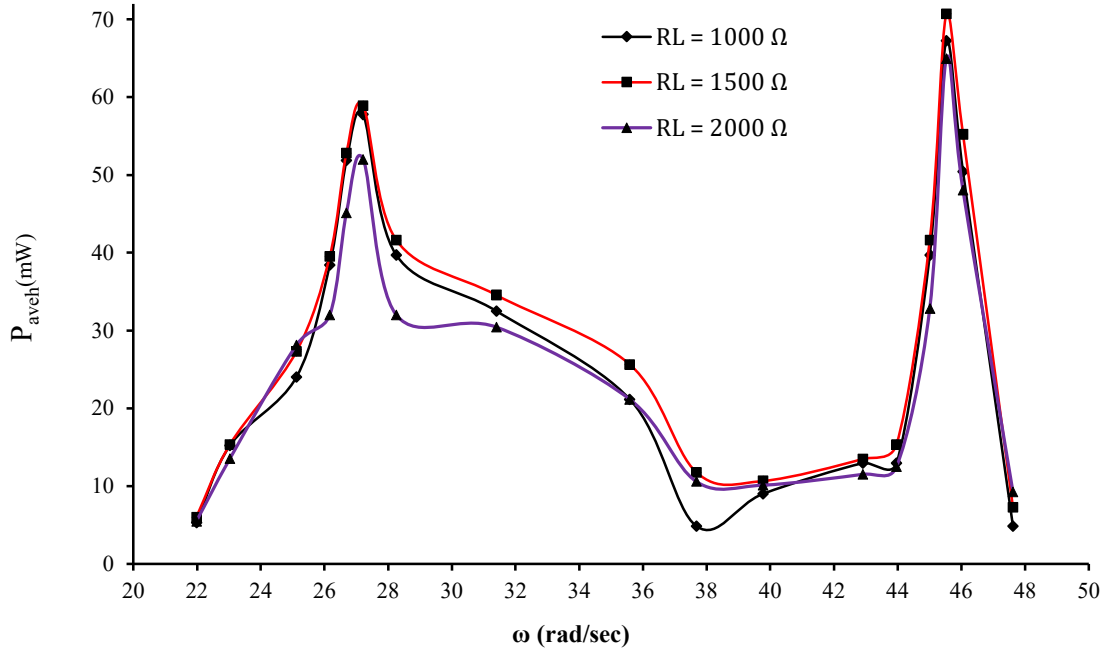

Figure 5.35 Average Harvested Power P_{aveh} vs. Excitation frequency ω for various R_L

5.5.4 Discussion on Results

i) For the case μ = 0.36

From figures 5.22 and 5.26, it is clearly seen that the band width of operating excitation frequency has been increased. The values of relative displacement amplitude Z is maximum at two resonant frequencies indicating that the open circuit voltage E and voltage across the electric resistive load V_R will be available over a wide band of excitation frequency. This result shows that the harvester power P_{aveh} of a 2 DOF VBEH

is increased as compared to that of a SDOF VBEH device. The power P_{aveh} is available over the wide band of excitation and the peak values of P_{aveh} are at the two resonant frequencies. It should be noted that the maximum values of P_{aveh} is available at a resistive load of 1500 Ω which is approximately equal to internal resistance R_L of electrical copper coil

ii) For the case μ = 0.3

From figures 5.27 to 5.30 it is clearly seen that the power P_{aveh} is available over the wideband of excitation with its peak values at the two resonant frequencies. The maximum power is available at a resistive load of 1500 Ω at 45.53 rad/sec.

5.6 Conclusions

i) The expression derived for non-dimensional power of a 2DOF VBEH shows that the power output of a 2DOF VBEH depends on the choice of the values of mass ratio μ, tuning ratio f, electrical damping ratio ξ_e, and normalized excitation frequency α. However, VBEH uses especially a low-frequency vibration sources, therefore the effect of α is not pronounced so much. Also, the choice of values of μ and f is also linked with effective non-dimensional bandwidth $\overline{b_e}$. Hence judicious choice of the values of μ, f, andξ_e has to be made while designing 2DOF VBEH i.e., choice of harvester mass-spring system and amplifier mass-spring system.

ii) This detailed analysis carried in sections 5.3, 5.3.1, 5.3.2, and 5.3.4 is useful to select the values of the mass ratio μ and tuning ratio f with a view to determine the mass and spring parameters of the proposed 2DOF VBEH model such that the power output of 2DOF VBEH is enhanced and is available over a wide band of the operational frequency. Also it is observed that when tuning ratio f = 1, and the mass ratio μ = 0.4, wide bandwidth $\overline{b_e}$ is available. However, if it is required to have even more bandwidth then one can obtain it for tuning ratio f = 1.2 and mass ratio μ = 0.4. If it is required to have less mass ratio such as μ = 0.3, in that case the tuning ratio f should be equal to 1.2. This choice of mass ratio μ will give power output of 2DOF VBEH over a widened bandwidth with the advantage that the weight of such 2DOF VBEH will be less.

Chapter – 6

OPTIMIZATION OF POWER OUTPUT OF A 2DOF VIBRATION-BASED ELECTROMAGNETIC ENERGY HARVESTER

6.0 Introduction

In chapter 5, analytical expressions for the power output and the operational frequency band of a 2DOF VBEH have been derived. The design details and conversion of the SDOF VBEH into 2DOF VBEH have been presented with a view to increase its power output and to widen its operating excitation frequency band. The power output of 2DOF VBEH is influenced by four major parameters, viz., the electrical damping ratio ξ_e, mass ratio μ, the tuning ratio f, and the excitation frequency ratio α. The power output of 2DOF VBEH obtained by applying a single variable optimization technique will be an optimal value of P_{ave} with respect to that variable only and may not be of the same value for the optimal value of P_{ave} obtained for other variables such as mass ratio μ. As such, the problem here is to obtain global optimal value of output power P_{ave} of 2DOF VBEH when ξe and α are varied simultaneously for a set of values of tuning ratio f = 0.8, f = 1.0 and f = 1.2, and for a given value of μ or a set of values of mass ratio, μ = 0.1, μ = 0.2, μ = 0.3, and μ = 0.4 for a given value of tuning ratio f. To achieve this goal, the method of drawing surface plots and contour diagrams has been used to obtain global optimal value of power output of a 2DOF VBEH device. The details of drawing these plots are presented in the sections to follow. From these plots, the global optimal non- dimensional value of power output P_{aven} under a given set of conditions can be obtained.

6.1 Surface Plots and Contour Diagrams for 2DOF VBEH

The expression for non-dimensional maximum average power P_{aven} available from a 2DOF VBEH device has been derived as (Refer to equation 5.22)

$$P_{aven} = \frac{\xi_e \mu f \alpha^6}{[\alpha^4+f^2-(1+(1+\mu)f^2)\alpha^2]^2+4(\xi_m+\xi_e)^2[f\alpha \ \ (1+\mu)f\alpha^3]^2} \tag{6.1}$$

It can be seen from equation 6.1, that the value of P_{aven} is controlled by mass ratio μ, tuning ratio f, frequency ratio α, and electrical damping ratio ξ_e.

Using the theoretical equation 6.1 for non-dimensional average power output P_{aven} from a 2DOF VBEH and associated variable which control the value of P_{aven}, a software tool MATLAB has been used to draw surface plots and contour diagram. (Appendix 2)

i) The resulting surface plots showing the non-dimensional average power output P_{aven} with respect to normalized excitation frequency α, at various values of electrical

dumping ratio ξ_e for given value of mass ratio μ are shown in figure 6.1 and 6.2 for tuning ratio f = 1, in figures 6.3 and 6.4 for f = 0.8, and in figures 6.5 and 6.6 for f = 1.2.

6.1.1 Case I f = 1

P_{aven} vs. ζ_e for μ = 0.1, 0.2, 0.3, and 0.4

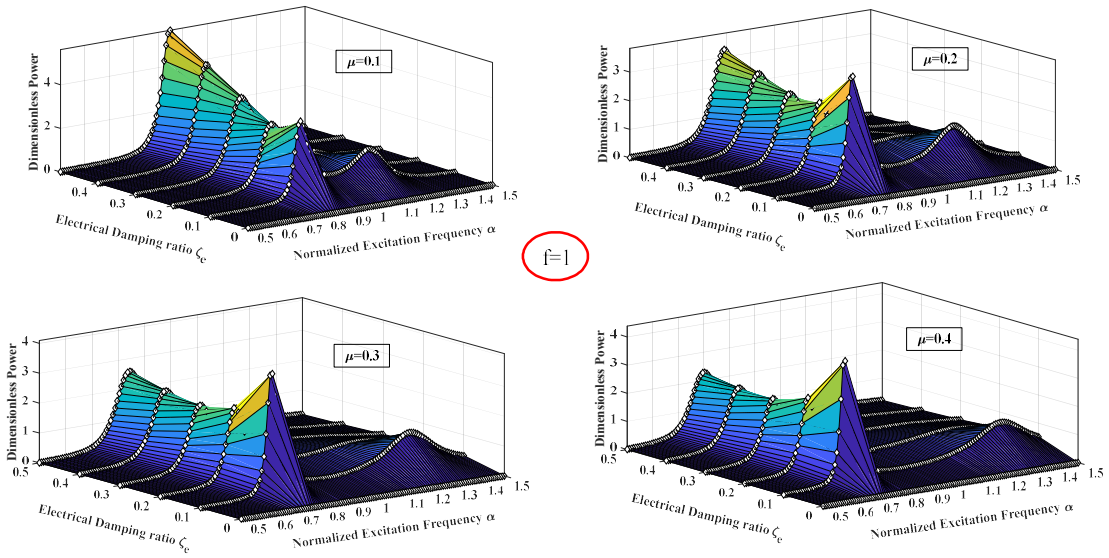

Figure 6.1 The power output P_{aven} of 2DOF VBEH at different values of excitation frequencies α and electrical damping ratios ζ_e, when mass ratio μ is 0.1, 0.2, 0.3, 0.4, tuning ratio f is 1 and mechanical damping ratio ζ_m= 0.046

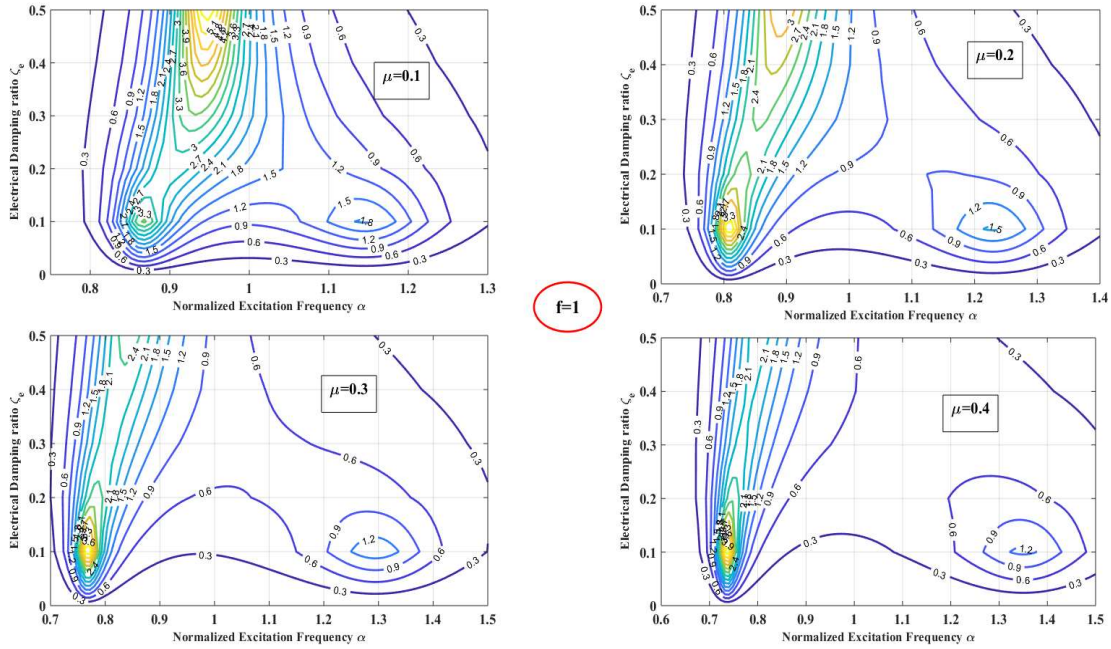

Figure 6.2 Contour of dimensionless power and optimal electrical damping ratios ζ_e at different excitation frequencies α when mass ratio μ is 0.1, 0.2, 0.3, 0.4, tuning ratio f =1 and ζ_m = 0.046

6.1.2 Case II f = 0.8

P_{aven} vs. ζ_e for μ = 0.1, 0.2, 0.3, and 0.4

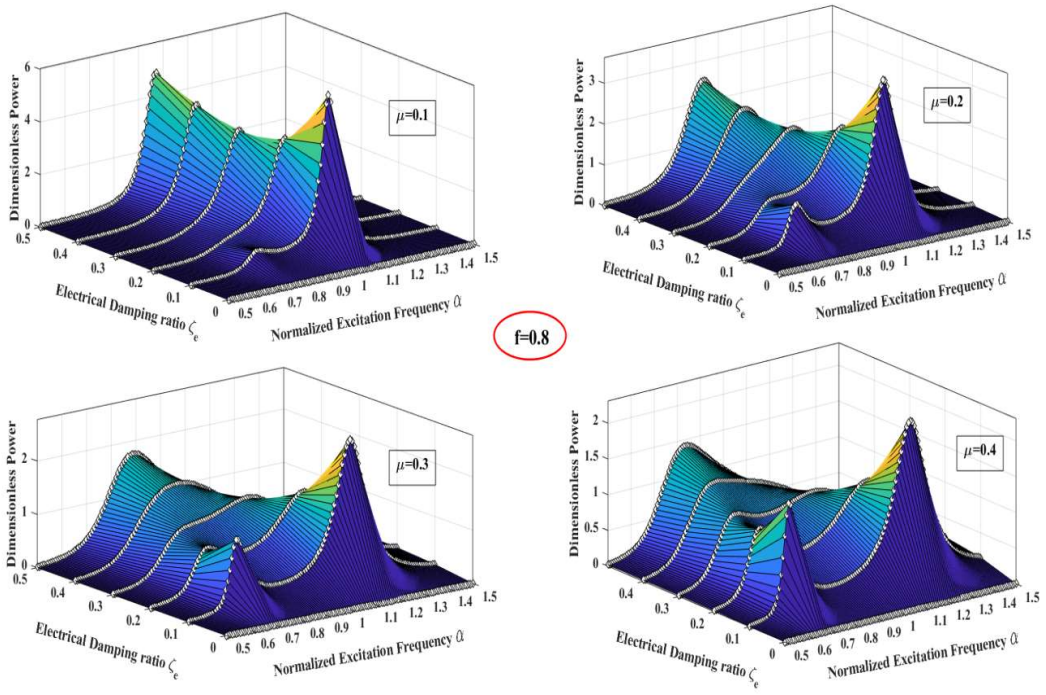

Figure 6.3 Output power P_{aven} of 2DOF VEH at different excitation frequencies α and electrical damping ratios ζ_e, where mass ratio μ is 0.1, 0.2, 0.3, 0.4, tuning ratio f is 0.8, and mechanical damping ratio ζ_m is 0.046

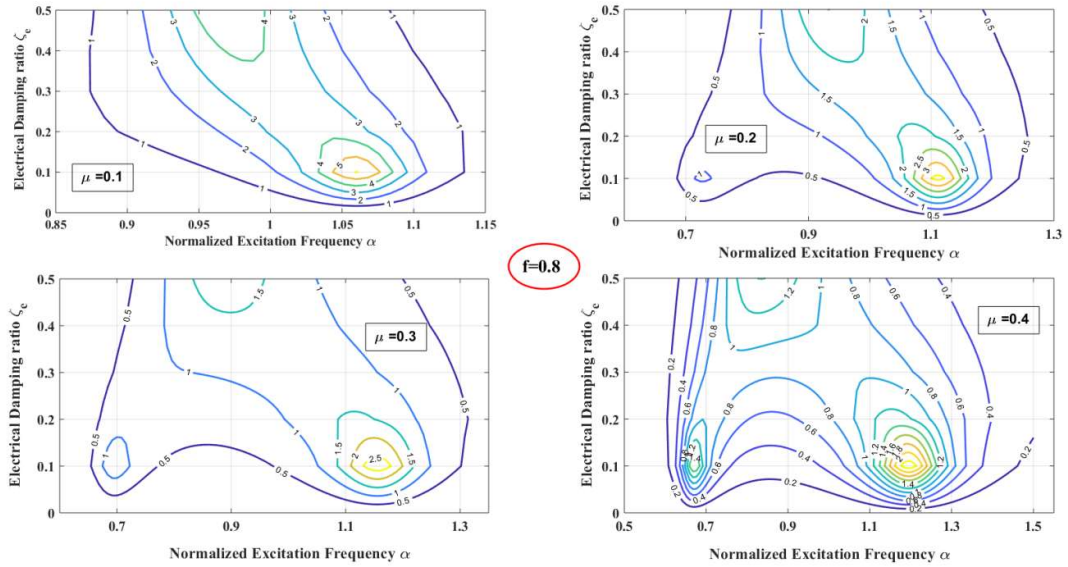

Figure 6.4 Contour of dimensionless power and optimal electrical damping ratios ζ_e at different normalized excitation frequency α, where mass ratio μ is 0.1, 0.2, 0.3, 0.4, tuning ratio f is 1, and mechanical damping ratio ζ_m is 0.046

6.1.3 Case III f=1.2

P_{aven} vs. ζ_e for μ = 0.1, 0.2, 0.3, and 0.4

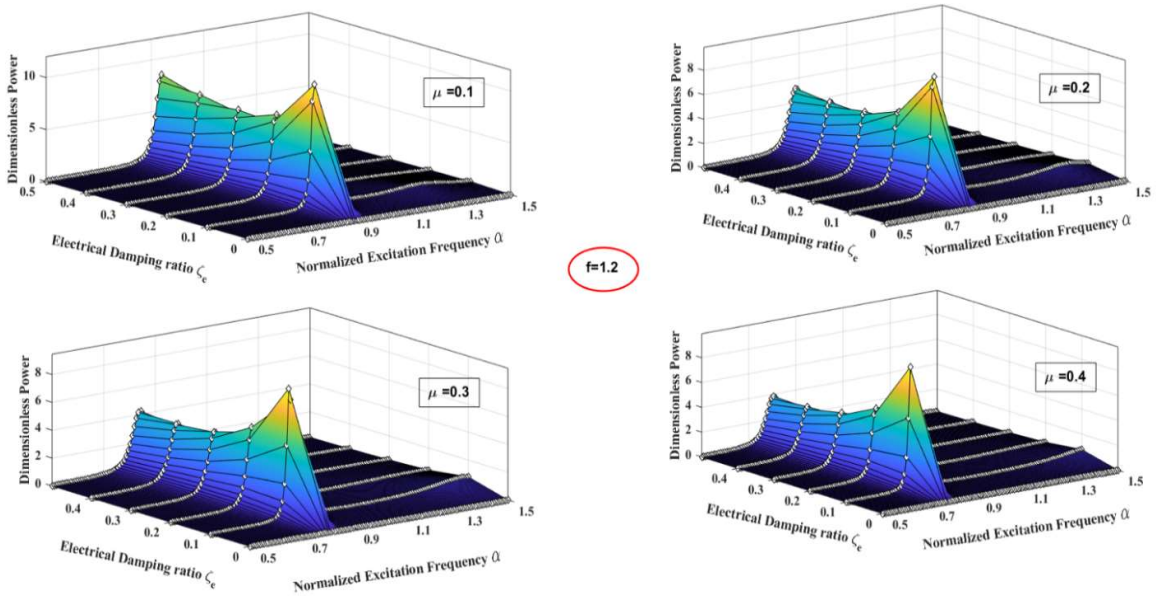

Figure 6.5 The power output P_{aven} of 2DOF VBEH at different excitation frequencies α and electrical damping ratios ζ_e, where mass ratio μ is 0.1, 0.2, 0.3, 0.4, tuning ratio f is 1.2, and mechanical damping ratio ζ_m is 0.046

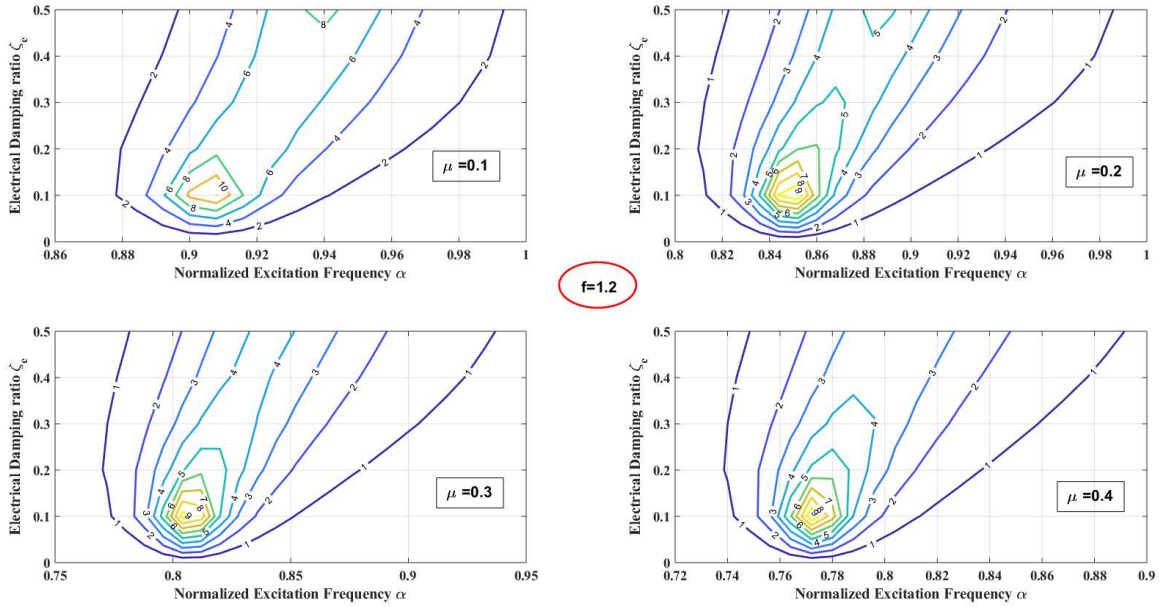

Figure 6.6 Contour of dimensionless power and optimal electrical damping ratios ζ_e at different excitation frequencies α, where mass ratio μ is 0.1, 0.2, 0.3, 0.4, tuning ratio f is 1.2, and mechanical damping ratio ζ_m is 0.046

6.2 Some Typical curves of P_{aven} vs. α

Some typical curves of P_{aven} vs. α, showing first and second mode normalized excitation frequency ω are shown in figures 6.7, 6.8, and 6.9

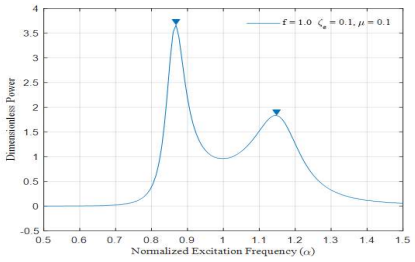

Figure 6. 7 Typical P_{aven} vs. curve for f = 1.0, ζ_e = 0.1, μ =0.1

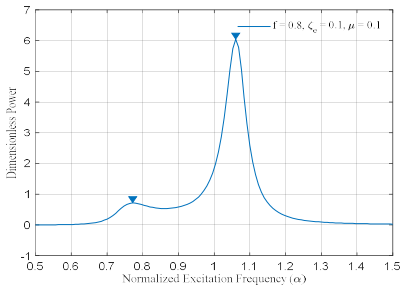

Figure 6. 8 Typical P_{aven} vs. curve for f = 0.8, ζ_e = 0.1, μ =0.1

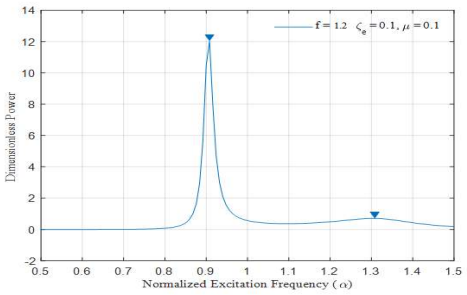

Figure 6. 9 Typical P_{aven} vs. curve for f = 1.2, ζ_e = 0.1, μ =0.1

In figure 6.7, (case f = 1), the first peak first peak P_{aven} is ≅ 3.5 units and the second peak P_{aven} is ≅ 1.75 units. (when ζ_e = 0.1 and μ = 0.1). In figure 6.8, (case f = 0.8), the second peak P_{aven} is ≅6 units. (when ζ_e = 0.1 and μ = 0.1). In figure 6.9, (case f=1.2), the first peak P_{aven} is ≅12 units. (when ζe = 0.1 and μ = 0.1)

Table 6.1, 6.2, and 6.3 show the values of P_{aven} at α_1 and α_2 for ζ_e = 0.1, 0.2, 0.3, 0.4, 0.5 and μ = 0.1, 0.2, 0.3, 0.4

Table 6.1 P_{aven} at first and second mode normalized frequencies α_1 and α_2

ξe	P_{aven} at α_1				P_{aven} at α_2			
	μ =0.1	μ =0.2	μ =0.3	μ =0.4	μ =0.1	μ =0.2	μ =0.3	μ =0.4
0.1	3.664	3.8376	4.0967	4.3883	1.835	1.5358	1.3726	1.271
0.2	2.9378	2.5518	2.56	2.6642		0.9108	0.7652	0.6836
0.3	3.5874	2.4576	2.2428	2.203				
0.4	4.5609	2.7784	2.3151	2.142				
0.5	5.6208	3.2646	2.5687	2.2732				

Table 6. 2 P_{aven} at first and second mode normalized frequencies

$\alpha_1 = \frac{\omega_{n1}}{\omega_1} = \overline{\omega_{n1}}$ and $\alpha_2 = \frac{\omega_{n2}}{\omega_1} = \overline{\omega_{n2}}$

ξe	P_{aven} at α_1				P_{aven} at α_2			
	μ =0.1	μ =0.2	μ =0.3	μ =0.4	μ =0.1	μ =0.2	μ =0.3	μ =0.4
0.1	0.7139	1.0762	1.3496	1.5901	6.0378	3.6294	2.7787	2.3133
0.2	3.883	2.1482	0.8974	0.9992			1.5704	1.2768
0.3	3.7167	1.8721	1.2716	0.943				0.9822
0.4	4.1828	2.0942	1.411	1.1328				
0.5	4.8736	2.5019	1.743	1.4048				

Table 6. 3 P_{aven} at α_1 and α_2

ξe	P_{aven} at α_1				P_{aven} at α_2			
	μ = 0.1	μ = 0.2	μ = 0.3	μ = 0.4	μ = 0.1	μ = 0.2	μ = 0.3	μ = 0.4
0.1	12.296	9.879	9.455	9.9255	0.7004	0.7941	0.8082	0.425
0.2	7.9881	6.1055	5.7607	5.6609		0.4426	0.4366	0.3039
0.3	7.3021	5.1645	4.5642	4.3796				
0.4	7.636	4.9953	4.2021	3.9291				
0.5	8.4141	5.1991	4.2288	3.7978			`	

6.3 Discussion on Results

In SDOF VBEH system, for mass ratio μ = 0.3, the available power output P_{ave} is 102 mW and for mass ratio μ = 0.36, the available output power P_{aven} is 124mW. In 2DOF VBEH, for mass ratio μ = 0.3 the available power output at first mode resonance frequency is 552 mW and at second mode natural frequency is 183 mW. Where as the harvested power output P_{aveh} for first mode of natural frequency is 58.51 mW and second mode natural frequency is 70.73 mW. For mass ratio μ = 0.36 the theoretical available power output at first board natural frequency is 576mW and second mode natural frequency is 128 MW. Where as harvested power output P_{aveh} for 1st board natural frequency is 69.36 MW and second board natural frequency is 44.83 MW. It is seen that the power output increases with increase in mass ratio μ.

For mass ratio μ = 0.3 theoretical effective non-dimensional bandwidth is 0.57 and experimental effective non-dimensional bandwidth is 0.55. The effective non-dimensionless bandwidth from the contour plot is 0.52. For mass ratio μ = 0.36 the theoretical effective non-dimensional bandwidth is 0.6 and experimental effective non-

dimensional bandwidth is 0.52. The values of theoretical and experimental effective frequency bandwidth $\overline{b_e}$ are in good agreement.

Case I: f = 1.0. From figures 6.1, 6.2, it is seen that P_{aven} increases with the increase in value of ζ_e for $\mu = 0.1$. The value of P_{aven} is at maximum at first mode resonant frequency α_1 of 2DOF VBEH. The case $\mu = 0.3$ and $\zeta_e = 0.1$ when (f =1.0) gives a better compromise between the maximum value of P_{aven} and bandwidth $\overline{b_e}$

Case II: f = 0.8. From figures 6.3 and 6.4 it can be seen that for small values of μ and ζ_e the maximum value P_{aven} occurs almost at the second normalized resonant frequency α_2 of 2DOF VBEH, however, the bandwidth $\overline{b_e}$ is less than that for the case f = 1.0.

Case III: f =1.2. From figures 6.5 and 6.6 it can be seen that for the values of $\mu = 0.1$, 0.2, 0.3, and 0.4, and for small values of ζ_e, almost all the non-dimensional power output P_{aven} of the 2DOF VBEH occurs at the first mode resonant normalize excitation frequency α_1. The value of P_{aven} in this case is the highest with extremely narrow bandwidth $\overline{b_e}$ i.e., in the neighborhood of first mode natural frequency α_1

6.4 Conclusions

i) The method surface plots and contour diagrams is extremely useful for estimating the global optimal value of power output from a 2DOF VBEH at its design stage. The variation of non-dimensional power output P_{aven} of 2DOF VBEH can be studied by varying the values of electrical damping ratio ξ_e and normalized excitation frequency α simultaneously for various values of mass ratio μ for a given value of tuning ratio f (i.e., f = 0.8 or f = 1.0 or f = 1.2). In all these cases, the increased P_{aven} is available over the widened operational excitation frequency band $\overline{b_e}$ compared to that for the traditional SDOF VBEH.

ii) With the use of the surface plots and contour diagrams, the researcher- designer of a 2DOF VBEH will have various options of choosing the values of essential parameters such as mass ratio μ, tuning ratio f, and electrical damping ratio ζ_e for the VBEH to be designed for a specific application. The choice of μ, f, and ζ_e will be based on the objective of getting maximum average power P_{aven} and bandwidth $\overline{b_e}$ over which this power is to be obtained.

iii) From the result of the comparison of theoretical power output and harvested power output of developed SDOF and 2DOF VBEH it can be seen that the harvested power is

much less than the power generated because of the effect of the shunted electrical load. Also it is seen that there is a good agreement between theoretical and experimental values of effective non-dimensional bandwidth $\overline{b_e}$.

Chapter – 7

DISCUSSION ON RESULTS AND CONCLUSIONS

7.1 Discussion on Results

In this section, the significant results of research work are recapitulated and a discussion on these results is taken up.

In chapter 3, some experimental and analytical studies on maximum average power output from a vibration-based electromagnetic energy harvester have been carried out. From the results of experimental analysis, it is observed that the maximum power Pave from VBEH is 45.1μW at the resonant frequency and some power is available in the neighborhood of resonance. The resistive load affects the value of maximum P_{ave} and the electrical damping ratios. From the results of analysis, in section 3.2.1 and 3.2.2, it is seen from figures 3.22, 3.23, and 3.24 that the value of dimensionless maximum average power obtained is 13.7 for $\zeta_m = 0.0046$, at $\frac{\omega}{\omega_n} = 1$. The results shown in figures 3.25, 3.26, and 3.27 it can be noted that the maximum average power obtained is 48 for $\zeta_e = 0.00516$, at $\frac{\omega}{\omega_n} = 1$. As such, to obtain maximum dimensionless average power from a VBEH, the value of ζ_m should be as small as possible.

In chapter 4, experimental studies on the effect of electrical load impedances on the power output of a vibration-based electromagnetic energy harvester have been carried out. The curves of P_{ave} vs. excitation frequency ω, for $\zeta_e = \zeta_{e1} = 0.005$ and of P_{ave} vs. excitation frequency ω,for $\zeta_e = \zeta_{e2} = 0.008$ and with the resistive load of 1600 Ω (which is approximately equal to the internal resistance of the coil) are shown in figure 4.29. It is seen that the value of P_{ave} based on the electrical damping ratio ζ_{e1} is less than that determined using the theoretical expression for ζ_e (method 2). From the curve of P_{aveh} vs. ω, it can be seen that the average harvested power P_{aveh} is maximum at the resonant frequency when the resistive load is 1600Ω. The value of the average harvested power output is very less than the average generated power output of VBEH.

In chapter 5, some theoretical and experimental studies on enhancing the power output and widening operational bandwidth of vibration-based electromagnetic energy harvester, have been carried out.

From figure 5.3, 5.4, 5.5 and 5.6, it is seen that, the values of useful bandwidth b increases with increases in mass ratio μ. For f = 1.2 the value of bandwidth are more for given value of μ this is clearly seen in figure 5.6.

From figure 5.7, 5.8, and 5.9, it is observed that, for f = 0.8 the band width is minimum for all values of mass ratio μ considered, at f = 1, bandwidth '$\overline{b_e}$' is wide enough from the point of design of 2DOF VBEH.

From figures 5.10,5.11,5.12,5.13, and 5.14 as the values of tuning ratio f increases, the first mode of natural frequency $\overline{\omega_{n_1}}$ decreases up to the f = 0.8 and increases thereafter till f = 1.4. Same trend is followed by the second mode of natural frequency $\overline{\omega_{n_2}}$. It is suggested that the design of 2DOF VBEH should be near the value of f = 1

For the case μ = 0.36, from figures 5.22 and 5.26, it is clearly seen that the band width of operating excitation frequency has been increased. The values of relative displacement amplitude Z is maximum at two resonant frequencies indicating that the open circuit voltage E and voltage across the electric resistive load V_R will be available over a wide band of excitation frequency. This result shows that the harvester power P_{aveh} of a 2DOF VBEH is increased as compared to that of a SDOF VBEH device. The power P_{aveh} is available over the wide band of excitation and the peak values of P_{aveh} are at the two resonant frequencies. It should be noted that the maximum values of P_{aveh} is available at a resistive load of 1500 Ω which is approximately equal to internal resistance R_L of electrical copper coil

For the case μ = 0.3, figures 5.27 to 5.30 It is clearly seen that the power P_{aveh} is available over the wideband of excitation with its peak values at the two resonant frequencies. The maximum power is available at a resistive load of 1500 Ω at 45.53 rad/sec.

In chapter 6, optimization of power output of a 2DOF vibration-based electromagnetic energy harvester has been carried out. In SDOF VBEH system, for mass ratio μ = 0.3, the theoretical available power output P_{ave} is 102 mW and for mass ratio μ = 0.36, the theoretical available output power P_{ave} is 124mW. For mass ratio μ = 0.3 the theoretical available power output at first mode resonance frequency is 552 mW and at second mode natural frequency is 183 mW. Whereas the harvested power output P_{aveh} for first mode of natural frequency is 58.51 mW and second mode natural frequency is 70.73 mW. For mass ratio μ = 0.36 the theoretical available power output at first mode natural frequency is 576mW and second mode natural frequency is 128 mW. Whereas harvested power

output P_{aveh} for first mode natural frequency is 69.36 mW and second mode natural frequency is 44.83 mW.

For mass ratio μ = 0.3 theoretical effective non-dimensional bandwidth is 0.57 and experimental effective non-dimensional bandwidth is 0.55. The effective non-dimensionless bandwidth from the contour plot is 0.52. For mass ratio μ = 0.36 the theoretical effective non-dimensional bandwidth is 0.6 and experimental effective non-dimensional bandwidth is 0.52.

Also, the effect of the tuning ratio f on the non-dimensional power output P_{aven} has been studied. The results are as follows:

Case I: f = 1.0. From figures 6.1, 6.2, it is seen that P_{aven} increases with the increase in value of ξ_e for μ = 0.1. The value of P_{aven} is at maximum at first mode resonant frequency α_1 of 2DOF VBEH. The case μ = 0.3 and ξ_e =0.1 when (f =1.0) gives a better compromise between the maximum value of P_{aven} and bandwidth $\overline{b_e}$

Case II: f = 0.8. From figures 6.3 and 6.4 it can be seen that for small values of μ and ζ_e the maximum value P_{aven} occurs almost at the second normalized resonant frequency α_2 of 2DOF VBEH, however, the bandwidth $\overline{b_e}$ is less than that for the case f = 1.0.

Case III: f =1.2. From figures 6.5 and 6.6 it can be seen that for the values of μ = 0.1, 0.2, 0.3, and 0.4, and for small values of ξ_e, almost all the non-dimensional power output P_{aven} of the 2DOF VBEH occurs at the first mode resonant normalize excitation frequency α_1. The value of $P_{aven,}$ in this case is the highest with extremely narrow bandwidth $\overline{b_e}$ i.e., in the neighborhood of first mode natural frequency α_1

7.2 Conclusions

The following significant conclusions are drawn from the discussion on results.

1. The results of the theoretical and experimental analysis of the developed VBEH show that the maximum available power from a VBEH is influenced considerably by the values of mechanical damping ratio ζ_m, both at resonance and off-resonance conditions, electrical damping ratio ζ_e and the resistive load R_L across the electromagnetic coil terminals. The ζ_m should be as small as possible and ζ_e should be nearly equal to ζ_m for maximum power generation from VBEH
2. The effect of variation of shunted electrical loads R_L (resistive), Z_1 (resistive and inductive) and $Z_{2,}$ (resistive, inductive, and capacitive) on the average harvested

power P_{aveh} is investigated at various excitation frequencies. It shows that the average harvested power P_{aveh} is maximum at resonance. The P_{aveh} decreases with an increase in electrical load on the harvester. It shows that the value of P_{aveh} is maximum at the resistive load of 1600 Ω, which is approximately equal to the internal resistance of the coil. This research finding is in line with the research results reported in the state-of-the-art of design and development of vibration-based energy harvesters.

3. Using the transient response curve of open-circuit voltage E vs. time t, the mechanical damping ratio ζ_m is estimatedas 0.025 and using the transient response curve of V_R vs. time t, The total damping ratio ζ is determined as 0.03, at the resistive load of 1600Ω. From the estimated values of ζ and ζ_m, the electrical damping ratio ζ_{e1} was calculated as $\zeta_{e1} = \zeta - \zeta_m = 0.005$, (method 1 of section 5.2). Also the value $\zeta_e = \zeta_{e2} = 0.008$ was estimated using the analytical formula for ζ_e. It shows that the value of the electrical damping ratio $\zeta_e = \zeta_{e1}$, obtained from method 1 of section 5.2, is less than that obtained from the analytical formula for ζ_e using method 2 of section 5.3. The experimental value of the electrical damping ratio $\zeta_e(0.005)$ is very small as compared to the value of the mechanical damping ratio ζ_m (0.025).This result is desirable to obtain maximum harvester power from a VBEH. This Conclusion will undoubtedly be beneficial in the design and development of vibration-based energy harvesters.
4. The value of the average generated power P_{ave} based on the electrical damping ratio ζ_{e1} (method 1) is less than that obtained using the analytical formula for ζ_e (method 2). The values of the average generated power Pave and average harvested power P_{aveh} of VBEH are maximum when the value of excitation frequency equals the natural frequency of the mechanical sub-system of the VBEH. These results bring out the importance of the experimental determination of the electrical damping ratio in the maximization of the out power of the VBEH shunted to electrical loads
5. The detailed analysis presented in sections 5.3, 5.4, 5.5, and 5.6 are the design sheets necessary to have the estimate of the mass ratio μ and tuning ratio f with a view to determine the mass and spring parameters of the proposed 2DOF VBEH model so that the output of 2DOF VBEH power harvested is enhanced and is available over a wide bandwidth of the excitation frequencyω, also it is observed that when tuning ratio f=1, and the mass ratio μ = 0.4, wide bandwidth b is available. However, if it is required to have even more bandwidth then one can obtain it for tuning ratio f = 1.2

and mass ratio $\mu = 0.4$. If it is required to have less mass ratio such as $\mu = 0.3$, in that case the tuning ratio f should be equal to 1.2. This choice of mass ratio will give output power of 2DOF VBEH over a wider bandwidth with minimum a weight of VBEH.

6. Figures 5.24 and 5.25 It is clearly seen that the band width of operating excitation frequency is increased over which, the relative displacement amplitude Z the value is maximum at two resonant frequencies, indicating that the open circuit voltage E and voltage across the electric resistive load VR will be available over a wide band of excitation frequency. This result increased harvester power P_{aveh} of 2 DOF VBEH devices over the comparable SDOF VBEH device. The power P_{aveh} is available over the wide band of excitation with its peak values at the two resonant frequencies. The maximum power is available at a resistive load of 1500 Ω and is minimum at R_L= 1000 Ω at 34.54 rad/sec
7. The use of method of the surface plots and contour diagram provides the researcher-designer of a 2DOF VBEH the options of choosing the values of essential parameters such as mass ratio μ, tuning ratio f, and electrical damping ratio ζ_e for the design of the VBEH for a specific application. The choice of μ, f, and ζ_e will be based on the objective of getting maximum average power P_{aven} and bandwidth over which this power is to be obtained.
   i. The value of ζ_e will be controlled by carefully designing electrical coil and magnet configuration and electrical load impedances connected to the VBEH device.
   ii. The charts suggest that the choice $\mu = 0.3$ and $f = 1.0$ (case 1) is a better compromise to obtain the maximum out power and wide operational frequency bandwidth.

Chapter – 8

CONTRIBUTIONS TO THE RESEARCH

The results of the present theoretical and experimental research work carried out in the areas of design, development and optimization of the performance of vibration-based electromagnetic energy harvester provides following outcomes as design guidelines for the designer/researcher of VBEH device.

i. The researchers/designers of a VBEH, for an available ambient vibration source will have to take into consideration the following facts that the maximum average power P_{ave} output of a VBEH is affected at and off the resonance by the values of electrical and mechanical damping ratios ξ_e and ξ_m and the pure resistive load across the vibration transducer coil terminals. For maximum P_{ave}, ξ_m should be as small as possible and $\xi_e = \xi_m$. The internal resistance of the coil R_C should be kept as small as possible using proper copper coil winding technology to achieve a high copper fill factor, at the same time the selection of the magnet oscillating in the copper coil is crucial to produce higher flux density in the coil circuit.

ii. Further, the researcher-designer of the VBEH has to keep in mind the effect of shunt electrical resistance R, inductance L, capacitance C impedances across the vibration transducer coil terminal on the harvested power of the VBEH by designing the R-L-C circuit in such a manner that the electrical natural frequency of the R-L-C circuit is made equal to the natural frequency of the harvester mass and suspension system. To achieve maximum harvester power, the load resistance R_L should be approximately the same as the internal resistance R_C of the transducer copper coil.

iii. The traditional VBEH has the drawback that it provides maximum average power only at resonant frequency or operation frequency band is narrow, in the small neighborhood of the resonance. It has been shown that it is possible to enhance or increase the power output of a traditional SDOF VBEH, by the method of its modification into 2DOF VBEH which simultaneously helps to widen its operational frequency band. The power of output of such a 2DOF VBEH is controlled by μ, f, ξ_e and α. The present research shows that the harvested power output is increased with widening of its operation frequency band of a 2DOF VBEH, also shown that it is affected by variations in 'μ'.

iv. The method of surface plots and contour diagrams is extremely useful for estimating global optimal value of power output of 2DOF VBEH, at its design stage. The use of method of surface plots and contour diagrams provides the researchers-designers the option of selecting the values of the necessary parameters such as mass ratio μ, tuning ratio f, and electrical damping ratio ξ_e for the design of a 2DOF VBEH for a specific application. The choice of these parameters will be based on objective of getting maximum power output and the extended effective frequency bandwidth $\overline{b_e}$ over which the power output is to obtained.

v. The present research has also shown that with the method surface plots and control diagrams for analyzing maximum non-dimensional power output P_{aven} of 2DOF VBEH, over a wide operational frequency band b, the researcher-designer has been provided with the options of choosing the essential parameters such as mass ratio μ, tuning ratio f and electrical dumping ratio ξ_e for the design of VBEH suitable for a given specific application and the characteristic parameters of the available ambient vibration source. In such a case the objective of the designer is to choose the value of μ, f and α for maximum power output P_{aven} over a wide excitation frequency band $\overline{b_e}$.

Chapter – 9

SCOPE FOR FURTHER RESEARCH

i. In continuation of the research work carried out, it is suggested to design and develop a multi-degree of freedom VBEH system with a view to increase its power output and widen the effective operation of frequency bandwidth, keeping in mind that the size and weight of such a multi-degree of freedom system VBEH be minimum.

ii. It is necessary to study the effect of change of coil-magnet relative motion architecture type on the output power of a VBEH. The study of flux-linkage with coil and magnet can be carried out to optimize the open circuit voltage of VBEH.

iii. It will be off interest to study the effect of using a non-linear spring in the harvester mass-spring system on the average power output of the VBEH and on operational frequency band.

iv. An extensive experimental study on the factors affecting the values of mechanical dumping and electrical damping in a VBEH is necessary as a slight change in values of these factors influence, to a great extent, on the harvested power output of a VBEH.

v. There is a further scope for carrying out studies on design and development of hybrid types of energy harvesters to take the advantage of their synergistic effect on power output and efficiency.

List of Publication

International Conference

1. Vijay Patil, Mahadev Sakri, “Effect of electrical damping ratio on maximum average power of an electromagnetic vibration harvester at resonance and off-resonance conditions” International Conference on Clean and Renewable Energy at National Institute of Technology Durgapur, July 10-12, 2019.

2 Vijay B. Patil, Mahadev Sakri “Investigative study on widening of operational bandwidth of a vibration based electromagnetic energy harvester” International Conference on Advances in Material Science, Mechanical and civil Engineering (AIP Proceeding) at Annasaheb Dange College of Engineering and Technology Ashta Sangli. Feb. 14-15, 2022.

International Journal

3 Vijay Patil, Mahadev Sakri, “Effect of electrical damping ratio on maximum average power of an electromagnetic vibration harvester at resonance and off-resonance conditions” International Journal of Recent Technology and Engineering (IJRTE) ISSN: 2277-3878, Volume-8 Issue-2S7, July 2019.
[DOI: 10.35940/ijrte.B1120.0782S719]

4 Vijay B. Patil, Mahadev Sakri, “Experimental studies on the effect of various types of shunted electrical loads on the performance of a vibration-based electromagnetic energy harvester” FME TRANSCTIONS journal (2021) 49, 163-172
[Web of science, DOI: 10.5937/fme2101163V, Impact factor 1.77, H index- 23]

References:

[1] *Srishti Banerji, Ashutosh Bagchi, Shervin Khazaeli,"Energy harvesting methods for structural health monitoring using wireless sensors: a review", International Conference on Resilient Infrastructure, London, STR-991, pp.1-10,(2016)*

[2] *A. -R. El-Sayed, K. Tai, M. Biglarbegian and S. Mahmud, "A survey on recent energy harvesting mechanisms," 2016 IEEE Canadian Conference on Electrical and Computer Engineering (CCECE), pp. 1-5, (2016)*

[3] *Matteo Scapolan, Maryam Ghandchi Tehrani, Elvio Bonisoli, "Energy harvesting using parametric resonant system due to time-varying damping" Journal of Mechanical Systems and Signal Processing, Vol. 79, pp. 149 – 165, (2016).*

[4] *G. Gatti, M.J. Brennan, M.G. Tehrani, D.J. Thompson, "Harvesting energy from the vibration of a passing train using a single-degree-of-freedom oscillator," Journal of Mechanical Systems and signal Processing, Vol. 66-67, pp. 785 – 792,(2016).*

[5] *Xueguang Liu, Xiaoxiao Feng, Ye Shi, Ye Wang, Zhijun Shuai," Development of a semi-active electromagnetic vibration absorber and Its experimental study", Journal of Vibration and Acoustics (ASME), Vol. 135 / 051015, pp 1-9, (2013)*

[6] *Lei Zuo and Wen Cui, "Dual-functional energy-harvesting and vibration control electromagnetic resonant shunt series tuned mass damper", Journal of Vibration and Acoustics (ASME), Vol. 135, No. 051018, pp 1-9, (2013)*

[7] *Carol L .Zoller and Remus DOBRA, "HP VEE simulation of an electromechanical vibration absorber", Research and Development in Mechanical Industry (RADMI), Serbia, pp 647-653, (2009)*

[8] *N.G. Stephen, "On the maximum power transfer theorem with in electromechanical systems",* Proceedings of the Institution of Mechanical Engineers, Part C: Journal of Mechanical Engineering Science*, Vol. 220, issue 8, 1261-1267. (2006)*

[9] *Stephen N. G." On energy harvesting from ambient vibration.", Journal of Sound and Vibrations. Vol. 293, pp. 409 – 425, (2006)*

[10] *Kangqi Fan, Geng Liang, Yiwei Zhang, Qinxue Tan, "Hybridizing linear and nonlinear couplings for constructing two-degree-of-freedom electromagnetic energy harvesters" International Journal of Energy Research, WILEY, pp 1–16. (2019)*

[11] *SadiaBakhtiar and FaridUllah Khan, "Analytical Modeling and Simulation of an Electromagnetic Energy Harvester for Pulsating Fluid Flow in Pipeline", Hindawi, The Scientific World Journal, Article ID 5682517, pp 1-9, (2019)*

[12] *Ahmed Munaz and Gwiy-Sang Chung, "An electromagnetic energy harvester based on multiple magnet scavenging power from low frequency vibration", Micro system Technologies, Springer, Vol. 23, issue 1, pp 91-99, (2015)*

[13] *Shih-Jui Chen and Jia-Yin Wu, "Fabrication of a 2-DOF electromagnetic energy harvester with in-phase vibrational bandwidth broadening", Journal of Smart Material Structures, IOP Publishing Ltd., Vol. 25, issue 9, pp. 1- 8, (2016)*

[14] *B. Fu, E. Blokhina, D. O'Connell, O. Feely and R. Frizzell, "A wideband 2-DOF resonator for electromagnetic energy harvesting systems," 21st IEEE International Conference on Electronics, Circuits and Systems (ICECS), pp. 878-881 (2014)*

[15] *B.L. Ooi and J.M. Gilbert, "Design of Wideband Vibration-based Electromagnetic Generator by means of Dual-resonator", Sensors and Actuators A, Vol. 213, pp. 9 – 18, (2014)*

[16] Slim Naifar et.al., "Survey of Electromagnetic and Magnetoelectric Vibration Energy Harvesters for Low Frequency Excitation", Measurement, Vol. 106, pp. 251 – 263, (2015)

[17] Jee Siang, M.H. Lim, M. Salman Leong, "Review of vibration-based energy harvesting technology: Mechanism and architectural approach", International Journal of Energy Research, Wiley, Vol. 42, issue 5, pp 1866 – 1893, (2018)

[18] Anwesamohanty, surajparida, rabindra kumar behera and tarapada roy, "vibration energy harvesting: a review", Journal of Advanced Dielectrics, Vol. 9, No. 4 (2019)

[19] Dong Hyun Bang and Jae Yeong Park, "Micro-Fabricated Silicon Spiral Spring based Electromagnetic Energy Harvester", Journal of the Korean Physical Society, Vol. 62, No. 12, pp. 1720~1725, (2013)

[20] Qian Zhang and EunSok Kim, "Vibration Energy Harvesting Based on Magnet and Coil Arrays for Watt-Level Handheld Power Source", Proceedings of the IEEE, Vol. 102, No. 11, pp. 1747-1761, November (2014)

[21] Chamanian, S., Baghaee, S., Ulusan, H., Zorlu, Ö., Külah, H., & Uysal-Biyikoglu, E., "Powering-up Wireless Sensor Nodes Utilizing Rechargeable Batteries and an Electromagnetic Vibration Energy Harvesting System", Energies Vol. 7, pp. 6323-6339, (2014)

[22] Hui Zhang, Lawrence R. Corr, Tianwei Ma, "Effects of electrical loads containing non-resistive components on electromagnetic vibration energy harvester performance", Mechanical Systems and Signal Processing, Vol. 101, pp. 55–66, (2018)

[23] Williams, C. B. and Yates, R. B., "Analysis of a micro-electric generator for micro systems.", Sensors and Actuators A, Vol. 52, pp. 8 – 11, (1996)

[24] P. V. Malaji, ShaikhFaruque Ali, "Broadband Energy Harvesting with Mechanically Coupled Harvesters", Sensors & Actuators, Vol. 255, pp. 1 – 9, (2016)

[25] Miah A. Halim, Hyunok Cho, Jae Y. Park, "Design and experiment of a human-limb driven, frequency up-converted electromagnetic energy harvester, Energy Conversion and Management, Vol. 106, pp. 393–404, (2015)

[26] Mohammed F. Daqaq, Ravindra Masana, Alper Erturk, D. Dane Quinn, "On the Role of Nonlinearities in Vibratory Energy Harvesting: A Critical Review and Discussion", Journal of Applied Mechanics Reviews (ASME), Vol. 66 / 040801-23, (2014)

[27] Noha A. Aboulfotoha, Mustafa H. Arafab ,Said M. Megahed, "A self-tuning resonator for vibration energy harvesting", Sensors and Actuators A, Vol. 201, pp. 328– 334, (2013)

[28] Xiudong Tang, Lei Zuo, "Enhanced vibration energy harvesting using dual-mass systems", Journal of Sound and Vibration, Vol. 330, pp. 5199–5209, (2011)

[29] Niell G. Elvin, Alex A. Elvin, "An experimentally validated electromagnetic energy harvester", Journal of Sound and Vibration, 330 pp. 2314–2324, (2011)

[30] C.B. Williams, C. Shearwood, M.A. Harradine, P.H. Mellor, T.S. Birch, R.B. Yates, "Development of an electromagnetic microgenerator", IEE Proceedings: Circuits, Devices and Systems Vol. 148, pp. 337–342, (2001).

[31] Yulong Zhang et. al., "Rotational electromagnetic energy harvester for human motion application at low frequency", Applied Physics Letters, Vol. 116, (2020)

[32] YiMing Lei and Zhiyu Wen, "Study on effects of the damping ratio on output performance of micro electromagnetic vibration energy harvesters", Microsystem Technologies, Vol. 20, pp. 221 – 226, (2014)

[33] Yulong Zhang et. al., "Rotational electromagnetic energy harvester for human motion application at low frequency", Applied Physics Letters, Vol. 116, (2020)

[34] ByungChul Lee, Gwiy Sang Chung, "Frequency tuning design for vibration-driven electromagnetic energy harvester", IET Renewable Power Generation, Vol. 9, Iss. 7, pp. 801–808, (2015)

[35] Lin Dong, M G Prasad and Frank T Fisher, "Two-dimensional resonance frequency tuning approach for vibration-based energy harvesting", IOP Publishing, Smart Materials and Structures, Vol. 25, issue 6, (2016)

[36] M. Z. A. Rahim, M. N. H. Hamid, Z. N. M. Yusuf, S. N. M. Soid and M. R. Ibrahim, "Modeling and Experiment of Electromagnetic Energy Harvester System by Using Dual Moving Mechanical Systems at Low Frequency Range", MATEC Web of Conferences, 217, (2018)

[37] Ping Li, Shiqiao Gao, and Binglong Cong, "Theoretical modeling, simulation and experimental study of hybrid piezoelectric and electromagnetic energy harvester", AIP Advances, Vol. 8, issue 3, (2018)

[38] B.L. Ooi, J.M. Gilbert, A. Rashid A. Aziz, "Switching damping for a frequency-tunable electromagnetic energy harvester", Sensors and Actuators: A, Vol. 234, pp. 311 – 320, (2015)

[39] Tanju Yildirim, Mergen H. Ghayesh, Weihua Li, GurselAlici, "A review on performance enhancement techniques for ambient vibration energy harvesters", Renewable and Sustainable Energy Reviews, Vol. 71, pp. 435–449, (2017)

[40] Jan Smilek and ZdenekHadas, "Coil Optimization for Linear Electromagnetic Energy Harvesters with Non-uniform Magnetic Field", Mechatronics, Advances in Intelligent Systems and Computing Vol. 644, pp. 734 – 742, (2017)

[41] H. A. Wheeler, "Simple Inductance Formulas for Radio Coils," in Proceedings of the Institute of Radio Engineers, vol. 16, no. 10, pp. 1398-1400, Oct. (1928)

[42] Wei-Che Tai, Lei Zuo, "On optimization of energy harvesting from base-excited vibration", Journal of Sound and Vibration, Vol. 411, pp. 47–59, (2017)

[43] P.V. Malaji, M. Rajarathinam, V. Jaiswal, S.F. Ali and I.M. Howard, "Energy harvesting from dynamic vibration pendulum absorber", Structural Engineering Convention (SEC-2016) CSIR-SERC, Chennai, India. 21-23 December (2016)

[44] ShaikhFaruque Ali, SondiponAdhikari, "Energy Harvesting Dynamic Vibration Absorbers", Journal of Applied Mechanics, Vol. 80 / 041004-1-9, (2013)

[45] E. Arroyo, A. Badel, "Electromagnetic vibration energy harvesting device optimization by synchronous energy extraction", Sensors and Actuators A, Vol. 171, pp. 266– 273, (2011)

[46] Seok-Chan Kim, Jin-Gyun Kim, Young-Cheol Kim, Seok-Jo Yang, Hanmin Lee, "A Study of Electromagnetic Vibration Energy Harvesters: Design Optimization and Experimental Validation", International Journal of Precision Engineering and Manufacturing-Green Technology, Springer, (2019)

[47] Clemens Cepnik, Ulrike Wallrabe, "Practical and Theoretical Limits of The Output Power of Electromagnetic Energy Harvesters at Miniaturization", Study lib, (2021)

[48] Giovanni Caruso, "Broadband Energy Harvesting from Vibrations Using Magnetic Transduction", Journal of Vibration and Acoustics, ASME, Vol. 137, issue 6, (2015)

[49] Nadav Cohen, "An energy harvesting mechanism travelling the human intestinal system", Proceedings of ISMA 2010, pp. 3677- 3690, (2010)

[50] *M. Z. A. Rahim, M. N. H. Hamid, Z. N. M. Yusuf, S. N. M. Soid and M. R. Ibrahim, "Modeling and Experiment Of Electromagnetic Energy Harvester System By Using Dual Moving Mechanical Systems At Low Frequency Range", MATEC Web Of Conferences, Vol. 217, (2018)*

[51] *N.G. Stephen, "On the maximum power transfer theorem with in electromechanical systems",* Proceedings of the Institution of Mechanical Engineers, Part C: Journal of Mechanical Engineering Science*, Vol. 220, issue 8, 1261-1267. (2006)*

[52] *C.B. Williams, R.B. Yates, "Analysis of a micro-electric generator for micro-systems", Sensors and Actuators A Vol. 52, pp. 8-11, (1996)*

[53] *M. Rajarathinam, S.F. Ali, "Energy generation in a hybrid harvester under harmonic Energy excitation", Energy Conversion and Management, Vol. 155, pp. 10– 19, (2018).*

[54] *Kouichi Takeya, Eiichi Sasaki, Yusuke Kobayashi, "Design and parametric study on energy harvesting from bridge vibration using tuned dual-mass damper systems", Journal of Sound and Vibration, Vol. 361, pp. 50–65*, (2016)

[55] *Q. Zhang and E. S. Kim, "Vibration Energy Harvesting Based on Magnet and Coil Arrays for Watt-Level Handheld Power Source," in Proceedings of the IEEE, vol. 102, no. 11, pp. 1747-1761, Nov. (2014).*

[56] *Lei Zuo and Pei-sheng Zhang, "Energy harvesting, ride comfort, and road handling of regenerative vehicle suspensions", Journal of Vibration and Acoustics (ASME), Vol. 135, 011002, pp 1-8, (2013).*

[57] *Ryan L. Harne, "Theoretical investigations of energy harvesting efficiency from structural vibrations using piezoelectric and electromagnetic oscillators", The Journal of the Acoustical Society of America, Vol. 132, No. 1, pp. 162 – 172, July (2012)*

[58] *Abu Riduan Md. Foisal ,Chinsuk Hongb, Gwiy-Sang Chunga, "Multi-frequency electromagnetic energy harvester using a magnetic spring cantilever" , Sensors and Actuators: A, Vol. 182, pp. 106– 113, (2012)*

[59] *P. D. Mitcheson, T. C. Green, E. M. Yeatman and A. S. Holmes, "Architectures for vibration-driven micropower generators," in Journal of Microelectromechanical Systems, vol. 13, no. 3, pp. 429-440, June. (2004).*

[60] *S. Roundy, P.K. Wright, J. Rabaey," A study of low-level vibrations as a power source for wireless sensor nodes", Computer Communications, Vol. 26, pp. 1131–1144, (2003).*

[61] *Christopher Mullen, Soobum Lee, "Experimental Verification and Optimization of a Linear Electromagnetic Energy Harvesting Device", Smart Materials and Nondestructive Evaluation for Energy Systems, Vol. 10171, pp. 1 – 12, (2017)*

[62] *Farid Khan, Boris Stoeber and FarrokhSassani, "Modeling of linear micro electromagnetic energy harvesters with non-uniform magnetic field for sinusoidal vibrations", Microsystem Technologies, Vol. 21, pp. 683 – 692, (2015)*

[63] *Joseph Davidson and Changki Mo, "Recent Advances in Energy Harvesting Technologies for Structural Health Monitoring Applications", Hindawi Publishing Corporation, Smart Materials Research, pp. 1 – 14, (2014)*

[64] *Haruhiko Shirai, Hiromichi Mitamura, Nobuaki Arai & Kazuyuki Moriya, "Study of Energy Harvesting from Low-Frequency Vibration with Ferromagnetic Powder and Non-magnetic Fluid", Plasmonics, Springer, Vol. 15, issue 2, pp. 559 – 571, (2019)*

[65] *Spreeman and Manoli, "Electromagnetic Vibration Energy Harvesting Devices" (Springer), (2012)*

[66] K. Ashraf, M. H. Md Khir, J. O. Dennis, and Z. Baharudin, "Improved energy harvesting from low-frequency vibrations by resonance amplification at multiple frequencies," Sensors Actuators, A Phys., vol. 195, pp. 123–132, (2013).

[67] Kai Tao, Jin Wu, Lihua Tang, Xin Xia, Sun Woh Lye, Jianmin Miao and Xiao Hu, "A novel two-degree-of-freedom MEMS electromagnetic vibration energy harvester", Journal of Micromechanics and Micro-engineering, Volume 26, Number 3, IOP Publishing Ltd, pp. 1 – 12, (2016).

[68] Osama J. Aldraihem, Amr Baz, "Energy Harvester with a Dynamic Magnifier", Journal of Intelligent Material Systems and Structures, Vol. 22, issue 6, pp. 521-530, (2011).

[69] Wanlu Zhou, Gopinath Reddy Penamalli and Lei Zuo, "An efficient vibration energy harvester with a multi-mode dynamic magnifier", Smart Materials and Structures, Volume 21, Number 1, pp. 1 – 9, (2011)

APPENDIX – I

Arduino Program

```
#define trigPin 7
#define echoPin 6
#define rpm_pin 2
float duration = 0;
float cm = 0;
float vtg = 0;
double rpm = 0;
int count = 0;
long prv_time = 0;
float mean_pos = 0;

void setup()
{
  Serial.begin(250000);
  delay(1000);
  pinMode(trigPin, OUTPUT);
  pinMode(echoPin, INPUT);
  pinMode(rpm_pin, INPUT);
  //analogReference(INTERNAL1V1);
  attachInterrupt(0, rpm_count, RISING);
  Serial.println("Data Aquasition System");
  Serial.println("Calculating Mean Position.....");
  Serial.println("Make sure motor is TURNED OFF");
  delay(1000);
  digitalWrite(trigPin, LOW);
  delayMicroseconds(2);
  digitalWrite(trigPin, HIGH);
  delayMicroseconds(10);
  digitalWrite(trigPin, LOW);
  delayMicroseconds(2);
  duration = pulseIn(echoPin, HIGH);
  mean_pos = duration * 3400 / 20000;
  Serial.print("Mean Position=");
  Serial.println(mean_pos);
}

void loop()
{
  digitalWrite(trigPin, LOW);
  delayMicroseconds(2);
  digitalWrite(trigPin, HIGH);
  delayMicroseconds(10);
  digitalWrite(trigPin, LOW);
  delayMicroseconds(2);
```

```
  duration = pulseIn(echoPin, HIGH);
  cm = duration * 3400 / 20000;
  vtg = (analogRead(A0) * 1.1 / 1024) * 1000;
  //UPWORD MOTION IS POSITIVE
  Serial.print(mean_pos - cm);
  Serial.print('\t');

  detachInterrupt(0);
  Serial.print(rpm);
  attachInterrupt(0, rpm_count, RISING);

  Serial.print('\t');
  Serial.print(vtg);
  Serial.print('\t');
  Serial.print(vtg/170);
  Serial.print('\t');
  Serial.println((vtg*vtg)/170);

  //float I = IPCurrent.getCurrentDC();
  //Serial.print('\t');
  //Serial.println(I);
  delay(0.5);
}

void rpm_count()
{
  delay(30);
  if (digitalRead(rpm_pin) == HIGH)
  {
    long t = millis() - prv_time;
    if (t > 0)
    {
      rpm = 60000 / t;
    }
    prv_time = millis();
  }
}
```

APPENDIX – II

MATLAB Code

```
clearall


Mu=[0:0.1:1]
f=1
Dummy=(1+(1+Mu).*f^2)*0.5
Omega1_f1=sqrt((Dummy)-(sqrt(Dummy.^2-f^2)))
Omega2_f1=sqrt((Dummy)+(sqrt(Dummy.^2-f^2)))
figure(1)
plot(Mu,Omega1_f1,'r-*',Mu,Omega2_f1,'b-o','LineWidth',2)
xlabel('\mu')
ylabel('{\omega_{n_{1}}}, {\omega_{n_{2}}}')
gridon
dum
=legend('{\omega_{n_{1}}}','{\omega_{n_{2}}}','Orientation','horizontal')
title(dum,'f=1')
text
b_1=(Omega2_f1-Omega1_f1)



f=0.8
Dummy=(1+(1+Mu).*f^2)*0.5
Omega1_f_dot8=sqrt((Dummy)-(sqrt(Dummy.^2-f^2)))
Omega2_f_dot8=sqrt((Dummy)+(sqrt(Dummy.^2-f^2)))
figure(2)
plot(Mu,Omega1_f_dot8,'r-*',Mu,Omega2_f_dot8,'b-o','LineWidth',2)
xlabel('\mu')
ylabel('{\omega_{n_{1}}}, {\omega_{n_{2}}}')
gridon
dum
=legend('{\omega_{n_{1}}}','{\omega_{n_{2}}}','Orientation','horizontal')
title(dum,'f=0.8')
text
b_f_dot8=(Omega2_f_dot8-Omega1_f_dot8)



f=1.2
Dummy=(1+(1+Mu).*f^2)*0.5
Omega1_f_1dot2=sqrt((Dummy)-(sqrt(Dummy.^2-f^2)))
Omega2_f_1dot2=sqrt((Dummy)+(sqrt(Dummy.^2-f^2)))
figure(3)
plot(Mu,Omega1_f_1dot2,'r-*',Mu,Omega2_f_1dot2,'b-o','LineWidth',2)
xlabel('\mu')
ylabel('{\omega_{n_{1}}}, {\omega_{n_{2}}}')
gridon
```

```
dum
=legend('{\omega_{n_{1}}}','{\omega_{n_{2}}}','Orientation','horizontal')
title(dum,'f=1.2')
text
b_f_1dot2=(Omega2_f_1dot2-Omega1_f_1dot2)



figure(4)
plot(Mu,b_1,'r-*')
holdon
plot(Mu,b_f_dot8,'b-o')
holdon
plot(Mu,b_f_1dot2,'m-s')
legend('f=1','f=0.8','f=1.2')
gridon



[r,c]=find(Mu==0.2)
dummy1=[Omega1_f_dot8(r,c), Omega2_f_dot8(r,c),b_f_dot8(r,c);...
        Omega1_f1(r,c), Omega2_f1(r,c), b_1(r,c);
Omega1_f_1dot2(r,c),Omega2_f_1dot2(r,c),b_f_1dot2(r,c)]
[r,c]=find(Mu == 0.3)


dummy2=[Omega1_f_dot8(r,c), Omega2_f_dot8(r,c),b_f_dot8(r,c);...
        Omega1_f1(r,c), Omega2_f1(r,c), b_1(r,c);
Omega1_f_1dot2(r,c),Omega2_f_1dot2(r,c),b_f_1dot2(r,c)]
[r,c]=find(Mu==0.4);


dummy3=[Omega1_f_dot8(r,c), Omega2_f_dot8(r,c),b_f_dot8(r,c);...
        Omega1_f1(r,c), Omega2_f1(r,c), b_1(r,c);
Omega1_f_1dot2(r,c),Omega2_f_1dot2(r,c),b_f_1dot2(r,c)]


[r,c]=find(Mu==0.5);


dummy3=[Omega1_f_dot8(r,c), Omega2_f_dot8(r,c),b_f_dot8(r,c);...
        Omega1_f1(r,c), Omega2_f1(r,c), b_1(r,c);
Omega1_f_1dot2(r,c),Omega2_f_1dot2(r,c),b_f_1dot2(r,c)]
```